

DRAFT - 9/23/94

NON-PROPRIETARY VERSION

Steam Generator Tubing Outside Diameter Stress
Corrosion Cracking at Tube Support Plates -
Database for Alternate Repair Limits,
Volume 1: 7/8 Inch Diameter Tubing

NP-7480-L, Volume 1, Revision 1

EPRI Project S404-29

EPRI Project Manager:
C. L. Williams

September, 1993

A. J. Baum
J. A. Begley
T. M. Frick
J. L. Houtman
W. R. Junker
R. F. Keating
P. J. Kuchirka
D. D. Malinowski
T. A. Pitterle
P. J. Prabhu
A. Sagar
R. M. Wepfer

This report was prepared by the Westinghouse Electric Corporation, Nuclear Services Division as an account of work sponsored by the Electric Power Research Institute, Inc. (EPRI). Neither EPRI, members of EPRI, Westinghouse Electric Corp., nor any person acting on behalf of them: (a) makes any warranty, express or implied, with respect to the use of any information, apparatus, method, or process disclosed in this report or that such use may not infringe privately owned rights, or (b) assumes any liabilities with respect to the use of, or for damages resulting from the use of, any information, apparatus, method, or process disclosed in this report.

9403160271 931025
PDR TOPRP EXIEPRI
B PDR

REPORT SUMMARY

The database required to support the alternate repair limits for outside diameter stress corrosion cracking (ODSCC) of steam generator tubes at support plate elevations has been developed from pulled tube examination results and tests of specimens produced in model boilers. Leak rate and burst pressure correlations with bobbin coil voltage have been developed from the overall data. Volume 1 of this report addresses the data and correlations for 7/8 inch diameter (OD) tubes.

BACKGROUND Outside diameter stress corrosion cracking (ODSCC) has been observed in PWR (pressurized water reactor) steam generators in the U.S. and abroad. The existing criteria governing the need for tube repair in the U.S. are too conservative and result in unnecessary repair with associated repair costs, radiation exposure, and reduced operating efficiency.

OBJECTIVES To develop the database which can be used to establish alternate repair limits for ODSCC in PWR steam generator tubes at support plate intersections.

APPROACH Data from operating experience (eddy current data and normal operating leakage or lack thereof) and data from pulled tubes (eddy current data, leak rate, burst pressure and destructive examination results) are collected and included in the database. In addition, ODSCC specimens were fabricated in the laboratory using model boilers and tested to supplement the pulled tube database.

RESULTS Eddy current tests on model boiler specimens were conducted using bobbin coil and rotating pancake coil (RPC) probes. Leak rate tests were performed on the specimens at typical normal operating conditions and at primary to secondary pressure differential following a postulated secondary side pipe break (steam line or feed water line break). The specimens were then subjected to burst pressure testing and destructive examination. The crack morphology of model boiler samples was similar to that of pulled tubes from operating steam generators (stress corrosion cracks with minor to negligible intergranular attack - IGA). Using bobbin coil voltage as the independent parameter, correlations were developed for leak rate and burst pressure.

EPRI PERSPECTIVE Degradation of tubes at support plate intersections and at eggcrate intersections is becoming one of the dominant tube degradation mechanisms in PWR steam generators. The existing repair criteria (based upon percent through-wall penetration as the extent of degradation) applied in the U.S. results in the unnecessary repair of structurally sound tubes. Therefore, development of alternate repair limits based upon eddy current signal amplitude could reduce repair costs and radiation exposure without affecting plant safety. The report TR-100407 outlines the EPRI recommended methodology for the development of alternate repair limits. The database needed to support the methods described therein is provided in this report.

ABSTRACT

Feasibility of alternate repair limits (ARC) for outside diameter stress corrosion cracking (ODSCC) observed at support plate locations of alloy 600 tubes in PWR steam generators was assessed. The database required to support the alternate repair limits was developed from available data from operating plants and from ODSCC specimens fabricated in the laboratory. Non-destructive (eddy current) examination, leak rate testing, burst testing and destructive examination of the test specimens were performed. Leak rate and burst pressure data, including those of tubes pulled from operating steam generators, were correlated with bobbin coil signal amplitude. This report documents the database developed for 7/8 inch diameter (OD) tubes to support the repair limits. Feasibility burst tests have also been performed for tubes with EDM (electric discharge machining) notches in quatrefoil and eggcrate tube support designs. Eddy current inspection requirements needed to support the ARC are defined and the means to reduce uncertainties addressed.

**Steam Generator Tubing Outside Diameter Stress
Corrosion Cracking at Tube Support Plates -
Database for Alternate Repair Limits,
Volume 1: 7/8 Inch Diameter Tubing**

TABLE OF CONTENTS

- 1.0 Introduction
- 2.0 TSP Region Pulled Tube Crack Morphology
 - 2.1 Introduction and Definitions
 - 2.2 Tub Examination Discussion
 - 2.3 Plant A Corrosion Degradation
 - 2.4 Plant L Corrosion Degradation
 - 2.5 Plant D Corrosion Degradation
 - 2.6 Plant P Corrosion Degradation
 - 2.7 Plant J-1 Corrosion Degradation
 - 2.8 Plant F Corrosion Degradation
 - 2.9 Plant W Corrosion Degradation
- 3.0 Non-Destructive Examination
 - 3.1 Voltage Normalization for ARC
 - 3.2 Voltage Renormalization for Alternate Calibrations
 - 3.3 Voltage Sensitivity to Crack Morphology
 - 3.4 Sensitivity to Bobbin Coil Probe Vendor
 - 3.5 Influence of TSP Design
 - 3.6 Influence of TSP Crevice Condition
 - 3.7 Approach for NDE Uncertainties
 - 3.8 Sensitivity to Probe Wear
 - 3.9 Bobbin Coil Analyst Variability
 - 3.10 NDE Conclusions
- 4.0 Pulled Tube Data Evaluation
 - 4.1 Pulled Tube Database Summary
 - 4.2 Tensile Properties of Pulled Tubes and Model Boiler Specimens
 - 4.3 Operating Plant Leakage Data for ODS/CC at TSPs
 - 4.4 Evaluation of Plant A Pulled Tubes
 - 4.5 Evaluation of Plant L Pulled Tubes
 - 4.6 Evaluation of Plant D Pulled Tubes
 - 4.7 Evaluation of Plant P Pulled Tubes
 - 4.8 Evaluation of Plant J-1 Pulled Tubes
 - 4.9 Evaluation of Plant F Pulled Tubes
 - 4.10 Summary of Pulled Tube Results

- 5.0 Laboratory Specimen Preparation and Testing
 - 5.1 Model Boiler Specimens
 - 5.2 Doped Steam Specimens
 - 5.3 Fatigue Precracked Specimens
 - 5.4 Chemically Dented Tubes
 - 5.5 Crack Morphologies
 - 5.6 Nondestructive Examination (NDE) Results
 - 5.7 Leak and Burst Test Objectives
 - 5.8 Leak Test Procedure
 - 5.9 Leak Test Results
 - 5.10 Burst Test Pressure
 - 5.11 Burst Test Results
 - 5.12 Destructive Examination of Laboratory Specimens
 - 5.13 Comparison with Pulled Tube Crack Morphology
 - 5.14 Review of Model Boiler Data for Acceptability
 - 5.15 Model Boiler Database Summary

- 6.0 Burst Pressure Correlations
 - 6.1 Introduction
 - 6.2 Database for Burst Pressure Correlation
 - 6.3 Burst Pressure vs. Voltage Correlation

- 7.0 SLB Leak Rate Correlation
 - 7.1 Introduction
 - 7.2 Database for SLB Leak Rate Correlation (7/8 Inch Tubing)
 - 7.3 Leak Rate Threshold Assessment
 - 7.4 Probability of SLB Leakage Versus Bobbin Voltage
 - 7.5 General Trends for SLB Leak Rate Correlation
 - 7.6 SLB Leak Rate Versus Voltage Correlation

Appendix A Destructive Examination Results for 7/8" Model Boiler Specimens

Appendix B Leak Rate Adjustments for 7/8" Tubing

Appendix C Crack Morphologies for ARC Applications

Appendix D Regression Analysis

1.0 Introduction

This report updates and revises the Revision 0 report describing the development of the database and correlations supporting the technical bases for alternate repair criteria (ARC) for outside diameter stress corrosion cracking (ODSCC) at tube support plates (TSPs) in PWR steam generators (SGs). Volume 1, this report, is directed toward 7/8 inch diameter (OD) tubing, while the Volume 2 report is directed toward 3/4 inch diameter specimens. This Revision 1 to Volume 1 of this report replaces the May 1992 version of the report in its entirety.

The database is derived from: 1) testing of laboratory induced ODSCC specimens, 2) examination of pulled tubes from operating SGs, 3) laboratory tests and evaluations to assess and refine bobbin coil voltage measurements and 4) field experience for operating leakage due to indications at TSPs. Specimen fabrication and testing was performed to develop the database required to support the ARC. The development activities were focused on a bobbin coil voltage based repair limit which integrates eddy current (EC) inspection results with tube integrity requirements. The ARC focus on directly relating bobbin coil voltage to the burst strength of tubes and the potential for tube leakage under normal operating and steam line break (SLB) pressure differentials as the applicable measures for tube integrity.

Regulatory Guide 1.121 (RG 1.121), which defines the NRC guidelines for the maintenance of SG tube integrity, specifies acceptance guidelines to be satisfied to minimize the potential for a tube rupture. Utilizing correlations of bobbin coil voltage with burst pressure, the repair limits can be developed to provide margins against tube burst such that the RG 1.121 burst strength requirements are satisfied. Leak rates under accident conditions, such as a postulated SLB event, can be maintained within acceptable values by limiting the number of tubes left in service which could potentially leak during an SLB event and projecting the end of cycle leak rate for these tubes. A correlation of SLB leak rate with bobbin coil voltage can be used for these analyses. ARC based upon relating eddy current (EC) measurements to the burst strength and the potential for tube leakage are appropriate criteria for demonstrating satisfaction of regulatory requirements for ODSCC within TSPs. This report emphasizes the development of the data base and NDE techniques to support burst pressure and leak rate correlations with bobbin coil voltage. Example correlations are developed based on the data given in this report.

The data described in this report are from 7/8 inch nominal diameter tubing with 0.050 inch nominal wall thickness. Correlations developed using this data base are semi-empirical in that bobbin coil-voltage is correlated with burst strength and the potential for tube leakage, and as such, there is no purely theoretical basis to adjust the criteria to other tube sizes.

To develop the database needed in support of an ARC for ODSCC at TSPs and to provide the technical basis for an ARC development, the following activities have been performed as documented in this report:

- o Background review of pulled tube examinations - Section 2.

- o Non-destructive examination (NDE) of 7/8 inch diameter tubing and NDE uncertainty assessments - Section 3.
- o Review and evaluation of pulled tube data to develop the current pulled tube database supporting ARC correlations - Section 4.
- o Preparation of test specimens in a model boiler and testing (eddy current, leak rate and burst testing, and destructive examination) of cracked specimens to develop a laboratory data base supplementing the pulled tube data for ARC correlations - Section 5.
- o Systematic development of the burst pressure correlation from the burst pressure database (pulled tube and model boiler specimens) and eddy current results - Section 6.
- o Systematic development of correlations for leak rates during a steam line break (SLB) and for probability of leakage during an SLB, as functions of bobbin coil voltage - Section 7.
- o Destructive examination results for 7/8" model boiler specimens - Appendix A.
- o Leak rate adjustment for 7/8" tubing - Appendix B.
- o Characterization of crack morphologies for ARC applications - Appendix C.
- o Regression analysis - Appendix D.

2.0 TSP Region Pulled Tube Crack Morphology

2.1 Introduction and Definitions

2.1.1 Introduction

The following provides summary information regarding OD originated corrosion at support plate crevice regions of alloy 600 tubing pulled from steam generators.

The type of intergranular corrosion with regard to crack morphology and density (number, length, depth) of cracks can influence the structural integrity of the tube and the eddy current response of the indications. To support the tube repair limits, the emphasis for destructive examination is placed upon characterizing the morphology (SCC, IGA involvement), the number of cracks, and characterization of the largest crack networks with regard to length, depth and remaining ligaments between cracks. These crack details support interpretation of structural parameters such as leak rates and burst pressure, crack length and depth, and of eddy current parameters such as measured voltage with the goal of improving structural and eddy current evaluations of tube degradation. In selective cases, such as the 1990 Plant A-2¹ pulled tubes, the pulled tube evaluations included leak rate measurements, in addition to the more standard burst pressure measurements, for further support of the integrity and tube repair limit evaluations.

2.1.2 Definitions

Before the support plate region corrosion degradation can be adequately described, some key corrosion morphology terms need to be defined. Intergranular corrosion morphology can vary from IGA to SCC to combinations of the two. IGA (Intergranular Attack) is defined as a three dimensional corrosion degradation which occurs along grain boundaries. The radial dimension has a relatively constant value when viewed from different axial and circumferential coordinates. IGA can occur in isolated patches or as extensive networks which may encompass the entire circumferential dimension within the concentrating crevice. Figure 2-1 provides a sketch of these IGA morphologies. As defined in this report, the width of the corrosion should be equal to or greater than the depth of the corrosion for the degradation to be classified as IGA. The growth of IGA is relatively stress independent. IGSCC (Intergranular Stress Corrosion Cracking) is defined as a two-dimensional corrosion degradation of grain boundaries that is strongly stress dependent. IGSCC is typically observed in the axial-radial plane in steam generator tubing, but can occur in the circumferential-radial plane or in combinations of the two planes. The IGSCC can occur as a single two dimensional crack, or it can occur with branches coming off the main plane. Figure 2-2 provides a sketch of these IGSCC morphologies. Both of the IGSCC variations can occur with minor to major components of IGA. The IGA component can occur simply as an IGA base with SCC protruding through the IGA base or the SCC plane may have a semi-three

¹ Actual plant names are on file at EPRI.

dimensional characteristic. Figure 2-3 provides a sketch of some of the morphologies possible with combinations of IGSCC and IGA. When IGSCC and IGA are both present at a given location, tube wall penetration of IGSCC extends deeper than the IGA and provides the leak path.

To provide a semi-quantitative way of characterizing the amount of IGA associated with a given crack, the depth of the crack is divided by the width of the IGA as measured at the mid-depth of the crack, creating a ratio D/W . Three D/W categories were defined: minor (D/W greater than 1); moderate (D/W between 1 and 2); and significant (D/W less than 1) where for a given crack with a D/W of 1 or less, the morphology is that of patch IGA.

The density of cracking can vary from one single large crack (usually a macrocrack composed of many microcracks which nucleated along a line that has only a very small width and which then grew together by intergranular corrosion) to hundreds of very short microcracks that may have partially linked together to form dozens of larger macrocracks. Note that in cases where a very high density of cracks are present (usually axial cracks) and where these cracks also have significant IGA components, then the outer surface of the tube (crack origin surface) can form regions with effective three dimensional IGA. Axial deformations of the tube may then cause circumferential openings on the outer surface of the tube within the three dimensional network of IGA; these networks are sometimes mistakenly referred to as circumferential cracks. The axial cracks, however, will still be the deeper and the dominant degradation, as compared to IGA.

Recognizing all of the gradations between IGA and IGSCC can be difficult. In addition to observing patch IGA, cellular IGA/SCC has been recognized. In cellular IGA/SCC, the cell walls have IGSCC to IGA characteristics while the interiors of the cells have nondegraded metal. The cells are usually equiaxial and are typically 0.1 to 0.2 in diameter. The cell walls (with intergranular corrosion) are typically 0.001 to 0.002 thick. The thickness and shape of the cell walls do not change substantially with radial depth. Visual examinations or limited combinations of axial and transverse metallography will not readily distinguish cellular IGA/SCC from extensive and closely spaced axial IGSCC with circumferential ledges linking axial microcracks, especially if moderate to significant IGA components exist in association with the cracking. Radial metallography is required to definitively recognize cellular IGA/SCC. Cellular IGA/SCC can cover relatively large regions of a support plate crevice (a large fraction of a tube quadrant within the crevice region).

A given support plate region can have intergranular corrosion that ranges from IGA through individual IGSCC without IGA components.

2.2 Tube Examination Discussion

2.2.1 NDE Characterization

Following tube removal, tube specimens were subjected to laboratory bobbin, RPC and sometimes UT inspection. In most cases, the post-pull bobbin coil voltages are higher than pre-pull voltages due to tearing of ligaments in the tube pulling operations. Pre-pull voltages are used for ARC applications. For the pulled tube results used in ARC applications, the bobbin coil and RPC inspection results as well as leak and burst test results are presented and evaluated for ARC applications in Section 4.

2.2.2 Leak Rate Testing

Following NDE characterization, some specimens were leak tested. Leak tests (performed by Westinghouse) were typically performed in two parts. The specimens were first tested under simulated normal operating conditions; with a primary to secondary pressure differential of . This pressure differential is slightly higher than the normal operating plant conditions of about . The primary side of the specimen was connected by insulated pressure tubing to an autoclave maintained at a pressure of by bottled nitrogen. The specimen was located in an autoclave maintained at and a pressure of . The pressure in the second autoclave was maintained by a back pressure regulator (BPR). Any water vapor passing through the BPR was then passed through cooling coils. The amount of condensed water was then measured as a function of time. Following the initial leak testing, a simulated steam line break (SLB) leak test was performed. For the SLB test, the primary pressure was increased to about while the secondary side was decreased to about , resulting in a nominal pressure differential of . This pressure differential is also conservative, since the reactor coolant pressure will be limited to the pressurizer safety valve setting of . Specific test conditions for a given indication may vary from these primary and secondary pressures. For ARC applications, the measured leak rates are adjusted to reference conditions using a leak rate adjustment procedure as described in Appendix B.

2.2.3 Burst Testing

Room temperature burst tests were performed following leak testing. Specimens were pressurized with water at a pressurization rate of approximately . Tygon tubing internal bladders were inserted into the specimens to permit testing in specimens with through wall cracks. No support plate restraint was provided. This setup provides exceptionally conservative results, since previous testing has shown that throughwall EDM slots, long do not burst inside of the crevice when the support plate restraint is provided. In most cases, tubing tensile properties are measured from a section of each pulled tube and the burst pressures used in correlations are normalized to a common flow stress.

2.3 Plant A Corrosion Degradation

2.3.1 Plant A, Unit 2 1990 Tube Pull Results at TSP Locations

Hot leg tubes R4-C73 and R21-C22 were pulled from Steam Generator B and hot leg tube R38-C46 was pulled from Steam Generator C. The sections pulled included the first support plate region from each tube. Laboratory NDE, leak and burst testing, and destructive examinations were performed. The following summarizes the data obtained at the first support plate region of each tube.

NDE Testing

Laboratory bobbin probe examination of tubes R4-C73 and R21-C22 was performed using two diameter bobbin probes. One was a brand new Echoram probe with very stiff spacers (it was difficult to insert the probe into the tube). The other was a slightly used (in terms of length of tubing previously examined) SFRM Zetec probe in which the spacers were less stiff (probe insertion into the tubes was easy). An indication was observed within both support plate crevice locations. Depth estimates were similar for both of the support plate crevice regions and for both of the probes. A range of deep covered all depth estimates. The voltage varied noticeably depending on the probe used, lateral pressures applied to the probe cables, and the orientation of the specimen, with the stiffer Echoram probe producing the smaller voltage variation. Later tests on model boiler specimens showed less variability between probes with the tubes vertical or horizontal. For tube R4-C73, the Echoram probe voltage variation ranged from volts. For tube R21-C22, the Echoram probe voltage variation ranged from volts.

While tube R38-C46 was reduced in diameter during the tube pull, the Zetec diameter bobbin probe could still be used for the laboratory examination. However, it passed through the deformed tube with difficulty. Consequently, the estimates of depth and voltage are not judged to be reliable. The field bobbin test produced a volt signal with an indicated depth of . This is considered more reliable than the laboratory result of volts and depth. Since the tube pull opened crack networks which were readily visible, the larger laboratory voltage is not surprising.

RPC results showed a main axial indication within the support plate crevice region of tube R4-C73. The length of the signal was and the depth was estimated as of tube wall based on an ASME drilled hole standard. In addition to the main signal, a less intense RPC signal was observed parallel to the main axial signal approximately away. Tube R21-C22 produced a single axial indication within its first support plate crevice region. The long RPC signal was estimated to be deep. Tube R38-C46 had a deep RPC signal that was long. Note that this tube was elongated during the tube pull. As a consequence of the reduced diameter, a diameter RPC probe was used.

Leak and Burst Testing

Following NDE characterization, the three tube sections from the first support plate region were leak and burst tested. Leak and burst test data are summarized in Section 4. Results from the SLB test are considered reliable. The measured SLB leak rates were for tube R4-C73, for tube R21-C22 and no leakage for tube R38-C46. These values are considerably below the maximum leak rate capability of the system, estimated to be approximately based on a test with the test specimen removed. Results for the normal operating conditions are considered to be less accurate. The observed leak rate for tube R4-C73 was . It was for tube R21-C22. No leakage was observed for tube R38-C46. These rates include any overflows from the back pressure regulator (BPR). Leakage through the BPR was encountered, especially with the testing of tube R21-C22. The BPR may have contributed to the entire amount of leakage observed² for the normal operating condition test. While this amount of overflow from the BPR is small in comparison to the SLB test leak rates, it is very large in comparison to potential leak rates from the normal operating conditions test. Consequently, the normal operating condition leak rate at the lower end of potential leak rates for these specimens should be considered zero. The upper value presented, at least for tube R21-C22, probably includes significant contributions from the BPR.

Room temperature burst tests were performed on the two specimens following leak testing. The first support plate region of tube R4-C73 burst at , the first support plate region of tube R21-C22 burst at , and the first support plate region of tube R38-C46 burst at

Characterization of the Corrosion Cracks

Figure 2-4 shows a sketch of the SEM fractographic observations on the burst fracture face of the first support plate region of tube R4-C73. Within the center of the burst opening, a long OD origin macrocrack was observed. The macrocrack was located at an orientation³ of and was entirely confined to within the support plate crevice region. It had only intergranular corrosion features. The macrocrack was composed of four microcracks, all of which had joined together by intergranular corrosion. The crack was through-wall for . A parallel axial macrocrack was observed near . It was

²Prior to initiation of the leak tests, the specimen fittings were tested to verify that they were leak tight. The fittings were tested by pressurizing the specimens with air and holding the specimens and their fittings under water. No fitting leaks were observed. The R4-C73 specimen was observed to leak air bubbles at the location of the support plate at a pressure of air. The R21-C22 specimen did not leak air bubbles at a pressure of . Consequently, it is believed reasonable that the normal operating leak rate for tube R21-C22 should be lower than that for tube R4-C73. This would also be consistent with the SLB leak results.

³As per the orientation system used in this report to describe tube examinations, 0° faces the steam generator divider plate and 90° is clockwise of 0° when looking in the primary flow direction (up for hot leg).

long and up to through-wall. In addition, numerous short axial cracks were observed at various locations within the crevice region. The depth of these short cracks ranged from minor penetrations to Figure 2-4 also provides a sketch estimating the crack distribution within the support plate crevice region as well as a description of the crack morphology of the main macrocrack. Figure 2-5 provides a sketch of the crack distribution and depth within the center of the support plate crevice region as determined by metallography. The main crack morphology was that of SCC with moderate IGA components ($D/W =$). The width of IGA surrounding the SCC is estimated to be approximately inch, except at the OD surface where the width was larger.

Other cracks tended to have less IGA components. Figure 2-6 provides micrographs showing both the main crack morphology as well as the crack morphology of one of the lesser cracks. The morphology of the latter crack, which has been opened wide by tube deformation, is more that of IGSCC ($D/W =$).

Figure 2-7 shows a sketch of the SEM fractographic observations on the burst fracture face of the first support plate region of tube R21-C22. Within the center of the burst opening, a inch long OD origin macrocrack was observed. The macrocrack was located at an orientation of and was entirely confined to within the support plate crevice region. The corrosion crack had only intergranular features. The macrocrack was composed of four microcracks. Three of the microcracks were joined by intergranular corrosion, while the top most microcrack was still separated from the others by metal. The macrocrack was through-wall for approximately inch. Figure 2-7 also provides a description of the crack morphology. The crack morphology was that of SCC with significant IGA components. The width of IGA surrounding the SCC is estimated to be approximately inch ($D/W =$). This tube had been plugged 4 years prior to the tube pull which may have contributed to the greater IGA width at the crack face and higher bobbin voltage than found for R4-C73. One additional crack was later observed on the specimen by metallographic examination. Figure 2-8 provides a sketch of the crack distribution and depth observed by metallography. Figure 2-9 provides micrographs of the cracks. As can be observed, the secondary crack morphology had lesser IGA components ($D/W =$).

Figure 2-10 shows a sketch of the SEM fractographic observations on the burst fracture face of the first support plate region of tube R38-C46. A inch long, OD origin, axial macrocrack was observed. The intergranular crack was up to through-wall and was contained within the support plate crevice region. The macrocrack was composed of numerous microcracks which had an unusual spatial distribution. They had orientations which ranged from axial to circumferential generating a spider-like crack distribution. It is believed that this network had a cellular IGA/SCC morphology. Three other crevice locations had less deep but significant intergranular crack distributions. Their locations are also shown in figure 2-10. Figure 2-11 shows the crack distribution and depth as determined by transverse metallographic examinations. Figure 2-12 shows photomicrographs of cracks in transverse sections obtained from within the crevice region. The cracks are opened wide by tube deformation. The morphology of the cracks is that of IGSCC with minor to moderate IGA components ($D/W =$).

2.3.2 Plant A, Unit-1 1992 Tube Pull Results at TSP Locations

Segments of tubes on the hot leg side were removed from tubes R14-C80, steam generator B, and R19-C41 steam generator A in late 1992. A total of three TSP intersections were removed. TSP intersections of these tubes had large () volt) voltage indications; R14-C80 at the second TSP and R19-C41 at the first TSP. The first TSP region of R14-C80 was called NDD. Following a similar methodology as previous tube exams, these tubes were subjected to eddy current characterization, leak and burst testing, and destructive metallographic examination.

NDE Testing

Eddy current data regarding these two tubes is summarized in Section 4. Field bobbin voltages were and volts for tubes R14-C80 and R19-C41, respectively. RPC volumetric characteristics were observed over approximately degrees on tube R19-C41 congruently with substantial axial indications (inch). Figures 2-13(a and b) and 2-14(a and b) show the pre-pull and post-pull RPC traces for tubes R14-C80 and R19-C41, respectively. The volumetric character of the R19-C41 indication is seen on both the pre and post-pull data. The post-pull indications for R14-C80 are more clearly defined than the pre-pull indications. However, the RPC voltages are essentially unaffected by the tube pulling operations.

Radiography did not identify indications, suggesting that the cracks were tight. UT inspection was able to resolve more axial indications than did the eddy current (RPC). Laboratory UT also suggested the presence of intermittent circumferential indications within the TSP crevice region. The intermittent circumferential indications may have been slightly opened by the tube pull process, based on previous UT inspections.

Leak and Burst Testing

The second TSP intersection of R14-C80 and the first intersection of R19-C41 were leak and burst tested. Neither developed leaks at either normal operating or accident (main steam line break) conditions. Room temperature burst test results indicate burst pressures of psi and psi. The methodology of leak and burst testing was consistent with that described in Section 2.2.1.

The burst openings occurred in axial macrocracks that were composed of numerous axially oriented intergranular microcracks of OD origin. The burst fracture microcracks of the second TSP region of R14-C80 were confined to a narrow axial band, whereas the burst fracture face of R19-C41 occurred in a patch of microcracks within the crevice region. The corrosion macrocracks for the burst openings were on average deep over inch length and deep on average over inch. Maximum depths were , for R14-C80 and R19-C41, respectively.

Characterization of Corrosion Cracks

Destructive examination results indicate that the Plant A-1 indications are entirely consistent with the existing ARC data base, both in the type of degradation observed and the NDE data associated with this degradation. The dominant corrosion mechanism was OD initiated IGSCC and all significant corrosion was confined to the crevice regions although R19-C41 had shallow, intermittent indications just above the TSP. In the case of the first TSP region of R19-C41, there was established intergranular cellular corrosion (ICC) found in association with the axial IGSCC. With an ICC morphology, a complex mixture of short axial, circumferential and oblique angled cracks interact to form cell-like structures. The ICC occurred in a large patch, approximately inch wide by inch high, with two smaller patches above this large patch. The IGSCC was deeper than the associated ICC. Only a very minor amount of ICC was found in association with the axial IGSCC detected in the second TSP region of R14-C80. Figures 2-15 and 2-16 show sketches of the OD crack distributions for these indications. Radial metallography was performed at a cellular patch of R19-C41. Figure 2-17 shows the cellular pattern obtained at a depth of about throughwall. With progressive radial grinding, the axial IGSCC was deeper than the associated ICC with the ICC disappearing at depths of

The density of axial IGSCC ranged from crack in for the second TSP region of R14-C80 to cracks in for the first TSP region of R19-C41. These are considered moderate crack densities. Higher crack densities are observed in the ICC patch regions. cracks in were counted in the main ICC patch in R19-C41. The measured D/W ratios ranged from in the second TSP region of R14-C80 to in the first TSP region of R19-C41. The individual microcracks within the ICC appeared indistinguishable from the individual microcracks within the axial IGSCC with respect to crack morphology. No surface IGA was observed at any location in either specimen.

Of interest is the detection of the ICC by the field RPC, relatively large bobbin voltages compared to the remainder of the pulled tube data base and rather high burst pressures. The influence of the ICC in tube R19-C41 on the burst capability of the intersection is negligible. This intersection burst at psi, and lies above the mean regression of the burst correlation.

2.3.3 Prior Pulled Tube Examinations from Plant A at TSP Locations

Prior to 1990, a total of 10 hot leg support plate intersection locations on steam generator tubing removed from Plant A-2 were examined. Of these support plate locations, were found to have OD origin intergranular corrosion. In addition, a support plate region of a tube removed in 1989 from Plant A-1 was examined. The support plate region of this tube also had OD origin intergranular corrosion. The following describes the extent and morphology of the degradation found.

Plant A-2, 1986 Examination

The first support plate region of hot leg tube R31-C46 from Steam Generator C was destructively examined. A volt, deep eddy current signal was detected in the field bobbin probe examination using a kHz frequency mix. Renormalization to the standard used in this report yielded volts. Destructive examination found a inch long macrocrack that extended from inch above the support plate bottom edge location to inch below the top edge location. The crack averaged through-wall with a local area penetrating through-wall for a length of inch. The macrocrack was composed of a number (at least) of axially orientated microcracks which had grown together by corrosion. The intergranular cracking was of OD origin and a number of shallow cracks existed parallel and nearby to the major macrocrack. The morphology of the cracking was predominately SCC, but moderate IGA components ($D/W =$) were also present. Figure 2-18 shows a sketch of SEM fractographic results of the main crack (only the mid to upper portion of the crack was examined). Figure 2-19 shows a sketch of the overall crack distribution and depth as viewed by metallography as well as a transverse micrograph showing the crack morphology. In addition to the main crack (which included a deep axial crack next to the main crack), smaller axial cracks were observed at other circumferential positions on the half-circumferential section examined.

Plant A-2, 1989 Examination

Two hot leg steam generator tubes from Plant A-2, Steam Generator C were examined to determine the origin of residual eddy current signals at support plate locations. The destructive examination included the crevice region at support plates 1-3 of tubes R16-C50 and R16-C53.

All six support plate intersections had residual type eddy current signals. The second support plate region of both tubes was chosen for more detailed examination. Following removal of both ID and OD deposits by honing, abrasion, and later by chemical cleaning, the eddy current examination was repeated. No significant change was observed in the eddy current signals indicating that the residuals were not related to surface deposits.

Destructive examination of tube R16-C50 found OD origin intergranular corrosion within the first and second support plate regions. No measurable corrosion degradation was found within the third support plate crevice region. The first support plate region had only an isolated region of minor OD origin, intergranular, axial SCC. The maximum depth of SCC was inch. The second support plate region from tube R16-C50 had experienced some negligible (no wall thickness change measurable) OD general corrosion with some intergranular penetrations. While most of the tube OD cracking within the TSP crevice regions had these features, at one location the intergranular corrosion was somewhat deeper though still regarded as minor. At this location, inch below the support plate top edge, the penetrations formed two short parallel axial cracks, inch long and up to inch deep. Consequently, all three support plate regions of tube R16-C50 had no degradation, or

only very minor IGSCC degradation. Bobbin voltages based on re-evaluation of the field data to ARC guidelines indicated small flaw voltages ranging from _____ volt.

Destructive examination of tube R16-C53 found OD origin intergranular corrosion within all three support plate regions. The first support plate region of tube R16-C53 had numerous OD origin, intergranular, axial stress corrosion cracks, but the depth of cracking was shallow (_____ inch maximum depth). At the second support plate of tube R16-C53, axial intergranular stress corrosion cracking was found on the tube OD concentrated near the support plate top edge and to a lesser extent near the support plate bottom edge. There were dozens of very tight stress corrosion cracks located discontinuously around the circumference, but located within all four quadrants of the tube. The maximum depth of penetration was _____. The third support plate region also had numerous but relatively shallow OD origin, intergranular, axial SCC. The maximum depth of degradation was _____ inch. Consequently, the only support plate region of tube R16-C53 with corrosion degradation of any potentially noticeable (not detectable by re-evaluation of the field data) depth was the second support plate region where the maximum depth was _____ inch (_____ through-wall). The morphology of these cracks ranged from that of IGSCC (Figure 2-20) to that of IGSCC with significant IGA components (Figure 2-21).

In summary, the 1989 pulled tubes were removed primarily to determine the cause of eddy current support plate residual signals. Laboratory eddy current testing showed that the residual eddy current signals were not caused by surface deposits. Destructive examination also showed that the residual signals were not caused by corrosion degradation, even though minor OD origin SCC was present at _____ support plate locations. Small flaw bobbin voltages could be detected for R16-C50 but not for R16-C53. For tube R16-C50 the deepest support plate region SCC was _____ inch while for tube R16-C53 the deepest crack was _____ inch. For the other support plate locations with cracks, the deepest cracks were _____ inch.

Plant A-1, 1989 Pulled Tube Examination

The first support plate crevice region of hot leg tube R20-C26 from Steam Generator C of Plant A-1 was destructively examined. Dozens of short, OD origin, intergranular, axial stress corrosion cracks existed within the crevice region and just above the crevice region. Most of these cracks were found within _____ wide axial bands on opposite sides of the tube. The band located at _____ extended from the support plate bottom edge to just above the support plate top edge. The deepest crack in this band penetrated _____ through-wall and was located approximately _____ inch below the top edge. The second band occurred between _____ and _____ with the cracking extending from the bottom edge to approximately _____ inch above the support plate top edge. Within the crevice region, the deepest crack in the second band of cracks occurred near the support plate top edge. This crack was _____ through-wall. Above the top edge, the depth of cracking decreased rapidly. At _____ inch above the top edge, the deepest crack was _____ through-wall. With respect to the length of individual cracks, they were typically much less than _____ inch long. Where individual cracks had grown together, cracks up to _____ inch long were found. Figure 2-22 sketches the crack distribution

2-23 provides a photomicrograph of typical cracks as observed in transverse metallographic sections that have been deformed to open cracks. The morphology is that of IGSCC with minor to moderate IGA components (D/W =). Figure 2-24 shows similar transverse micrographs, but ones in which not all cracks were opened during the tube deformation.

Field eddy current inspection (bobbin probe) of the first support plate region revealed (by initial interpretation) no corrosion degradation. Later analysis suggested a very low voltage (volts) indication signal, partially hidden between larger voltage dent signals. Laboratory bobbin probe inspection produced similar results, with an indication voltage of volts within the overall volt dent signal. The phase angle of the indication component, within the overall dent signal, suggested a deep indication. RPC testing revealed many indications confined to within the crevice region. This pulled tube, with a difficult to detect indication of depth and individual crack lengths inch, was instrumental in initiating the ARC activities of this report. In this case, the objectives of the ARC program (successfully achieved) was to demonstrate that indications at TSPs that are difficult to detect are not a concern relative to structural integrity of the tube.

2.4 Plant L Corrosion Degradation

A total of tubes and TSP intersections were removed from steam generators C and D of Plant L in 1991. The Plant L pulled tube data base represents the largest single source of pulled tube data directly applicable to the 7/8 inch tubing database. Destructive examination for the majority of the Plant L tubes was performed by ABB Combustion-Engineering, while limited laboratory work was performed by Westinghouse on six burst crack samples.

The pulled tubes from Plant L are; R12-C8, R29-C70, R30-C64, R16-C74, R20-C66, R8-C66, R8-C69, and R12-C70. All pulled tubes included the first, second and third TSP regions.

intersections were destructively examined and intersections were burst tested. All TSP intersections destructively examined were tested for leaks at normal operating and SLB pressure differentials by pressurization of the tubes with water at room temperature during the burst test sequence. No samples experienced leakage during these tests. This includes two intersections with relatively large bobbin voltages, and volts, by re-evaluation (field voltages were and volts, respectively).

All of the Plant L pulled tubes with the exception of R12-C8 were active up to the time they were removed from the steam generator. Tube R12-C8 had been plugged in 1989, and pulled in 1991. The corrosion morphology of this tube, in particular the first TSP intersection, is uniquely different from the remainder of the domestic steam generator pulled tube data base.

NDE Results

Re-evaluation of the field bobbin data for the Plant L produced indication voltages ranging from to volts. The re-evaluation was considered necessary since the field data was collected using a different calibration setup as compared to the ARC guidelines and changes in the plant eddy current analysis guidelines occurred during the plant outage. Throughwall

depth estimates by bobbin ranged from [redacted] volt indications (third TSP region of R29-C70, third TSP region of R8-C66, and third TSP region of R30-C64, respectively) to [redacted] throughwall for an indication of [redacted] volts. Of the [redacted] intersections destructively examined, [redacted] had depth estimates greater than [redacted], and [redacted] were or greater. RPC voltages could be applied to [redacted] destructively examined intersections. A complete listing of the eddy current data is furnished in Section 4. A description of the eddy current data evaluation is included as Appendix A to Volume 1, Revision 0 of this report but is not repeated in this revision to Volume 1.

Leak and Burst Test Results

As previously stated, no specimens leaked during the leak tests. Burst pressures ranged from [redacted] psi (first TSP region of R8-C69, [redacted] volts) to [redacted] psi (third TSP region of R12-C8, [redacted] volts). The low burst pressure of [redacted] psi represents an outlier to the data based on its recorded voltage. In general, four of the Plant L indications lie in the lower portion of the mean regression for the burst correlation; the burst pressures are consistent with the crack lengths and depths but not consistent with the low recorded voltages. One postulated reason has been the large number of noncorroded ligaments remaining between microcracks permitted good signal conductivity throughout the intersection, thereby lowering the voltage.

Destructive Examination Results

Corrosion Degradation of Plant L Tube R12-C8, S/G D

Extensive OD origin intergranular corrosion was found within the first TSP region of this tube. Very high densities of axially oriented IGSCC microcracks were observed, and all corrosion was confined within the TSP region. The microcracks at the first TSP had significant amounts of IGA associated with them. A description of the microcracks would be that of IGA fingers, with the depth of the cracks typically being [redacted] times longer than the width of the IGA associated with the crack. The microcracks were less than [redacted] inch in axial extent. As stated previously, crack density was high, estimated to be possibly [redacted]. This crack density was higher than any previously observed in the destructive examination of tubes from domestic units. Because of the high crack density and IGA associated with the crack, local regions sometimes formed patches of IGA. The depth of these IGA patches was no more than [redacted] of the depth of crack penetration through the IGA patch. The largest circumferential length of continuous IGA observed was [redacted] inch, or approximately [redacted] degrees with a depth of [redacted]. The maximum depth of IGSCC in the same area was [redacted] as shown in the micrograph of Figure 2-25. Larger axial macrocrack networks were also formed from the high density axial microcracks.

The first TSP region of R12-C8 was initially separated circumferentially near the center of the crevice region by applying a tensile force axially to the tube. The fracture would have occurred where the volumetric corrosion degradation was deepest. SEM fractography of the separation showed intergranular corrosion greater than [redacted] deep over [redacted] degrees of the circumference. It is believed that the corrosion front was composed of a large number of

axially oriented cracks that frequently had interconnecting IGA components. The deepest region of corrosion was deep, via IGSCC, over approximately degrees of the circumference. Above this local region with the deepest corrosion, the tubing was deformed to open any axial crack networks. Many were revealed. One of the deeper looking ones was broken apart and SEM fractography performed. A fairly uniform crack front was observed from the support plate crevice center to the support plate crevice top. The front ranged from throughwall, with an average depth of . Several ledges were observed in the fractograph where it is believed that individual, axially oriented, microcracks had joined together to form the macrocrack. Below the support plate center, only metallography was performed. Transverse metallography revealed the morphology of the axial cracking and IGA as shown in Figure 2-26. From the fractography and metallography data, it is concluded that axial macrocrack networks existed from the bottom edge of the support plate crevice region to the top edge, with the crack front having a fairly uniform depth. It is currently believed that the appearance of significant IGA in this intersection is a resultant of the tube's removal from service and continued exposure to possibly caustic secondary side conditions.

In direct contrast with the first TSP region of R12-C8, the second TSP region had a crack density of approximately , and morphology of the penetrations was that of narrow IGA fingers. The maximum depth of cracking observed was , while the associated patch IGA penetration was reported by ABB to be throughwall.

The third TSP region yielded results very similar to the second TSP, moderate crack density and minimal IGA involvement. The maximum depth of cracking was listed as throughwall, with the ABB listed patch IGA depth of . Patch IGA was identified at seven locations around the circumference at the mid-support plate region that were very small in circumferential extent. The third TSP region of this tube was burst tested, and burst occurred at psi.

Corrosion Degradation of Plant L Tubes R29-C70, R30-C64, R16-C74, R20-C26, R8-C66, R8-C69 and R12-C70

The remaining pulled tubes differ from R12-C8 in crack densities and evidence of patch IGA type degradation. Crack densities were listed as either low or moderate, and only minor IGA evidence was detected. The IGA extent was limited to the surface, and never penetrated more than a few grains into the tube wall. Only tube R16-C74 produced a morphology other than axially oriented IGSCC. The first TSP region of this tube had what appeared to be cellular IGA/SCC, up to about deep. This indication was one of the first indications examined by radial metallography to characterize cellular corrosion. Figures 2- and 2- show the cellular pattern including grind depths of mils. It is seen that the cellular pattern becomes dominantly axial at the mil grind depth.

Tube R29-C70 had low crack density, and relatively high burst pressure, psi, psi, and, psi. Fractography of the burst faces showed IGSCC macrocracks that were inch in length. The microcracks were separated by ligaments with dimple rupture features, suggesting that the ligaments tore during burst testing. The

maximum depth of IGSCC was _____, respectively, for the first, second, and third TSP regions.

Destructive examination of Tube R30-C64 indicated similar corrosion morphology at the first, second and third intersections. The morphology was dominated by axially oriented IGSCC with only minor to moderate IGA components, without the presence of affective surface IGA (minor surface IGA, _____ grains deep was occasionally present). Crack densities were moderate, _____ for the three intersections. Axial burst openings were produced by the burst test, and the burst pressures ranged from _____ psi to _____ psi. The IGSCC macrocracks were all confined within the plates, and burst faces measured were _____ inch long. The maximum depth of IGSCC observed was _____, respectively.

The remaining intersections all appeared to have similar morphologies; dominant IGSCC with minor to moderate cellular corrosion IGA, with occasionally appearing insignificant (_____ grains deep) surface IGA. The first support plate region of R16-C74 differed only slightly from the remaining intersections in that cellular IGA/SCC was more visible and confirmed by radial metallography. Still though, the dominant mechanism detected was axially oriented IGSCC. Fractography of the burst opening indicated numerous axially oriented, OD origin, intergranular microcracks, up to _____ deep. The depth of penetration of the cellular corrosion was less than the dominating IGSCC. The main macrocrack was _____ inch long and averaged _____ deep. The burst pressure of this intersection was _____ psi.

Summary of Plant L Degradation

All three support plate regions of Plant L plugged tube R12-C8 had multiple axial IGSCC macrocrack networks from the bottom to the top edge of the crevice. The first support plate region had the deepest cracking, _____ maximum throughwall. Maximum crack depths were _____ throughwall at the second and third TSP regions, respectively. In addition, effective IGA patches were observed. In the case of the first support plate crevice locations, the IGA patches occurred in regions with the highest crack densities. The depths of the IGA patches were typically half that of the associated axial cracking. For the second and third TSP regions, ABB C-E reported the maximum depths of IGA to be _____. The support plate regions from the other seven pulled Plant tubes had corrosion more typical of other plants: a small to moderate number of axial IGSCC, minor to moderate IGA components to the cracking, and little or no separate IGA (patch IGA). While the IGSCC on these tubes had IGA components, the appearance was more that of stress corrosion cracking than that of IGA fingers as was observed at the first support plate region of tube R12-C8. Finally, cellular IGA/SCC was locally observed at the first support plate crevice region of tube R16-C74. Cellular IGA/SCC may have also been present, and even played a major role, in the corrosion degradation at the first support plate region of tube R12-C8. Non-confirmed cellular IGA/SCC was also suspected in local areas of the crevice regions of another _____ of the total _____ crevice regions examined.

2.5 Plant D Corrosion Degradation

In 1992, tubes (intersections per tube) were pulled from Plant D-1 in direct support of ARC applications. additional tubes had been previously pulled from the hot leg region of Plant D steam generators. tubes were pulled from Plant D-1 SG-4 in 1983. The first support plate region of each tube was destructively examined. In 1984 tubes were pulled from Plant D-2, SG-1 and tubes were pulled from Plant D-2, SG-4. The first support plate region of each of these tubes was destructively examined. In 1985 tubes were pulled from Plant D-2. The first support plate regions of each tube were pulled, but only locations were destructively examined. In addition, the fourth and fifth support plate regions of two of these tubes were also pulled. Of these additional four support plate locations, three were destructively examined. Of the support plate regions destructively examined from the 1983 - 1985 tube pulls, a total of had OD origin intergranular corrosion. The following describes the extent and morphology of the degradation found at these hot leg support plate crevice regions as obtained from a review of the final tube examination reports as well as a review of the raw data obtained during the examinations. The 1985 and 1992 tube pull campaigns provided more complete support plate corrosion data since the support plate crevice regions were the principal region of interest and since burst testing of some of the degraded support plate crevice regions was also performed. Only those tube examination data considered relevant to the ARC data base are discussed below.

2.5.1 Plant D, Unit 1 1992 Tube Pull Results

Four hot leg tube segments from S/G 12 were removed, however, one of these tubes did not include TSP regions. The removed tubes used in the ARC data base are R11-C60, TSP regions 1 and 2, R18-C16, TSP regions 1 and 2, and R18-21, TSP regions 1 and 2.

NDE Results

Bobbin voltages for the TSP regions of these tubes ranged from volts. The bobbin depth predictions ranged from about deep. The second TSP region of tube R18-C21 did not exhibit a bobbin or RPC indication in the field (maximum destructive exam depth of). However, laboratory testing indicated confirmation of axial cracking. Tube R18-C16, second TSP region, had a volt bobbin indication, but did not exhibit an RPC indication (maximum destructive exam depth of throughwall). Laboratory UT generally gave the indication of multiple short axial and circumferential indications in several patches. Some specimens appeared to show signs of circumferential indications. Upon metallographic review, these indications were determined to be areas of ICC, which gave the appearance of circumferential indications when examined by RPC.

Leak and Burst Testing

The first TSP regions of R18-C16 and R18-C21 were leak tested at elevated temperature and both normal and SLB pressure differential conditions. Neither specimen indicated evidence of

leakage. The other TSP regions of each tube were leak tested at room temperature. These specimens developed axial burst openings simultaneously with the development of leakage.

Room temperature burst test results ranged from psi. All pertinent data concerning the burst test results are included in Section 4. The first TSP region of R18-C21 burst at a pressure of psi, and had the largest voltage of the specimens, volts. This tube had slightly higher than average material properties, and based upon the morphology, had an effect upon the measured burst strength. The specimen with the smallest voltage, TSP region 2 of R18-C16, had a voltage of and also had a burst pressure of psi. All burst specimens had axial burst openings. All of the burst data from these tubes lie well above the mean voltage-burst regression fit.

Destructive Examination Results

The leak and burst fracture faces were opened for fractographic examinations. The fracture faces were found to contain the deepest average crack depths. The OD origin axial intergranular macrocracks were composed of many shorter intergranular microcracks, and most of the ligaments separating the microcracks had only intergranular features, indicating that they had interconnected by corrosion prior to the burst test. The loss of ligaments, in macrocracks of the shallow depths found for these indications is unusual and results in higher than typical voltages which is the probable cause for the high outlier behavior on the voltage-burst correlation.

The depth of penetration of the observed cracking was consistent with bobbin voltages and the maximum and average depths of penetration were relatively normal. Tube R18-C21, TSP region 1 had the deepest cracking, maximum and average. The second TSP region of R18-C21, which had a NDD by bobbin field call, had a maximum depth of cracking of only . The TSP regions of these tubes had combinations of axially oriented intergranular stress corrosion cracking and intergranular cellular corrosion. This corrosion was of OD origin, and occurred in bands and patches as shown in Figure 2-29. The indications on tubes R11-C60 (Figure 2-30) and R18-C60 (Figure 2-31) show similar crack morphologies although more as isolated patches.

All specimens had either a band or up to patches of corrosion on the OD surface. All corrosion was confined to the TSP crevice region. Corrosion within the patches appeared to be predominantly composed of short axial cracks. Short cracks oriented at oblique or circumferential direction between the axial cracks were detected, producing an ICC morphology in the patch area. In addition to the patches of ICC, larger axial macrocracks composed of numerous aligned axial microcracks were detected. These microcracks appeared to exist independently of the patch ICC. These axial macrocracks were confined to narrow axial zones composed of many closely spaced axial microcracks. The axial burst openings, with the possible exception of the first TSP region of R18-C16 occurred in the band or patch corrosion areas, and not within the large axial macrocracks. Burst opening location was still controlled by the area of deepest corrosion penetration, and occurred in axial macrocracks.

The individual microcracks in the band and patch corrosion areas have an IGSCC morphology with minor to moderate IGA components associated with the IGSCC. Cracking densities ranged from moderate to high. Typical D/W ratios in the IGSCC areas ranged from [redacted] and in the areas of minor IGA, the D/W ratios ranged from [redacted].

Plant D-2, 1985 Examination

support plate regions of five tubes (R6-C40, R7-C38, R11-C25, R12-C42, and R18-C77) pulled from the hot leg region of Plant D-2 were destructively examined. Burst tests had been performed prior to the destructive examination on tube sections from four of the support plate crevice regions of R7-C38. Three of the sections were burst tested without simulated support plate collar while the fourth used a collar which caused the burst to occur away from the degraded support plate crevice region. For the three bursts that occurred in the crevice locations, SEM fractography of the burst fracture faces was performed in addition to the more normal metallography. Finally, bend tests (deformation of the tubing to open cracks for visual purposes) were performed on selected locations to assist in understanding the overall crack distribution.

[redacted] of the [redacted] support plate locations examined had intergranular corrosion, primarily as axial SCC, confined to the crevice region. Maximum depths of degradation ranged from [redacted]. The degradation was located from near the support plate bottom edge to near the top edge with the degradation being in the form of numerous axial microcracks that were frequently close together. No degradation was observed at or beyond the edges of the crevice. In some instances the microcracks had grown together by intergranular corrosion. The first support plate regions of tubes R7-C38 and R18-C77 were found to have the deepest and highest density of SCC ([redacted] or more individual cracks were found at mid-support plate circumferential planes with maximum SCC depths of [redacted] and [redacted], respectively). The SCC aspect ratios (length of the microcrack divided by its depth) from SEM fractography ranged from [redacted] with the larger ratios associated with the more shallow cracks. The aspect ratio was less than [redacted] and typically [redacted] for crack depths of [redacted] or greater. It was concluded that any individual SCC was short with a maximum length approaching [redacted] inch as the SCC became deeper. Many of the individual cracks (microcracks) were separated by structurally sound, non-corroded metal, that tore by tensile tearing during burst testing. This is schematically shown in Figure 2-32 which is typical of burst test effects on cracks with remaining noncorroded ligaments. These ligaments between cracks tended to be on the order of [redacted] mil in width for the support plate locations with the highest densities of SCC. For low crack density support plate locations, the ligaments were larger, up to [redacted] inch in width.

Tube R7-C38 had corrosion at the first, second, and third support plate locations (each of the crevice regions examined). The maximum depths were [redacted], respectively. The morphology was of axial IGSCC at all three locations with the first support plate location having the smaller D/W ratios (i.e., with the larger IGA components associated with the cracking). The first support plate region had [redacted] axial cracks uniformly distributed around the circumference at a mid-crevice location. No cracks were found at the top and bottom support

plate crevice locations. Figure 2-33 shows a photomicrograph of one of the smaller D/W ratio cracks. D/W ratios typically varied from although isolated ratios of greater than were observed. No IGA was observed at the OD surface. The second support plate crevice region had cracks at a mid-crevice region with most of the cracking located on opposite quadrants of the tube. No cracking occurred at the top and bottom crevice edges. D/W ratios were typically near and no IGA was observed at the OD surface. Figure 2-33 also provides a photomicrograph of degradation located at the second crevice region. The third support plate crevice region had axial cracks located at a mid-crevice region with most of the cracking again located on opposite quadrants of the tube. D/W ratios were typically near. Intergranular penetrations, approximately deep, were observed at isolated locations on the OD surface.

Tube R18-C77 had corrosion at the first, second, third, fourth, and fifth support plate locations. The maximum depths of corrosion were respectively. All locations had an axial IGSCC morphology although some locations (particularly the second and fourth support plate crevice regions) had isolated regions with patch IGA, usually at locations where axial cracks were particularly close together. See Figure 2-34 as an example of the patch IGA on R18-C77. The depth of the patch IGA was less than, but approaching, the depth of the penetrating axial cracking. A count of the number of cracks observed around a mid-crevice region was made at the first support plate crevice region. cracks were observed and photographs of were taken. The other four TSP regions did not have a total count performed on the original metallographic mounts; however, photomicrographs taken showed cracks, respectively, at the second, third, fourth and fifth mid-crevice locations. D/W ratios for the deeper cracks typically ranged from for the first, second, third, fourth, and fifth support plate crevice regions, respectively. Other than for the locations with IGA patches, only isolated shallow intergranular penetrations were observed on the OD surface away from the cracking.

Summary of Plant D Pulled Tube Data

The tube examination performed in 1983 on Plant D-1 steam generator tubing removed from support plate crevice locations found the beginning of intergranular stress corrosion. Most of the degradation observed was undeveloped and too shallow to form definitive conclusions regarding the corrosion morphology. The 1992 tube pull results show that the IGSCC occurring in the plant D-1 tubes is predominantly axial IGSCC, and can exist with patches of axial and short obliquely oriented cracks which tend to form a patch or cell-like structure. The burst test results indicate that maximum corrosion of throughwall in a macrocrack network with an average depth of penetration of has little effect upon the free span burst capability of a tube. The corrosion which was deep enough to influence the burst capability was readily detectable by both bobbin and RPC probes in the field.

2.6 Plant P Corrosion Degradation

Two tubes were removed from Plant P in 1991 and were examined for degradation at the tube support plate locations. This work was performed by ABB Combustion Engineering, and a summary of the reported results has been provided below.

2.5.1 Results of 1991 Tube Pull of Plant P TSP Intersections

Hot leg tubes R11-C48 and R16-C60 were pulled including the first, second, and third tube support plate intersections and the tubesheet expansion transition. Pull forces were lbs. or less during the removal of the tube sections containing the TSP intersections. Laboratory NDE, leak and burst testing, and destructive examinations were performed. The following summarizes the data obtained at each support plate region of the tubes.

NDE Testing

The field eddy current identified indications only at the first TSP on both tubes, volts on R16-C60 and volts on R11-C48, while re-evaluation of the field data to ARC guidelines also identified a volt indication at the second TSP of R16-C60. The relatively low pull forces resulted in a voltage increase from volts on R11-C48 but had no significant affect on R16-C60 voltages.

The laboratory post-pull bobbin coil indicated a very shallow indication of about volts at the second TSP of R16-C60 but the MRPC did not suggest the presence of degradation at this location. This contrasts to the field data of volt bobbin and volt RPC indications.

Ultrasonic testing was also performed of the samples. UT signals were noisy, as some of the deformation incurred during the tube removal process apparently hampered correct centering of the probe in the tube. Characterization and sizing of defects could not be done accurately. Indications were reported up to in. length and deep on R11-C48 at the first tube support plate intersection. On R16-C60, small crack-like indications in. length and and deep were reported at the first and third TSP intersections, respectively.

Radiography did not produce any observable indications.

Leak and Burst Testing

Following NDE characterization, the first and second TSP regions of tube R16-C60, and the first TSP region of R11-C48 were leak and burst tested.

Based on the relatively low bobbin voltages and low depth estimates for these intersections, respectively) leakage at normal operating or SLB pressure differentials was not anticipated. The results of the leakage testing

portion of the examination of these tubes showed this to be true. For these tubes, leak testing was performed at room temperature, as part of the pressurization during burst testing.

Burst testing was performed by sealing each end of the tube with mechanical fittings, the upper one of which was connected to 1/8 inch, high pressure tubing to permit pressurization of the sample. Some of the fittings initially leaked and were sealed by soldering. The tests were initially conducted without an internal bladder to determine at what pressure leakage occurred. If a burst was not obtained, the test was interrupted, a bladder was inserted, and the test resumed until a burst, as indicated by a "fish mouth" opening, occurred. All burst openings were axially oriented. Tube R16-C60, TSP regions one and two, burst at pressures of psi and psi, respectively.

Tube R11-C48, first TSP region, was burst tested with a carbon steel collar simulating the TSP, located around the original crevice area. The tube burst at psi outside of the collar, in an undegraded free span section of tubing. The presence of the collar showed that the burst will not occur within the crevice area when the TSP is present.

Destructive Examination Results

The burst specimens, TSP regions 1 and 2 of tube R16-C60, and TSP region 1 of tube R11-C48 were sectioned, and transverse samples cut from the upper, mid-plane and lower portion of the burst opening. Additionally, the mid-section area of each of the third TSP regions of each tube were sectioned and examined. The second TSP region of R11-C48 was partially examined, and crack penetration depths of throughwall were identified. Longitudinal sections were prepared for all six TSP intersections with the exception of TSP 2 of R11-C48.

The highest crack density, , was found near the top surface of the first TSP region of R16-C60 (Figure 2-35). Maximum depth of IGSCC penetration was and average depth of was determined for the burst crack. Many areas of IGSCC present over the entire circumference were identified. Only small patches of shallow (grains deep) IGA were observed along the tube OD. The mid-plane region of the intersection identified several areas of IGSCC, with a maximum depth of penetration of . Crack density was moderate at this location. Much lesser extents of degradation were identified at the bottom of the intersection. The burst crack length was determined to be approximately inch in length.

The top and bottom areas of TSP 2 of R16-C60 showed little and no evidence of IGSCC or corrosion in general. Corrosion crack density at mid-plane (Figure 2-36) was judged moderate (cracks). The maximum and average depths of penetration for the burst crack were and , respectively. Again, several shallow, small patches of surface IGA were identified. The burst crack length of this intersection was inch.

Only minor extents of cracking, less than deep, maximum were identified in the third TSP regions of R16-C60.

Crack density in the first TSP region of R11-C48 (Figure 2-37) was moderate, cracks, with a maximum penetration depth of . The greatest extent of IGSCC occurred at the mid-plane elevation. Presence of the steel collar prevented this intersection from bursting. Examination of the transverse specimens for this intersection indicate the IGSCC did not progress to a throughwall condition during straining due to the internal pressurization. While the outer edge of the cracks were slightly opened, no crack propagation was detected.

Summary of Plant P Degradation Morphology

The Plant P tubes were found to contain multiple axially oriented microcracks which formed larger macrocracks. Insignificant surface IGA, only a few grains deep, were detected. Degradation was confined to the TSP crevice regions, and did not extend out of the plate area. Axial burst openings occurred as a result of burst testing. Thin ligaments of non-corroded material was located between the generally short (. inch) microcracks, which provided some structural support. The IGSCC plus cellular patch corrosion morphology of the Plant P pulled tubes is consistent with the ARC data base.

2.7 Plant J-1 Corrosion Degradation

Several hot leg tube segments were removed from French Plant J-1 in 1991. Metallographic examinations of these tubes show IGSCC and patch IGA and ICC most similar to tube R12-C8 from Plant L. The crack densities were in the high range, cracks per elevation. The extent of IGA associated with individual cracks had moderate D/W ratios (), while the extent and depth of IGA is more significant than the Plant L tube R12-C8, which has been identified to contain the most extensive amounts of IGA seen in domestic units at the tube support plates. The origin of the patch IGA in Plant J-1 appears to be that of closely spaced axial IGSCC and ICC interacting near the surface to form IGA patches. French descriptions of the morphology combine ICC with IGA. The second TSP of R5-C28 was burst without TSP constraint at a burst pressure of psi, and provides a data point for ARC correlations. As shown for R5-C28, second TSP region in Figure 2-38, the OD surface of the intersection exhibits a morphology of ICC, with many axial and obliquely angled cracks interconnecting to effectively form a cellular structure. Figure 2-39 is a transverse photomicrograph of the R5-C28, second TSP region intersection which tends to show the morphology as ICC and closely spaced axial IGSCC as opposed to the more volumetric characteristics usually associated with pure IGA. Additionally, the D/W ratios are not representative of IGA, which is typically less than (significant category). Figure 2-40 shows transverse micrographs from R5-C28, second TSP region, just above (ECH 2, same as Figure 2-39) the TSP midplane and just below (ECH 5) the midplane. The darkened areas on the tube OD are classified as IGA by EdF. The terminology of this report would classify these regions as IGSCC with patches of ICC and surface IGA. Radial micrographs performed on tube R9-C22 and R4-C64 show similar corrosion patterns that classified as cellular from radial metallography of domestic pulled tubes. It was also observed that the depth of corrosion degradation in the patch IGA areas compared to IGSCC is similar to that seen in domestic units, one-third to one-half of the depth of IGSCC. In tubes with throughwall

IGSCC, the maximum depth of patch IGA was reported to range from inch deep (throughwall) to inch deep (throughwall). The circumferential extent of the cellular corrosion covered large portions of the tube OD surface, in bands that covered the entire height of the crevice area on some tubes and progressed from partially to entirely around the tube circumference. Most IGA patch areas (suspected to be the morphology referred to as intergranular cellular corrosion) were smaller in circumferential extent, normally of circumference.

2.8 Plant F Corrosion Degradation

Three cold leg tube segments were removed from tubes R13-C42, R16-C29 and R16-C42, steam generator B. The removed section from tube R16-C29 included only the first TSP location, while the other two tubes included the first and second TSP regions.

NDE Results

Except for the second TSP region of R13-C42, all TSP regions had OD origin indications of volts confined to the crevice area. Indicated bobbin depths ranged from deep (volts) to deep (also volts). The volt indication (first TSP region of R16-C29) had an indicated depth of . The RPC data and laboratory UT data exhibited considerable width, suggesting the presence of ICC or possibly IGA in association with the axial IGSCC. The UT results (laboratory) confirmed the field indications. The laboratory eddy current data is somewhat influenced by dent signals that were not present in the field data. The cause of these post-pull dent signals is attributed to tube deformation suffered during the tube pulling process. Radiography did not detect indications, suggesting that the degradation was tight and/or very shallow.

Leak and Burst Test Results

All tube sections produced axial burst openings and the burst openings were centered within the crevice regions. The UT data indicated that the circumferential position of the deepest indications were coincident with the burst locations. The burst pressures for these tubes were all exceptionally near to each other. The measured burst pressures ranged from psi to psi. Free span sections of each tube were also tested. The variance between the TSP and free span regions were a maximum of psi, or about , indicating that the existing degradation had virtually no effect upon burst capability. Tube material properties were considered normal for the distribution of Westinghouse tubing.

Since the indicated depths of penetration were so shallow, it was judged that leak testing would not provide relevant data, since these indications assuredly would not have leaked at the bounding SLB pressure differential of psi.

Destructive Examination Results

The burst openings occurred in axial macrocracks that were composed of numerous axially oriented intergranular microcracks of OD origin. The corrosion macrocracks for the burst openings were deep on the average over macrocrack lengths of inch. The maximum crack depths were deep. In the case of the first TSP region of R13-C42, the laboratory UT data indicated the crack depth to be up to , while the destructive examination results showed that the cracking was a maximum of deep. While the UT provides more detailed resolution than RPC, in the presence of ICC the UT depth prediction results can become less reliable due to the morphology. The ligaments separating the microcracks had only intergranular origin. The loss of ligaments by corrosion in macrocracks deep is very unusual and similar to the 1992 Plant D-1 tube pull results. Like Plant D-1, the Plant F burst results are high outliers on the burst pressure versus voltage correlation. For both of these plants, the voltages are unusually high for shallow indications as a consequence of loss of ligaments. All intergranular corrosion was confined to the crevice region.

All five TSP regions had narrow bands of corrosion centered within the crevice as shown in Figures 2-41 to 2-43. The bands ranged from inch high and were present almost entirely around the circumference except for the first TSP region of R13-C42, where the band was approximately degrees. Corrosion within the bands appeared to consist of many short axial cracks. Crack densities at the shallowest depths were typically cracks in degrees, while the highest density approached cracks in degrees.

From the metallographic examinations, it was concluded that the dominant OD origin corrosion morphology was axial IGSCC. In all cases there was also some ICC found in association with the axial IGSCC, but it was never the dominant mechanism. In some areas where the crack density was high, the morphology approached that of IGA. Some local, shallow IGA was also detected. With progressive grinding through the tube, it was shown that the axial IGSCC became more dominant with depth while the ICC and IGA tended to disappear more quickly.

2.9 Plant W Corrosion Degradation

Two hot leg tube segments were removed from tubes R6-C58 and R21-C64, steam generator 3, from plant W, Unit 1. The first and second TSP regions of R6-C58 and the first TSP region of R21-C64 were removed and destructively examined. Only R6-C58 had ODSCC indications and is described in this section.

These tubes were selected to obtain a range of indications observed in the 1993 field eddy current inspection.

NDE Results

The two removed TSP regions of R6-C58 had similar eddy current indications, both in the field and the lab. The indications were OD origin, confined to the TSP crevice region, and had considerable width in the field RPC data (and lab UT data), suggesting intergranular cellular corrosion (ICC), in addition to the axial cracking.

Field bobbin voltages were volts and volts, with associated depth estimates of and , for the first and second TSP regions of R6-C58, respectively. A inch SAI, was called by RPC for the first TSP region. RPC data for the second TSP was noisy, but a inch long by degree indication was identified.

X-ray data only identified a small patch of circumferential indications near the center of the first TSP crevice of R6-C58.

Leak and Burst Test Results

The first TSP segment of tube R6-C58 was leak tested at elevated temperature and pressures. No leakage was detected. Both TSP regions were burst tested and developed axial burst openings. The openings were centered within the crevice region for the first and second TSP regions of R6-C58. Burst pressures were psi and psi, for the first and second TSP regions of R6-C58.

Destructive Examination Results

The burst openings occurred in axial macrocracks composed of numerous axially oriented microcracks of OD origin for tube R6-C58. All intergranular corrosion for tube R6-C58 was confined within the TSP. The burst opening macrocrack length and maximum and average depths for this tube were; inch, maximum depth, and average depth for the first TSP region, inch, maximum depth and average depth for the second TSP region of R6-C58.

From the metallographic examination, the dominant OD origin corrosion morphology was axial IGSCC. The TSP regions of R6-C58 had significant intergranular cellular corrosion (ICC), found in association with the IGSCC, as shown in Figure 2-44. The ICC patch in the first TSP region of R6-C58 was about inch wide by inch high, while a patch in the second TSP region was inch. The axial burst opening occurred within the patches. The axial IGSCC was deeper than the associated ICC. The ICC depths ranged from about TW. The density of IGSCC was typically high in the local patch areas, about cracks in degrees. However, very few or no cracks were detected outside of the patch areas. Little or no surface IGA was detected.

Summary of Plant W, Unit 1 Degradation

Tube R6-C58 was dominantly degraded by OD origin IGSCC, with lesser extent IGSCC. Burst was controlled by the more deep IGSCC macrocracks. OD corrosion was confined to the TSP regions. Burst pressures were consistent with the voltage/burst correlation although the first TSP indication is below the mean of the correlation. A slightly alkaline crevice chemistry was determined to have existed. Field and laboratory inspection techniques accurately described the presence of the axial cracking. The presence of some form of cellular corrosion phenomena was identified using both the field and laboratory inspection techniques. As was seen in other cases of ICC, UT had difficulty accurately predicting the depth of penetration within the patch area. However, the ability of the ICC to be identified was not challenged. Still the ICC remain at depths typically less than half of the depth of penetration of the dominant IGSCC, which controls the burst location during burst testing. These tube examination results are consistent with the ARC data base.

Figure 2-1. Patch and Uniform IGA Morphology in a Transverse Tube Section.
A similar observation would be made from a longitudinal section.

Figure 2-2. Schematic of Simple IGSCC and Branch IGSCC. Note that branch and simple IGSCC are not distinguishable from a longitudinal metallographic section. From a longitudinal section, they also look similar to IGA (see Figure 2-3)

Figure 2-3. Schematic of IGA with IGSCC Fingers and IGA with IGA Fingers. Note that neither of the above variations is distinguishable from a longitudinal section.

Figure 2-4. OD Corrosion at the First TSP Crevice of Plant-A-2 Tube R4-C73

Figure 2-5. Sketch of Crack Distribution at the First TSP of Plant A-2 Tube R4-C73. Depth of crack penetration is also shown.

Figure 2-6. Photomicrographs of Cracks in Plant A-2 Tube R4-C73. Top micrograph is from a transverse section through one half of the main burst crack. The crack morphology is that of IGSCC with some IGA components (width of IGA is $\frac{1}{16}$ inch on one side of the crack). Bottom micrograph is from a transverse section through a typical crack located near the burst crack. The morphology is that of IGSCC with only minor IGA components. (Note: crack is opened wide by tube deformation)

Figure 2-7. OD Corrosion at the First TSP Crevice of Plant A-2 Tube R21-C22

Figure 2-8. Sketch of Crack Distribution at the First TSP of Plant A-2 Tube R21-C22

Figure 2-9. Photomicrographs of Cracks in Plant A-2 Tube R21-C22. Top micrographs are from a transverse section through one half of the main burst crack. The crack morphology is that of IGSCC with significant IGA components (width of IGA is inch on one side of the crack). Bottom micrograph is from a transverse section through the only other crack found in the crevice region. The crack morphology is more that of IGSCC. (Note: crack has been opened wide by tube deformation)

Figure 2-10. OD Corrosion at the First TSP Crevice of Plant A-2 Tube R38-C46

Figure 2-11. Sketch of Crack Distribution at the First TSP of Plant A-2 Tube R38-C46

Figure 2-12. Photomicrographs of Cracks in Plant A-2 Tube R38-C46. The crack morphology is that of IGSCC with minor IGA components. Mag. 100X

Figure 2-13a

Field RPC probe eddy current inspection data for the second support plate region of Tube R14-C80. Multiple axial indications (cracks) are observed. The maximum signal strength is volts, as corrected for alternative plugging criteria.

Figure 2-13b Laboratory RPC probe eddy current inspection data for the second support plate region of Tube R14-C80. Multiple axial indications (cracks) are shown in the data display. The largest signal strength was volts.

Figure 2-14a Field RPC probe eddy current inspection data for the first support plate region of Tube R19-C41. Multiple axial indications (cracks) are observed. The maximum signal strength is volt, as corrected for alternative plugging criteria.

Figure 2-14b

Laboratory RPC probe eddy current inspection data for the first support plate region of Tube R19-C41. Multiple axial indications (at least cracks) are shown in the data display. The largest signal strength was volts.

Figure 2-15

Sketch of the crack distribution found at the second support plate crevice region of Tube R14-C80. Included is the location of the burst test fracture face opening. The OD origin intergranular corrosion was confined to the crevice region, including that found on the burst fracture face.

Figure 2-16

Sketch of the crack distribution found at the first support plate crevice region of Tube R19-C41. Included is the location of the burst test fracture face opening. All deep OD origin intergranular corrosion was confined to the crevice region, including that found on the burst fracture face. Some minor intergranular corrosion was observed up to inch above the crevice top.

Figure 2-17

Radial metallography of the SP1 region of Tube R19-C41 showing intergranular cellular corrosion (ICC).

Figure 2-18 OD Corrosion at the First TSP Crevice of Plant A-2 Tube R31-C46

Figure 2-19

Photomicrograph of a Crack in Plant A-2 Tube R31-C46. The crack morphology is that of IGSCC with moderate IGA components. Top figure shows the secondary crack distribution at the first TSP.

Figure 2-20

Photomicrographs of a Transverse Section of Plant A-2 Tube R16-C53
at the First TSP Crevice Region. Mag. 100X

Figure 2-21

Additional Photomicrographs of Cracks in Plant A-2 Tube R16-C53
at the First TSP Crevice Region. Mag. 100X

Figure 2-22 Sketch of Crack Networks at the First TSP of Plant A-1 Tube R20-C26

Figure 2-23

Transverse Metallographic Section Through Plant A-1 Tube R20-C26 at the Mid-point of the First TSP Crevice Region (90° deformed half). Photomicrographs of areas A and B are also shown.

Figure 2-24 Crack Details in Areas C, D, and E of Transverse Metallographic Section Shown in Figure 2-20 (Plant A-1 Tube R20-C26)

Figure 2-25

Photomicrographs of a Transverse Section of Plant L Tube R12-C8, just below the circumferential fracture at the center of the first TSP. The circumferential location is that where deepest corrosion was found. The deepest axial IGSCC is through-wall. IGA patches are observed: through-wall and inch long, through-wall and inch long, and through-wall and inch long. The axial IGSCC had IGA components to individual cracks. Their L/W ratios vary from .

Figure 2-26

Axial Photomicrograph of Plant L Tube R12-C8 from the Center of the First TSP Crevice to the Bottom Edge of the Crevice at a Location with Deepest Corrosion. A uniform corrosion front, about through-wall is observed. The section is believed to cut through a region composed of numerous axial microcracks.

Figure 2-27

Photomicrographs of Radial Metallography Performed on a Region of Plant L Tube R16-C74. Cellular IGA/SCC was found with little change in the cell shape and cell wall thickness at depths of _____ mils below the OD surface. Note that the cut section was flattened, preferentially opening the circumferential wall of the cells. Mag. 11.5X

Figure 2-28 Higher Magnification Photomicrographs of Radial Section Shown in Figure 2-25. Top photo 50X, bottom 200X

Figure 2-29a Sketch of the crack distribution at the crevice region of SPI of Tube R18-C21HL. The large opening is from the burst test.

Figure 2-29b

Sketch of the crack distribution at the crevice region of SP2 of Tube R18-C21HL. The large opening is from the burst test.

Figure 2-30a Sketch of the crack distribution at the crevice region of SPI of Tube R11-C69HL. The large opening is from the burst test.

Figure 2-30b Sketch of the crack distribution at the crevice region of SP2 of Tube R11-C60HL. The large opening is from the burst test.

Figure 2-31 Sketch of the crack distribution at the crevice region of SPI of Tube R18-C16HL. The large opening is from the burst test.

Figure 2-32 Sketch of the possible ways individual microcracks interconnect by tensile tearing during a burst test.

Figure 2-33

Tube R7-C38 from Plant D-2, first and second support plate regions, transverse OD metallography, Mag. 100X.

Figure 2-34 Tube R18-C77 from Plant D-2, fourth and fifth support plate regions, transverse OD metallography, Mag. 100X.

Figure 2-35

Transverse View of Top of TSP Region of R16C60
TSP #1 -

Figure 2-36

Transverse View of Mid-Plane Region of R16C60
TSP #2

Figure 2-37

Transverse View of Mid-Plane Region of R11C48
TSP #1 -

Figure 2-39. Transverse micrograph just above midplane of TSP-1 from Tube R5C28

Figure 2-40. Transverse micrograph above (Ech 2) and below (Ech 5) TSP-1 midplane of Tube R5C28. Darkened OD regions are areas of greatest IGA involvement.

Figure 2-41a

Sketch of the OD origin crack distribution found at the first support plate crevice region of Tube R13-C42. Also shown is the location of the burst fracture opening. (While the burst opening extended outside of the SP crevice region, the corrosion cracking on the burst fracture was confined to within the crevice region.)

Figure 2-41b

Sketch of the OD origin crack distribution found at the second support plate crevice region of Tube R13-C42. Also shown is the location of the burst fracture opening. (While the burst opening extended outside of the SP crevice region, the corrosion cracking on the burst fracture was confined to within the crevice region.)

Figure 2-42

Sketch of the OD origin crack distribution found at the first support plate crevice region of Tube R16-C29. Also shown is the location of the burst fracture opening. (While the burst opening extended outside of the SP crevice region, the corrosion cracking on the burst fracture was confined to within the crevice region.)

Figure 2-43a

Sketch of the OD origin crack distribution found at the first support plate crevice region of Tube R16-C42. Also shown is the location of the burst fracture opening. (While the burst opening extended outside of the SP crevice region, the corrosion cracking on the burst fracture was confined to within the crevice region.)

Figure 2-43b

Sketch of the OD origin crack distribution found at the second support plate crevice region of Tube R16-C42. Also shown is the location of the burst fracture opening. (While the burst opening extended outside of the SP crevice region, the corrosion cracking on the burst fracture was confined to within the crevice region.)

Figure 2-44a

Sketch of the OD origin crack distribution found at the first support plate crevice region of Tube R6-C58. Also shown is the location of the burst fracture opening. (While the burst opening extended outside of the SP crevice region, the corrosion cracking on the burst fracture was confined to within the crevice region.)

Figure 2-44b

Sketch of the OD origin crack distribution found at the second support plate crevice region of Tube R6-C58. Also shown is the location of the burst fracture opening. (While the burst opening extended outside of the SP crevice region, the corrosion cracking on the burst fracture was confined to within the crevice region.)

3.0 Non-Destructive Examination

An extensive NDE program was implemented to characterize the laboratory cracked specimens and to assess the sensitivity associated with application of the bobbin coil voltage limits for the tube repair limits.

The test program included tests to address some of the variables associated with field characterization of degradation as follows:

1. Bobbin probe voltage sensitivity to the length of the cracks, depth of the cracks, presence of inclusions in the cracks and parallel cracks.
2. Multiple probes to address probe-to-probe variations utilizing probes from Echoram and Zetec.
3. Influence of tube to TSP crevice condition on bobbin coil response including open crevices, packed crevices, incipient denting and fully developed denting.
4. Bobbin probe voltage sensitivity to probe wear to establish field inspection requirements for acceptable NDE uncertainties.
5. Variability among calibration standards, and normalization of the frequency mix.
6. Use of RPC to augment bobbin probe inspections.
7. Detectability of IGA and volumetric tube degradations using bobbin coil probe and the amplitude of their signals.

The NDE results for the laboratory specimens are utilized in later sections to develop correlations of eddy current voltage response to potential leakage and burst pressure for application to tube repair limits.

Establishing a relationship between the bobbin coil response and tube integrity (leakage, burst considerations) is important to inspection planning. A relationship helps determine the importance of detecting degradation with a small amplitude. That is, can "small" indications be left in service and have negligible consequences for safe operation. Degradation exceeding present repair limits, whose bobbin coil eddy current response was not detected as readily as would equivalent size notches, has been confirmed by destructive examinations.

The morphology of the intergranular corrosion can explain the reduced eddy current response for small cracks. The observed field degradation, multiple short cracks (microcracks), coupled with an intergranular nature, allows paths for the eddy currents to pass uninterrupted through ligaments remaining between microcracks which can grow together to form longer

microcracks. An appreciation for why this phenomenon can account for diminished eddy current response has come from the use of liquid metal modeling techniques. Using this technique, degradation is simulated as inserts in liquid metal, and degradation morphologies that are difficult or impossible to machine can be easily simulated. The difference in response between "real" cracks and notches have been modeled by varying the contact between the faces of the crack. In that work, interfacial contact of $\frac{1}{2}$ reduced the eddy current response by a factor of $\frac{1}{2}$. An example of this behavior was found for the doped steam specimens cracked with high applied hoop stresses. These specimens were found to have lower voltages than expected for the crack sizes present in these tubes. This result is judged to be the consequence of crack face contact as a result of removing the applied stress. Similarly, the voltage sensitivity tests reported here show large voltage increases as ligaments between cracks are lost. The presence of crack ligaments and partially degraded grain boundaries provides an explanation for the limited eddy current response associated with field induced degradation. Further, the presence of these ligaments and the low instance of primary coolant leakage associated with this degradation mode suggests that there is residual strength associated with these ligaments. Thus, significant degradation depths may result in less severe loss of strength than used in determining the repair limits based only on crack depth, e.g. 40% through-wall. For this reason, repair limits are based on voltage responses correlated to tube integrity through the voltage versus burst pressure and leakage correlations.

3.1 Voltage Normalization for ARC

To provide for repeatability of the voltage measurements, a common voltage calibration is used for ARC applications. Bobbin probe voltages are calibrated to the $\frac{1}{8}$ inch holes on an ASME standard. The ASME standard includes four flat bottom holes of $\frac{1}{8}$ inch depth and $\frac{1}{8}$ inch diameter. The dimensions on the $\frac{1}{8}$ inch holes should be manufactured to a tolerance of ± 0.001 inch. For $\frac{7}{8}$ inch diameter tubing with 0.050 inch nominal wall thickness, the bobbin voltages for the ASME $\frac{1}{8}$ inch holes should be normalized to 1.0 volts at 10 kHz and 0.5 volts for the 100 kHz mix. The 0.5 volt for the mix results is obtained when the reference EPRI laboratory standard is setup to 1.0 volts at 10 kHz. If the particular probe and standard being applied for a voltage measurement does not yield the same voltage ratio for 10 kHz to within about $\pm 5\%$, voltages should be normalized to 1.0 volts for the mix.

RPC probe voltages should be normalized to 1.0 volts for the $\frac{1}{8}$ inch long, throughwall notch at 10 kHz. The calibration must be established at the frequency used for reporting the RPC amplitudes.

Alternate voltage normalizations based on throughwall holes or slots were also evaluated for ARC applications as described in Section 3.10. No advantages were found for these alternate normalizations and the $\frac{1}{8}$ inch hole normalization is required for bobbin voltages.

3.2 Voltage Renormalization for Alternate Calibrations

In France and Belgium, kHz differential inspections are applied for TSP intersections with 7/8 inch diameter tubing. The French normalization is to volts for four throughwall mm diameter holes, while the Belgium normalization is volts for four throughwall mm diameter holes. By both hole volume scaling and direct measurements, the French and Belgium normalizations are equivalent within . Thus a U.S. ARC voltage to French/Belgium voltage renormalization can be obtained from either or both French and Belgian data.

French to U.S. voltage renormalization has been evaluated using comparisons between calibration standards and model boiler specimens with both U.S. and French probes and equipment. Table 3-1 summarizes voltage ratios based on calibration standards. U.S. Zetec and Echoram probes were applied with the U.S. calibration standards and equipment, and French and Echoram probes were used with the French calibration standards and equipment. The Zetec and Echoram probes, when normalized to the hole, yield about differences in voltages for the four throughwall holes using U.S. Equipment, with the Echoram probe showing the larger voltage increase between and holes. With the French equipment, the Echoram probe shows a smaller voltage increase than the French probe between and holes. The appropriate French to U.S. voltage renormalization would utilize U.S. equipment for the U.S. normalization and French equipment for the French normalization. However, the results of Table 3-1 show insignificant differences between choice of equipment for the French normalization. The results show U.S./French voltage renormalization factors of about

Laborelec has performed measurements in Plant K-1 SGs using U.S. equipment/probe/standards for the ARC voltage measurements and Belgian equipment/probes/standards for the Belgian voltage measurements. The ARC voltage measurements were obtained using Zetec equipment, an Echoram probe and an ASME standard cross-calibrated to the reference laboratory standard. Voltage data were obtained for indications up to Belgian volts. Data have also been obtained on model boiler specimens using Zetec equipment, a French probe, the reference ASME standard and a standard with throughwall mm diameter holes for the French voltage normalization. These data points range up to French volts with points overlapping the Belgian data up to volts. To develop a correlation for renormalizing Belgian/French voltages to the U.S. calibration, the Belgian and model boiler data were combined and the overlapping data up to volts were used as shown in Figure 3-1(a). The y-axis intercept is negative for the overall fit as the large slope associated with the deeper, higher voltage indications dominates the data. For this reason, a constant renormalization factor of (typical of that found for depth ASME holes) is suggested below Belgian/French volts. The correlation of Figure 3-1(a) can be acceptably used to convert Belgian and French data for use in the voltage/burst and voltage/leakage correlations.

The fitted correlation of Figure 3-1(a) is compared with the higher voltage, six model boiler data points in Figure 3-1(b). It is seen that the correlation tends to underestimate the U.S. voltages at the higher voltage range. This is consistent with the ASME standard data of Table 3-1 which shows a throughwall ratio of $\frac{1}{2}$ for the U.S./French normalizations compared to the asymptotic value of $\frac{1}{3}$ obtained for the data up to 1000 volts. A polynomial could be fit to the total voltage range to improve the overall fit. However, the region of interest for ARC applications is up to about 1000 French/Belgian volts (1000 U.S. volts) so the simpler linear regression is being applied for the voltage renormalizations.

3.3 Voltage Sensitivity to Crack Morphology

A series of eddy current tests were performed to establish voltage trends with crack morphology to characterize voltage as a measure of tube integrity. In most cases, machined specimens were used to simulate degradation features. This section describes using simulated cracks and volumetric indications. In addition, voltage measurements for laboratory specimens and pulled tubes with IGA degradation are summarized to assess detectability of IGA.

Voltage Sensitivity Using Slits in Copper Foil. To establish the general trends of bobbin coil voltage amplitude to crack morphology, sensitivity tests were performed using slits in a cylindrical copper foil to simulate varying crack lengths, ligaments and parallel cracks around the tube circumference. The copper foil was placed around a plastic tube. The various crack morphologies simulated by the slits in the copper foil, and the associated voltage responses are shown in figure 3-2. For each combination of simulated cracks in figure 3-2, the total crack network length is equal to the TSP thickness of 0.75 inch. The vertical cuts between the parallel axial cracks simulate loss of ligaments between cracks.

The voltage trends of figure 3-2 show that the voltage increases with:

- Increasing crack length
- Increasing number of cracks around the tube circumference, and
- Loss of ligaments between cracks.

Voltage Sensitivity Tests Using Slots in Alloy 600 Tubing. Additional information on the functional dependence of bobbin signal voltage on length and depth of axial cracks was obtained using EDM (electric discharge machining) slots in 7/8 inch OD, 50 mil wall alloy 600 tubing as shown in figure 3-3. The signal voltages for the slots represent the upper bound for the signal voltages expected for actual cracks of similar length. For the 0.1 inch deep slots, the signal voltage increases steeply with slot length up to about 0.5 inch and continues to increase up to one inch, after which it tends to level off. For the 0.2 inch deep OD slots, the signal amplitude increases with slot length up to about 0.5 inch after which it levels off. The signal amplitude increases by a factor of about 2 for 0.1 inch deep slots as the slot length increases from 0.25 inch to 0.5 inch; it increases by a factor of about 3 for the 0.2 inch deep OD

slots over the same range of crack length. It may further be noted that for longer slots, there is a greater increase in the signal voltage as the depth increases from a shallow depth to . For example, for slots, the voltage increases by a factor of about as the depth increases from where as for mil long slot it increases by only a factor of for the same range of depth change. Voltage increases in an exponential manner with depth for a given slot length. For example, the voltage for a slot increases from about volts at depth to volts at depth. Overall, the voltage amplitude is particularly sensitive to deep wall penetration and crack length; this is the desired dependence for voltage as a severity index for tube integrity.

Figure 3-3 also shows the data for three slots with depth varying along slot length. The central of each slot had depth which tapered off to at the ends. The signal amplitudes for these slots with tapered ends are, as expected, higher than for the through-wall rectangular slots when plotted against the through-wall slot lengths. Figure 3-4 shows a plot of percentage increase in signal amplitude above that for a uniform through-wall slot resulting from the tapers as a function of the deep portion of the slot length. As the through-wall length increases, the influence of the partial depth slot decreases such that for lengths greater than about inch, the partial depth slot length has negligible influence on the voltage amplitude.

Figure 3-5 shows the signal amplitudes for the axial slots obtained by using the rotating pancake (RPC) probe with a mil diameter coil. This data is qualitatively similar to the bobbin data of figure 3-3.

General observations from this eddy current evaluation of axial slots are:

- Both bobbin and RPC voltage amplitudes increase sharply with axial crack length up to about one inch for deep slots.
- The voltage increase with length is much smaller for partial depth OD axial slots and voltage does not increase significantly with length for slots greater than about long.
- Voltage increases exponentially with depth.
- Signal amplitude is dominated by the deep portion of the slot.

These results support the use of the voltage amplitude as a crack severity index for tube integrity assessments. Voltages increase with increasing crack length, with increasing depth particularly near through-wall penetration and with loss of ligaments between cracks.

The general concept of relating voltage to burst pressure can be demonstrated by combining data for voltage vs. slot length with burst pressure vs. slot length data. Figure 3-6 demonstrates the resulting voltage/burst correlation. Voltages for slots are not typical of

cracks but the general trend and slope are similar to that developed in section 6 from burst testing of cracked tubes. As intuitively expected and shown even for machined specimens, a given voltage amplitude does not define a unique crack morphology, i.e., different crack morphologies could lead to the same voltage amplitude. These crack morphologies would have different burst strengths and thus a spread in burst pressures for a given voltage is expected. This spread is accommodated in the repair limits by using a voltage/burst correlation at the lower confidence band of the test data. Various crack morphologies involving variables such as length, depth, ligaments, multiple cracks, etc. influence the spread of the data and thus the resulting tube repair limit.

Voltage Sensitivity to Volumetric (Non-Crack) Indications. It is desirable to compare voltage amplitudes for volumetric indications to those associated with repair levels for ODSCC cracks. Given degradation specific repair limits for ODSCC at TSPs, these comparisons help to guide the importance of distinguishing ODSCC from other types of degradation. These voltage comparisons provide guidance on setting the bobbin voltage threshold for RPC inspection. Typical bobbin coil voltage amplitudes were developed from laboratory simulations of volumetric degradation as developed below:

Pitting: Figure 3-7 shows the bobbin signal amplitude vs diameter of machined through-wall holes simulating deep pits. Pitting observed in operating steam generators occurs as multiple pits for which voltages are significantly higher than the voltage expected for single Rules/Pits of comparable depth. The data from ASME flat-bottom holes of partial depths may be used for estimating the signal voltages expected from partial depth OD pits.

Thinning: Cold Leg Pulled tube data from two different plants with cold leg thinning were reviewed and are summarized as follows. In one case, a flaw at the second TSP in the cold leg with a maximum wall penetration of had a bobbin amplitude of volts. Figure 3-8 shows a photograph of the OD surface at the degraded location. In the second example, which was also at the second TSP in the cold leg, a maximum wall penetration of yielded a bobbin amplitude of volts. Examination of the pulled tubes showed no cracks in these tubes and the degradation was identified as "cold leg thinning."

These data indicate that bobbin voltages would exceed about volts, as limited by pitting degradation, before being a concern for tube integrity. A single pit, simulated by mil through-wall holes would have voltages of about volts, respectively. Single pits of this size are significant of a tube integrity issue. Pitting typically occurs as multiple pits in operating steam generators with higher voltage levels. Cold leg thinning at depth will yield a bobbin amplitude of over volts.

IGA Detectability. Limited laboratory specimens with pure IGA and pulled tubes at TSP intersections with significant IGA are currently available for assessments of detectability and tube integrity. Available laboratory IGA specimens were prepared as long (inches), uniform IGA to assess detectability in unexpanded regions of tubesheet crevices. Data from three domestic tube to TSP intersections from Plant L¹ (R12 C8), one from Plant M-2, and three from Plant N-1 (non-Westinghouse unit) are available. Some French data obtained from Electricite de France (EdF) for TSP indications can also be assessed. The general morphology of the French indications is cellular + SCC with IGA patches and is more like Plant L tube R12 C8 than indications in other domestic plants.

Three sets of laboratory IGA specimens were available for NDE assessments. Two were Westinghouse samples and the third represents samples prepared under a later EPRI program. The two Westinghouse sets of specimens represent laboratory IGA under accelerated conditions and provide uniform wall penetration IGA over inch lengths. Bobbin coil detection for these specimens is shown in figure 3-9. Figure 3-9a represents specimens prepared using sensitized tubing and shows very high bobbin coil amplitudes. Figure 3-9b shows bobbin coil responses using non-sensitized material. The non-sensitized material shows much lower amplitudes. These examples show that although bobbin coil cannot distinguish IGA from other forms of degradation, IGA is detectable by bobbin coil, with voltage amplitudes exceeding volts for uniform IGA penetration of .

Methods of sample preparation were refined for the specimens prepared in the EPRI program to further improve comparisons with field experience. These specimens were in the range of nearly uniform wall penetration of IGA. Figure 3-10 shows typical NDE results for deep IGA. The bobbin coil differential tests reveal the uniform IGA whereas the RPC results are not particularly revealing. Voltage amplitudes are not available for the samples that were destructively examined. Bobbin coil measurements of laboratory samples were performed with the results given in table 3-2. These samples show voltage amplitudes of about volts where the IGA depth is expected to be deep and are NDD (no detectable degradation) where depths of a few percent are expected. Deep cracks within the samples were detected with amplitudes of volts. These samples are more representative of field IGA than the figure 3-9 samples although only limited pulled tube data for uniform IGA are available for direct comparisons.

A pulled tube from Plant M-2 shows IGA with cracks up to depth. This tube had a voltage amplitude of volts, which is high compared to tubes with principally ODS/SCC at comparable depths as shown in Section 4.11. The signal amplitude is comparable to the laboratory specimens of table 3-2, although lower than the specimens of figure 3-9.

¹Actual plant names are on file at EPRI.

Three pulled tube results from Plant N-1 with egg crate supports and IGA degradation also support IGA detectability at voltage levels comparable or higher than that for ODS/SCC with minor IGA (see Section 4.11). The pulled tube (R12 C8) indications from Plant L were detected by pre-pull bobbin coil inspection. Section 4-11 describes comparisons of the voltage and maximum depth for indications from Plant L to other pulled tube results. It is seen that the Plant L voltage levels are typical of the rest of the population of pulled tubes with less IGA involvement than the Plant L tube R12 C8 crack morphology, which shows patches of IGA with IGA/SCC cracks.

Section 4-11 also describes voltage amplitudes for tube to TSP intersections removed from French and Belgian units. The French and Belgian data, which have cellular corrosion morphologies, show voltage responses toward the high range of the data.

Overall, the available pulled tube results show comparable voltage responses relative to maximum depth with no definable dependence on IGA or cellular involvement within the broad scatter of the data. The laboratory uniform IGA samples show significant voltage responses at depth. The available pulled tubes with significant IGA levels show IGA with cracks and have been found to be detectable indications using bobbin coil data although the bobbin data cannot distinguish IGA from other forms of degradation.

3.4 Sensitivity to Bobbin Coil Probe Vendor

To address concerns that the results of the study might be limited to a specific probe, probes from different eddy current probe vendors (Echoram and Zetec) were used. Both probes were nominally inch in diameter and incorporated the latest technology for centering. The coils on each probe were nominally inch wide and were spaced by inch. Initially each of the probes was used with two different sets of frequencies duplicating typical field inspection configurations. The first set of frequencies (configuration I) was kHz. The second (configuration II) was kHz. The results described in this section were obtained from the initial comparisons of the two probes. An update of the probe comparisons using all available model boiler data is given in Section 3.10 as part of an assessment of alternate voltage normalizations.

Comparisons were made between the data obtained from probe Er and probe Zt for the cracked tube specimens. The probes have different frequency response characteristics: Probe Zt gives a greater response at kHz, while probe Er has a larger response at kHz since it is designed for higher frequency operation than the Zt probe. This difference is not a significant issue and is noticeable only as a consequence of the way in which the voltage calibrations have been derived. Table 3-3 gives the voltage measured by probe Zt divided by the voltage measured by probe Er for the EDM calibration notches. As can be observed for each frequency, the difference between the probe responses is a constant factor for all notches.

This apparent variation between the probes can be eliminated by calibrating each of the frequencies individually rather than using the kHz calibration factor, or by calibration at the planned mix frequency.

The results of figures 3-11 to 3-13 show that both the Zetec and Echoram probes yield essentially the same voltage amplitudes for ODSCC flaws when voltages are normalized to the ASME hole as described in Section 3.1. A further discussion of this comparison is given in Section 3.10.

The results for the kHz Mix channel are dependent on the method for voltage calibration. Plots of the measured voltage for various indications from probe Zt versus the voltage from probe Er indicate a one to one correspondence for both amplitude and depth (figures 3-11 to 3-13). The correspondence between the mix channels of the two probes is due to the fact that the kHz channel is being used both as the "primary" mix frequency and to set the calibration factor. If another frequency is used as the primary mix frequency (i.e., kHz) the apparent mix amplitudes will differ. Table 3-4 gives the measurement of the ASME holes using a kHz mix for the two different probes. As can be seen the results from the two probes differ by a constant multiplier. As with the individual frequencies, this factor can easily be accommodated by using a different calibration procedure.

The bobbin coil inspections were supplemented by two RPC examinations, also with probes from the two eddy current probe vendors noted above. Only one set of frequencies (kHz) was used for both RPC probes. The data gathered during this phase of the program were used primarily as a qualitative tool in assessing the extent of the degradation.

3.5 Influence of TSP Design

The effect of various support configurations on degradation response was estimated from measurements with similar degradation. In performing these measurements, simulated supports of various geometries and materials (see table 3-5) were slid over the test specimens so that the degradation was approximately centered in the support. The NDE measurements were made in the presence of different support plate simulants surrounding the degradation.

In general the only significant effect of the supports was to cause a variation of approximately 10% in the amplitude of the degradation response. Figures 3-14 and 3-15 show the amplitudes of the degradation response within the various supports normalized by that obtained with the carbon steel ring. Note that the egg crate and quatrefoil responses are slightly larger than that obtained from the solid support configurations. Figure 3-16 shows that the drilled stainless steel configuration is the only support that has any influence on the phase angle (or depth) of the indications and even this is restricted to approximately a effect.

An exception to this was sample BW-5 where the residual response from the support was comparable to that of the degradation. For this sample the presence of the support caused the response to be mis-identified. For this sample the degradation response was on the order of _____ volt and was located in the vicinity of a dent response resulting from sample fabrication. The support mix residual from the calibration support ring was on the order of _____ volts. The addition of the support to the dent and the degradation was sufficient to cause the indication to be distorted so that it was not uniquely identifiable. After leak testing, the degradation response grew in amplitude sufficiently (from _____ volt) such that it could be identified under all support plate conditions.

3.6 Influence of TSP Crevice Condition

For some specimens, the crevice between support and the tube was packed with magnetite and the sample was inspected again with the bobbin coil. It may be noted that crevice packing did not cause (and is different from) denting or other mechanical deformation of the tube except in the one case described below (It is known that even minor denting results in significant bobbin coil response). Table 3-6 compares the data from the two inspections. With the exception of sample BW-11 the amplitude of the responses from the samples changed by approximately ____%. Sample BW-11 showed a ____% increase in amplitude. When the support was removed from the sample the degradation response had indeed increased, indicating that the presence of magnetite in the crevice did not cause the increase in response, rather the process of packing the crevice had mechanically deformed the sample causing further loss of ligaments and a subsequent increase in response. Additional evidence for the minimal impact of the presence of magnetite in the crevice is derived from the comparison of the data from corrosion samples with tightly packed crevices. A comparison of the EC data before and after the removal of magnetite with the packed support ring in place (figure 3-17) shows a ____ increase in response in the presence of magnetite, with a scatter of approximately _____.

As part of the test program, _____ fatigue crack and _____ doped steam corrosion crack samples were tested to determine the influence of the dented support plate crevice condition. Table 3-7 summarizes the results of the eddy current inspection of these samples before and after denting (note samples FAT 1, 2, and 3 had been leak tested previously). Denting resulted in a significant change in the amplitude of the fatigue crack eddy current responses. Prior to denting, all but one of the fatigue cracks had amplitudes which approached that of the through-wall EDM notch (____ Volts). After denting, two of the fatigue cracks could not be distinguished from the response of the dents, despite the fact that the dent response was about _____ times smaller than the initial fatigue crack response. Initially the corrosion cracks produced smaller responses than the fatigue cracks. In spite of this, their responses on average, could be detected in the presence of the dent. These results represent large indications in the presence of small dents. In field applications, small to moderate indications typically cannot be separated from dent signals that exceed the amplitude of the indication at TSP edges; it may be possible to detect ODSCC signals much smaller than the dent signals in the TSP center.

The difference in the behavior of the two crack types (and further within the fatigue samples) in the presence of denting is a consequence of the heavier oxide coating on the crack faces of the corrosion samples as opposed to the leak tested fatigue cracks. Under the compressive loads of denting, the crack faces are forced together. The presence of the oxides on the corrosion crack faces prevents interfacial contact and therefore results in a minimal change in the crack response. On the other hand, the faces of a fatigue crack, being free of oxides, come into intimate contact permitting the eddy currents to flow unimpeded across the crack, significantly reducing the response. The significant loss in response of the fatigue cracks demonstrates that interfacial contact does indeed result in a reduced eddy current response.

It is not expected that service-induced degradation will respond to denting as have the fatigue cracks. Rather, it is expected that the compressive stresses from denting would not play a direct role in providing interfacial contact in the case of corrosion cracks and hence field induced cracking would respond as the doped steam samples did, with little change in amplitude. However, it may be noted that bobbin coil detectability of cracks at dented intersections is unreliable when the degradation signal overlaps the dent signal (e.g. both at edges of TSP) and when degradation amplitude is much smaller than the dent amplitude.

3.7 Approach for NDE Uncertainties

In most prior evaluations, SG NDE uncertainty is determined as the difference between bobbin coil indicated depth versus actual depth from destructive tube examinations. This is not the case for voltage measurements such that the NDE uncertainties for voltage do not have such a unique interpretation. For voltage plugging criteria based upon voltage versus burst pressure correlations, the NDE voltage "uncertainties" affect both the voltage measurement and the spread or uncertainty in the burst pressure correlation. The goal for the voltage measurements is to minimize the uncertainty on repeating a measurement so that the uncertainty on the burst correlation is reduced to the extent practical. The remaining voltage measurement uncertainties end up as part of the burst correlation uncertainty. For example, assume that a number of perfectly identical samples were prepared such that burst pressures would be identical. If voltage measurements were then made with different probe diameters, calibration standards, open crevices, packed crevices, copper deposits in crevices, etc., the voltage measurement variability would then result in a spread in the voltage versus burst correlation. Clearly the goal is to minimize the burst correlation uncertainty (lower confidence limit used for plugging criteria) by controlling the voltage variability. The voltage measurement procedures must be consistent between laboratory and field implementation to apply the laboratory specimen NDE/burst data for developing plugging limits. Inclusion of field voltage measurements for tubes pulled prior to implementing the procedures to improve measurement repeatability tend to increase the spread in the burst correlation. The NDE voltage uncertainty is defined as the uncertainty in voltage repeatability emphasizing differences between the laboratory and the field measurements. As applied for the plugging limit development, the variables affecting the burst correlation are split into NDE uncertainties for determining voltage and burst correlation uncertainties as given in Table 3-8.

The potential contributors to the NDE repeatability uncertainty are probe centering (principally probe wear), calibration standards, probe design differences, eddy current analysis variability and eddy current system variability. Eddy current system variability results from noise due to instrumentation and cabling. This contributor is on the order of ± 1 V and can be ignored when combined with the probe wear uncertainty for applications to plugging limits above a few volts.

Probe design differences are eliminated by requiring that only bobbin coil probes with 1/2 inch coils and 1/2 inch spacing between coils be used for voltage measurements. These values are commonly used by nearly all probe vendors. The voltage amplitude is a function of coil to coil spacing. For differential responses and a center to center coil spacing of 1/2 inch, the influence of small changes in coil spacing such as associated with manufacturing tolerances is small. This sensitivity is shown in Figure 3-18. The data base for the voltage/burst correlation includes magnetic bias and non-magnetic bias bobbin probe data. Most of the pulled tube data, were obtained with magnetic bias probes while the model boiler data were obtained with non-magnetic bias probes. In either case, the differences in voltage measurements between these probe types is negligible. A systematic comparison of magnetic and non-magnetic bias probes was performed by B&W in evaluating pulled tube data from Plant R. Eddy current data were obtained with both probe types on 8 pulled tube indications and various machined hole standards. The differences between probe types was $\pm 10\%$, which is less than the analyst variability of $\pm 15\%$ as developed below. Thus, either probe type is acceptable for application of the plugging limits of this report.

As noted in Table 3-8, the use of field voltage measurements for pulled tubes obtained prior to implementing the present voltage calibration requirements contributes to the spread or uncertainty in the burst correlation. Uncertainties associated with field crevice conditions, like the human factors, are more significant at the low amplitudes near detection thresholds than at the voltage plugging limits. This has been the experience in Plant L SGs where distorted indications have been primarily low amplitude indications. Again, the larger amplitudes near voltage plugging limits provide more reliable quantification of the indications than associated with current experience with depth limits for tube plugging. This is supported by the 10% eddy current analyst variability uncertainty developed from the larger Plant L indications as described in Section 3.9.

An uncertainty in the burst correlation that adds conservatism to the correlation is the effect of tube pull forces on crack morphology and potential reduction in burst pressures. Although not a major concern for axial indications, effects of the tube pull such as loss of ligaments can occur. Since pre-pull field voltage amplitudes rather than post-pull values are used in the burst correlation, the pull force effects add conservatism. Post-pull voltages are commonly higher than pre-pull values, particularly for indications that tend toward lower burst pressures on the voltage/burst correlation. For example, Plant L tube R8C69 had post-pull voltages for both bobbin and RPC probes that were higher than pre-pull voltages by a factor of 1.5 or more.

3.8 Sensitivity to Probe Wear

Eddy current test parameters can exist over which there is little systematic control and which may vary between tubes or along the length of a tube. The centering of the eddy current probe as it passes the degradation poses the greatest concern of this type. This study has shown that probe centering can vary the amplitude of a signal, in the worst case, by a factor of two. The laboratory study used field probes which had excellent centering characteristics. At the beginning of a field inspection sequence, the probe centering characteristics would mimic those found in the laboratory. As the inspection continues the probe is expected to wear and its centering capability to degrade. The time frame for this to occur is unknown because it is a complex function of inspection extent, centering device design and material, tube geometry, the presence of oxides, etc.

A means of assessing the probe's centering capability is through the use of an appropriate verification standard as illustrated in Figure 3-19. Such a standard can be as simple as holes drilled in a segment of tubing. The holes are displaced axially in different planes with each spaced degrees around the circumference from its neighbor. The amplitude ratio between the holes then determines the degree of centering of the probe. A standard of this type would be implemented during inspections to periodically verify probe centering during the inspection.

The bobbin probe centering mechanism wears with usage. This could affect the eddy current signal. The effect of wear on signal voltage was evaluated using a "-hole standard." The holes were mils in diameter, % deep, degrees apart circumferentially, and inches apart, axially. A inch diameter probe fabricated by Echoram was used for this evaluation. The centering mechanism in this probe consists of sets of spring loaded plastic buttons (hemispherical) degrees apart and protruding approximately mils from the probe body. The test runs were made with the tubes in a vertical position. The tubes were rotated after each run to provide for the randomness in the probe to tube orientation expected in the field. For the new probe, the standard deviation for the voltages obtained from the identical holes for repeated test runs was of the average voltage amplitude.

The centering buttons of the probe were worn by repeatedly running the probe through a tube with an abrasive tape on the tube ID. The data from the -hole standard were collected for different levels of probe wear. At the level of probe wear represented by a reduction in height of the centering plastic buttons (i.e., about mils radial reduction), the standard deviation in the voltage for the four holes was found to be within . Increasing the probe wear beyond this level resulted in rapid deterioration of the quality of the data. The results of the tests are shown in the upper part of Figure 3-20. The reduction in height of the centering buttons appears to envelope typical field wear between probe changeouts during an inspection. Thus, even for a worn probe, the variation in voltage measurements can be represented by a standard deviation of . These data can be used to estimate the NDE uncertainty associated with probe wear. Since acceptable field measurements would be made for probe wear between and about mils radial material loss, all the data for mils wear can be combined to define the NDE uncertainty.

Probe wear approaching the mil wear data of Figure 3-20 is minimized by field application of the probe wear standard requiring probe replacement if the worn probe voltage for any hole differs from the new probe voltage for the same hole in the wear standard by more than . Combining the data of Figure 3-20 from mils wear yields an average voltage of volts with a standard deviation of volts or of the mean voltage, as shown in the upper part of Figure 3-21. Thus, the uncertainty allowance for probe wear can be represented by a standard deviation of . The remaining concerns over probe centering are the impact of tube to tube variations in diameter and ovality. Neither of these are anticipated to be major sources of variability.

Channel head mockup tests were performed to evaluate field implementation of the probe wear standard of Figure 3-19. During field implementation of the probe wear standard, the wear standard must be utilized essentially in line with an ASME calibration standard and both located within the channel head below the tubesheet. This application introduces the effects of bends in the probe leads, as well as probe wear, on the variation in voltages between new and worn probes as measured against the holes in the wear standard. The effects of bending the probe leads can be a function of the location of the eddy current fixture in the channel head. A probe pusher, foot cable extension and a robot fixture for tube location were used in these tests. This testing was performed at tube locations using both Echoram and Zetec new and simulated worn probes as summarized in Figure 3-22. This figure also shows the approximate location of the standard, which rested on the bottom of the channelhead pointed away from the manway. Moving the eddy current fixture between tube locations can potentially move the location of the standard. repeat voltage measurements were made at tube locations and measurements were made at locations. For field application of the probe wear standard, probe wear acceptability requires that the change in voltage between a new and worn probe for each of the holes be less than of the new probe hole voltage. Four different probes from each manufacturer were used to represent a new probe and three levels of probe wear. Simulated probe wear was obtained by machining the centering devices to the material losses given in Figure 3-22. For the Echoram probes, the material loss represents the thickness removed at each of the three centering buttons, which represents a reduction in the probe radius. For the Zetec probes, the material loss represents the radial reduction in the centering petals. The bobbin voltages were normalized to a hole ASME standard at tube location R23C44 following the pull of the probe for each probe diameter tested. The voltage normalization for these tests was different than used for the probe wear tests described above, such that the voltages are not directly comparable. The data from these tests can be compared with the above described tests by comparing the standard deviation of the results as a percentage of the mean voltage.

The mockup test data were evaluated to assess the fraction of the wear standard measurements, as a function of probe wear, that would exceed the allowable change in the hole voltage measurements. For example, with repeat tests at each probe wear value, there are probe wear measurement combinations. Each of the measurements for a new probe is compared with all measurements on a worn probe. If the voltage difference for any one of the four holes between new and worn probes changes by , the occurrence would be considered to require probe replacement.

The results are summarized in Table 3-9. It is seen that very few Echoram probe replacements would be required up to probe wear of 0.005 mils. These replacements represent premature probe replacement, as the standard deviation on voltage variations is only 0.005 at this wear level. This is consistent with the prior test for the vertical wear standard, as shown in Figure 3-20, for which the voltage variations did not increase substantially until 0.005 mils radial wear was reached. The results for the Zetec probe show more dependence on tube location, with relatively high fractions (0.1) of all measurements exceeding voltage changes at probe wear values of 0.005 and 0.01 mils. Overall, the Echoram probe with its spring loaded centering buttons appears to have only minor sensitivity to the location of the probe fixture for the range up to 0.005 mils radial wear that was tested. The Zetec probe, with fixed centering petals, appears to show more sensitivity to fixture locations, particularly at locations (R8C92, R2C88, and R23C44) adjacent to or behind the end of the wear standard (see Figure 3-22).

The standard deviation of 0.005 for the Echoram probe in the horizontal wear standard tests is the same as that found for the vertical wear standard tests for 0.005 mil radial wear (Figure 3-20). Thus, there does not appear to be a significant dependence on orientation of the standards and probe over this range of probe wear. The Zetec probe, with fixed diameter centering petals, shows the standard deviation increasing from 0.005 wear to 0.01 mils radial wear, and to 0.02 mils radial wear. Combining these results with the overall likelihood of probe replacement from Table 3-9, the probability of probe replacement is about 0.005 at wear levels resulting in about 0.005 voltage variability and about 0.01 at wear levels with about 0.01 voltage variability. Thus, applying the probe wear standard with a limit of a 0.005 voltage change between new and worn probes effectively limits the voltage variability due to probe wear to about 0.005 for worn probes. Only a small fraction of indications measured with a given probe would be made at this stage of probe wear. Since the wear standard measurements are not a strong function of the measurement location, the data can be used as an additional assessment of the NDE uncertainty associated with probe wear. Figure 3-20 shows the signal amplitude variations as a function of probe wear for both the Echoram and Zetec probes for the measurements taken with the wear standard horizontal in the channelhead. The Echoram probe does not show a strong function of probe wear up to the 0.005 mils of wear tested for this case. This result is consistent with the upper figure given in Figure 3-20 which indicates substantial voltage variability only at about 0.005 mils of probe wear. The Zetec probe shows increasing amplitude variability at 0.005 mils or larger wear, with significant variability 0.01 mils wear. At 0.01 mils wear, there is a significant likelihood that probe replacement would be required for field applications of the wear standard based on one of the 4 hole voltages differing by 0.005 from the new probe value as shown above.

The data of Figure 3-20 show that the trends in voltage variability with wear are similar for both the Echoram and Zetec probes. Prior to wear values for which probe replacement is likely (0.005 mils for the Echoram probe, 0.01 mils for the Zetec probe), the voltage variability is similar for both probes and the same NDE uncertainty for probe wear can be used for both probes. This similarity is further shown in Figure 3-21, where distributions of voltage variability can be compared for Zetec and Echoram probes.

The standard deviation is _____ for the Echoram probe and _____ for the Zetec probe. If the _____ mil wear data is included in the voltage variability distribution for the Zetec probe, the standard deviation increases from _____

The field application of the wear standard requires probe replacement when the voltage difference between that measured for a new probe (at time of probe replacement) and subsequent measurements changes by more than _____ of the new probe voltage for any of the _____ holes in the standard. As discussed earlier in this section, this occurred in the tests a few times at an Echoram probe wear of _____ mils or a Zetec probe wear of _____ mils and in most tests for a Zetec probe wear of _____ mils. These results correspond to a few premature probe replacements where voltage variability is _____ (standard deviation) and nearly _____ chance of probe replacement where voltage variability is _____. Thus, the NDE uncertainty for probe wear, when the wear standard is implemented for field applications can be represented by a normal distribution with a mean of _____, and a standard deviation of _____ with a cutoff on the distribution at an error of _____.

3.9 Bobbin Coil Analyst Variability

To assess analyst variability on voltage measurements, an assessment was performed by comparing voltage measurements from six analysts evaluating the largest indications (included in the evaluation) at TSP intersections found in the 1991 Plant L inspection. The steps included in this assessment of analyst variability included:

- Preparation of eddy current analysis guidelines including Plant L examples.
- Preparation of tapes of bobbin data for the largest indications found in the last inspection. A total of _____ indications were used in the evaluation.
- Selection of six eddy current analysts including primary vendor analysts and subcontracted analysts typically used in Plant L inspections.
- Discussion of the Plant L guidelines with the six analysts utilizing a Westinghouse analyst having previous experience with the guidelines to explain the guidelines using Plant L examples.
- Independent evaluation of the _____ Plant L bobbin indications to obtain data points to evaluate the eddy current analyst variability and define the associated NDE uncertainty.

Figure 3-23 shows the distribution of voltage amplitudes for the _____ indications obtained as the average of the six independent evaluations for each indication. The voltages ranged from about _____ volts to _____ volts with an average amplitude of _____ volts. Figure 3-24 shows the distribution of analyst differences from the mean for each of the _____ indications. The mean of the difference is _____ voltage with _____ of the _____ data points between _____ and _____ volts. The distribution is narrower than a normal distribution and shows exponentially decreasing trends from the _____ voltage difference peak of the distribution. At cumulative probability, the analyst variability is _____ volts or _____ of the _____ average voltage.

Based on this evaluation, a uncertainty at cumulative probability was derived and can be applied for the eddy current analyst variability as part of the NDE uncertainty. Assuming a normal distribution for the data of Figure 3-24 yields a standard deviation of or an uncertainty of cumulative probability. The normal distribution assumption thus yields a conservative estimate of the analyst variability uncertainty.

3.10 Assessment of Throughwall Holes and Slots for Voltage Normalization

As an alternative to the ASME hole bobbin voltage normalization, it is possible to normalize voltages to throughwall holes or slots. The most desirable voltage normalization would result in the smallest difference in crack voltages between different probe designs. In Section 3.4, it was shown that normalization to the holes resulted in small differences between the Zetec and Echoram probes for model boiler specimens. The model boiler data, which has increased somewhat since the Section 3.4 evaluation, can be used to assess throughwall hole and slot voltage normalizations. This assessment is described in this Section.

The comparison of the Zetec and Echoram probes, based on ASME hole normalization as measured, was updated to include the complete model boiler database for indications measured with both probes. Figure 3-25 shows a plot of the measured Zetec versus Echoram voltages. The overall agreement between the probes is seen to be good with a few larger differences which would include analyst variability as well as probe differences. The probe to probe difference can be quantified by the distribution of the ratio of Echoram to Zetec voltages as shown in Figure 3-26. The mean ratio between probes is with an overall spread between . The Echoram probe tends on the average to yield higher voltages than the Zetec probe for the hole normalization.

To assess alternate voltage normalizations against the model boiler data, it is necessary to develop voltage adjustment factors for each probe to modify the data obtained with the hole normalization. Alternate normalizations were evaluated using throughwall holes of inch diameter (ASME standard hole) and throughwall slots of inch length. Voltages for each probe for these throughwall defects were obtained by normalizing each probe to volts on the laboratory standard hole at the kHz mix. The results for alternate probes and the ratio to the Zetec laboratory probe are shown in Table 3-10. A new Zetec probe of the same design as the laboratory probe was included in the data collection and found to yield the same voltage response as the laboratory probe. The Echoram laboratory probe is seen to yield higher voltages for throughwall holes than the Zetec probe and higher voltages for the inch EDM slot. The Echoram probe showed better agreement with the Zetec probe for inch slots than for the shorter slot or throughwall holes. An alternate Echoram probe design (BPRMS versus lab. FSBM) resulted in lower throughwall voltages than the Zetec probe.

Based on the results of Table 3-10, Echoram laboratory probe voltages obtained with hole normalization must be reduced by a factor of _____ for throughwall holes and _____ for throughwall slots. Figures 3-27 and 3-28 show the comparisons of the Zetec and Echoram probes for the hole normalization while Figures 3-29 and 3-30 show the comparisons for the slot normalization. The mean ratio of Echoram to Zetec voltages for the model boiler specimens, which was _____ for the _____ hole normalization, is _____ for throughwall hole normalization and _____ for the throughwall slot normalization. Thus the throughwall hole normalization offers no improvement on probe to probe differences over the _____ hole while normalization to the short slot offers about a _____ improvement. The _____ throughwall inch slots yield a voltage of about _____ volts for the current _____ normalization which is well above the voltage range of interest for ARC applications. Overall, it is judged that the throughwall hole or slot voltage calibrations yield negligible improvement in probe to probe differences over the _____ ASME hole calibration. Consequently, the _____ hole normalization is retained for ARC applications.

It can be noted from the results of Table 3-10 that different throughwall hole standards yield about _____ differences in voltage responses even after the voltages were adjusted for the measured hole size to _____ inch holes. These differences are likely due to both measurement tolerances on the actual hole sizes and to variations in axial alignment between holes along the tube axis. Thus it would not be expected that use of throughwall holes for voltage normalization would substantially reduce the standard to standard variability compared to the _____ ASME holes. Cross-calibration of throughwall hole standards to a laboratory reference standard appears as desirable for throughwall holes as for _____ holes.

The differences in throughwall hole and slot voltages were also obtained for 3/4 inch diameter tubing as shown in Table 3-11. In this case, the hole and slot dimensions were scaled from the 7/8 inch tubing values by the diameter ratio to obtain scaled voltages. The probe to probe differences in voltage responses are similar to the 7/8 inch tubing results. The ratios of the 7/8 to 3/4 inch tubing voltages for the throughwall simulations are given in Table 3-12. On a theoretical basis, ratios of _____ would be expected for throughwall holes and slots based on the diameter ratio squared for holes and the diameter ratio for slots. The measured ratios are essentially the theoretical ratios for the smaller hole and slot sizes measured as given in the table. However, the ratios decrease for both larger hole and slot sizes. These results indicate that a constant voltage ratio between 7/8 and 3/4 inch tubing should not be expected to obtain equivalent voltages for structural or tube integrity considerations. Thus merging of the 7/8 and 3/4 data sets should not be expected for a constant voltage factor unless an increased voltage uncertainty or spread in the data is acceptable for the merged data sets.

Data obtained in this study was also used to assess the bobbin voltage dependence on throughwall hole diameter as shown in Figures 3-31 and 3-32. It is seen that the measured values support the expected diameter squared dependence of voltage on hole diameter. Also included in this study is the sensitivity of bobbin voltages to the use of a _____ foot cable extension.

Laboratory measurements are often made without a cable extension while field measurements involve use of cable extensions. For comparisons of laboratory and field voltages, it is desirable to know the influence of cable length. Figure 3-33 shows the ratio of voltages with the cable extension to those without the foot extension. For voltages above about volt, which are of primary interest to ARC applications, the influence of cable extensions is less than on bobbin voltages. Below volt, the influence of cable length is about . Thus it is acceptable for ARC applications to measure voltages with or without a cable extension.

3.11 NDE Conclusions

1. The use of probes from Echoram or Zetec has negligible influence on voltage amplitude measurement, as demonstrated by measurements of model boiler specimens.
2. Alternate TSP designs have minor influence on bobbin voltage measurements with differences bounded by about and drilled stainless steel, quatrefoil and eggcrate designs tend to yield slightly higher voltages than drilled carbon steel TSPs.
3. Small indications, where their amplitude approaches the size of the mix residual, can be influenced by the presence of the support.
4. The eddy current response is essentially unaffected () for a packed tube to tube support plate crevice as compared to an open crevice.
5. Large amplitude cracks which are likely to have oxide coating on the crack surfaces remain detectable by eddy current in the presence of minor denting. Small amplitude cracks and cracks with clean surfaces (i.e., fatigue generated cracks) may be masked by the dent signal for dented intersections.
6. Use of ASME standards cross calibrated against the reference laboratory standard for the ASME hole are recommended for application of the tube repair criteria. Calibration at the mix frequency minimizes effects of variations in frequency response between probes. Calibration at kHz can be performed if, for the probes used in the inspection, the ratio of the mix to kHz voltage is the same as obtained for the laboratory probes within about .
7. NDE uncertainties contribute to the spread or uncertainty in the voltage vs. burst pressure correlation and tend to lower the structural limit for tube burst which is based on the lower confidence interval. The use of reference calibration standards, frequency mixes, etc., are directed toward minimizing the NDE uncertainties associated with voltage measurement repeatability. Other NDE considerations remain as part of the burst correlation uncertainty although the principal variable in the burst uncertainty is crack morphology differences.

8. Probe centering characteristics, related to probe wear, can contribute to the uncertainty of the eddy current signal. This uncertainty was found by probe wear test simulations to have about a standard deviation. Probe wear influence on the signal uncertainty can be controlled by the use of an appropriate wear standard. The staggered hole standard can be applied to limit the upper bound voltage amplitude uncertainty from probe wear to .
9. Eddy current analyst variability was evaluated for Plant L indications (from the 1991 outage) utilizing six analysts typical of personnel utilized at Plant L inspections. Evaluation of the bobbin voltage differences between the six analysts and the average amplitude from the six analysts' data leads to a bobbin voltage uncertainty of at cumulative probability.
10. Voltages obtained with the French and Belgian voltage normalizations can be adjusted to the ARC normalization using a correlation obtained from field data.
11. Voltage calibrations based on throughwall holes or slots yield negligible improvement in probe-to-probe voltage variability over the ASME hole calibration based on measurements of cracks in model boiler specimens.

Table 3 - 1

Comparisons of Voltage Amplitudes for 7/8" Tubing
Between U.S. - ASME and European Standards

Table 3 - 2

Bobbin Coil Detectability of IGA Samples

Table 3 - 3

**Comparison of the EDM Notch Amplitude of Probe ZT and Probe ER
(Ratio Probe ZT / Probe ER)**

Table 3 - 4

**Comparison of ASME Hole Amplitude Response of Probe ZT and Probe ER
(Ratio Probe ZT / ER)**

Table 3 - 5

Support Plate Configuration Matrix

	<u>Drilled</u>	<u>Quatrefoil</u>	<u>Eggcrate</u>
Material			
Carbon Steel	X		X
Stainless Steel	X	X	
Crevice Condition			
Open	X	X	X
Packed	X		

Table 3 - 6

**Comparison of Tight (Magnetite Packed) and Open Crevices
for Probe ZT and Probe ER
(Ratio Tight/Open)**

Table 3 - 7

Influence of Denting on Indication Response

Table 3 - 8

Variables Influencing NDE Voltage and Burst Correlation Uncertainties

NDE Voltage Uncertainties (Voltage Repeatability)

- Probe centering: probe diameter and wear considerations⁽¹⁾
- Calibration standards: dimensional tolerances⁽²⁾
- Probe design differences⁽³⁾

Burst Correlation Uncertainties

- Crack morphology (length, depth, ligaments, multiple cracks, IGA involvement) variability for same voltage amplitude
- Tubing dimensional tolerances⁽⁴⁾
- Variations in field crevice conditions (open, packed, deposits, TSP corrosion, small dents, etc.)⁽⁵⁾
- Effects of tube pull forces on crack morphology and associated burst pressures⁽⁶⁾

Notes:

1. Minimized in the field during APC implementation by use of a hole probe wear standard.
2. The influence of dimensional tolerances of the calibration standards on voltage normalization is eliminated by calibrating the field standards to the laboratory reference standard.
3. Uncertainty minimized by specifying coil to coil spacing (coil centers are separated by mils).
4. The influence of tubing dimensional tolerances as they affect burst pressure are inherently included in the spread of burst pressures from pulled tubes and laboratory specimens.
5. The influence of field crevice conditions as they affect burst pressure are inherently included in the spread of burst pressures from pulled tubes.
6. Results as pre-pull field measured voltages rather than post-pull voltages are used in burst correlation.
7. The use of field voltage measurements for pulled tubes obtained prior to implementing the voltage calibration requirements contributes to the spread or uncertainty contained in the burst correlation.

Table 3 - 9

Channelhead Mockup Probe Wear Standard Test Results

Table 3-10
7/8" TUBING VOLTAGE DEPENDENCE ON PROBE DESIGN - VOLTAGES FOR
VOLT ON ASME HOLE, LABORATORY STANDARD KHZ

Table 3-11
3/4" TUBING VOLTAGE DEPENDENCE ON PROBE DESIGN - VOLTAGES FOR
VOLT ON ASME HOLE, LABORATORY STANDARD

KHZ

Table 3-12
RATIO OF 7/8 TO 3/4 INCH DIAMETER TUBING VOLTAGES

Figure 3 - 1(a) Belgian/French Voltage (7/8" Tubing) Renormalization
to U.S. APC Calibration for Belgian Plant K-1 (1992 Data)
and Model Boiler Data Below Volts

Figure 3 - 1(b). Belgian/French Voltage Renormalization (7/8" Tubing) to
U.S. APC Calibration - Comparison of Correlation with
Model Boiler Data above Volts

Voltage Sensitivity to Crack Network Morphology

Figure 3 - 2. Voltage Sensitivity to Crack Network Morphology

Figure 3 - 3. Bobbin Coil Voltage Dependence on Slot Length and Depth

Figure 3 - 4. Bobbin Coil Voltage Increase Due to Tapers at Ends of Through-wall Axial Slots

Figure 3 - 5. RPC Voltage Dependence on Slot Length and Depth

Figure 3 - 6. Burst Pressure vs Bobbin Coil Voltage for EDM Slots

Figure 3 - 7. Bobbin Coil Voltage Dependence on Diameter of Through-wall Holes

Figure 3 - 8. Photograph of Plant P-2 Pulled Tube With Cold Leg Thinning

Figure 3 - 9. Bobbin Data and Typical Metallographic Sections of 0.75 Inch OD Simulated IGA Specimens

Figure 3 - 10. Inspection Results for 0.875 Inch OD Simulated IGA Specimens

Figure 3 - 11. Voltage Comparison of Indications Found With Two Eddy Current Probes
(kHz Mix)

Figure 3 - 12. Comparison of kHz Mix Amplitude Response from Two Probes
(Model Boiler Specimens)

Figure 3 - 13. Comparison of kHz Mix Phase Response from Two Probes
(Model Boiler Specimens)

Figure 3 - 14. Comparison of Bobbin Signal Amplitudes in Different Support Configurations

Figure 3 - 15. Influence of Support Geometry on Eddy Current Response

Figure 3 - 16. Bobbin Coil Phase Angle Ratios from Different Support Configurations

Figure 3 - 17. Comparison of Tight and Open Crevice Indication Response

Figure 3 - 18

Signal Amplitude (Arbitrary Units) vs. Center-to-Center Coil Spacing

Figure 3 - 19

Probe Wear Calibration Standard

Figure 3 - 20

Bobbin Coil Amplitude Dependence on Probe Wear

Figure 3 - 21

Voltage Variability Due to Bobbin Probe Wear

Figure 3 - 22

Tube Locations for Channelhead Mockup Probe Wear Tests

epri, d33 8905

Figure 3 - 23

Figure 3 - 23 Distribution of Plant L Voltage Indications Used for
EC Analyst Variability Evaluation

Figure 3 - 24 Distribution of Voltage Differences Between Individual Analysts and Mean Values

Zetec vs. Echoram Probe Voltage

ASME Normalization

Figure 3 - 25

Eddy Current Probe Comparison

Echoram Probe/Zetec Probe

Figure 3 - 26

Zetec vs. Echoram Probe Voltage

TW Hole Normalization

Figure 3 - 27

Eddy Current Probe Comparison

Echoram Probe/Zetec Probe (TW Hole Norm.)

Figure 3 - 28

Zetec vs. Echoram Probe Voltage

TW Slot Normalization

Figure 3 - 29

Eddy Current Probe Comparison

Echoram Probe/Zetec Probe (TW Slot Norm.)

Figure 3 - 30

Four Hole Response

kHz Calibration

Figure 3 - 31

Four Hole Response

kHz Calibration

Figure 3 - 32

Influence of Extension

Mix and kHz

Figure 3 - 33

Preliminary Copy

4.0 Pulled Tube Data Evaluation

4.1 Pulled Tube Database Summary

The available pulled tube data base for ODSCC at TSPs in Westinghouse steam generators is summarized in Table 4-1 for both 3/4 and 7/8 inch diameter tubing. The number of 3/4 inch pulled tubes is provided as a general comparison with the 7/8 inch data and is not utilized in the 7/8 inch evaluation of this report. Both tubing sizes have a comparable number of pulled tube intersections although the 7/8 inch tubing has more tube burst data. None of the pulled tubes have been reported as leakers during plant operation. The field eddy current data for all pulled tubes were reviewed for voltage normalization consistent with the standard adopted (see Section 3.1) for the ARC development.

Operating plant leakage experience for ODSCC at TSPs is summarized in Section 4.3. Evaluations of the 7/8 inch diameter, pulled tube burst and leak rate data are given in Sections 4.4 to 4.12. The pulled tube results support ODSCC as the dominant degradation mechanism. The most extensive leak rate and burst test data for 7/8 inch diameter pulled tubes are from Plant L, as described in Section 4.5.

4.2 Tensile Properties of Pulled Tubes and Model Boiler Specimens

The 7/8 inch diameter model boiler specimens have below average tensile properties, while the pulled tube data have both higher and lower tensile properties than average values. The tensile property differences between model boiler and pulled tube data are less for 7/8 inch tubing than found for 3/4 inch tubing. The 3/4 inch model boiler tubing had above average material properties while the 7/8 inch model boiler tubing had properties slightly below average. For the 7/8 inch tubing ARC development, all model boiler and pulled tube burst pressure data are renormalized to approximate average tensile properties (ksi for $S_y + S_u$) for 7/8 inch tubing as described in this section.

Tubing manufacturing data have been utilized to develop mean tensile properties together with the standard deviation and lower tolerance limit at room temperature and 650°F. These data are given in Table 4-2. Also given in the table are the values for ($S_y + S_u$). An $S_y + S_u$ value of ksi (twice the flow stress) at room temperature is used to normalize the measured burst pressures for the model boiler and pulled tube data. The ratio of the Lower Tolerance Limit (LTL) flow stress at 650°F to a ksi flow stress at room temperature is utilized to adjust the voltage/burst correlation obtained at room temperature to obtain the operating temperature LTL correlation.

Table 4-2 also includes the tensile properties for the 7/8 inch model boiler specimens and for each of the available pulled tubes. Since burst pressures are proportional to the flow stress, the measured burst pressures are normalized to approximate mean properties by the ratio of the tubing mean ($S_y + S_u$) of ksi (flow stress of ksi) at room temperature to the tube specific ($S_y + S_u$) given in Table 4-2.

4.3 Operating Plant Leakage Data for ODSCC at TSPs

Table 4-3 summarizes the available information on three suspected tube leaks (3/4 inch tubing) attributable to ODSCC at TSPs in operating steam generators. These leakers occurred in European plants with two of the suspected leakers occurring at one plant in the same operating cycle. In the latter case, five tubes including the two with indications at TSPs were suspected of contributing to the operating leakage. Leakage for the two indications at TSPs was obtained by a fluorescein leak test as no dripping was detected at psi secondary side pressure.

For the Plant B-1 leakage indication, other tubes also contributed to the approximately gpd total leak rate. Helium leak tests identified other tubes leaking due to PWSCC indications. Using relative helium leak rates as a guide, it was judged that the leak rate for the ODSCC indication was less than gpd. These leakage events indicate that limited operating leakage has occurred for indications above about volts in 3/4 inch diameter tubing, which is equivalent to about volts for 7/8 inch tubing.

4.4 Evaluation of Plant A Pulled Tubes

Three tubes from Plant A-1 and five from Plant A-2 with eddy current indications have been pulled and destructively examined. Two TSP intersections from Unit-1 and three from Unit-2 have been leak and burst tested in support of ARC. The NDE and destructive examination data are summarized in Table 4-4. Four of the tubes were pulled explicitly to support ARC applications and have bobbin voltages cross calibrated to the reference ASME laboratory standard. The bobbin voltages range from volts and include the highest bobbin voltages for 7/8 inch diameter, domestic pulled tubes. The destructive exam depths ranged from . Crack morphologies range from a dominant single crack to axial SCC plus cellular corrosion patches.

Tube R21C22 from Unit-2 has been identified as a potential low leakage outlier for the leak rate correlation based on statistical analyses. This indication is moderately above the mean burst correlation and does not indicate potential outlier behavior for burst. The remaining Plant A tubes show burst and leakage behavior near the mean of the correlations. As noted in Table 4-4, Tube R21C22 was plugged in 1986 with a volt indication (volt in original field call) and pulled in 1990 with a volt signal. The bobbin voltage of volts for this indication is much higher than expected compared to R4C73 which has a very similar 2

crack size and morphology. The destructive exam results for these tubes described in Section 2 show the crack morphologies for R21C22 and R4C73. Crack sizes and morphologies are comparable except that R21C22 has mils of IGA penetration on the crack face while R4C73 has mils. Other pulled tube exams of tubes plugged for multiple years prior to removal have shown greater IGA involvement than tubes active prior to the tube pull. It is expected that the 4 years of tube plugging for R21C22 increased the IGA involvement which likely increased the bobbin voltage from volts. The IGA involvement of R21C22 would have negligible influence on the burst pressure or leakage of this indication. Thus the bobbin voltage of volts for R21C22 is judged more appropriate for ARC applications and is used for the ARC database.

Tube R20C26 from Unit-1 was not burst tested and would not leak at SLB conditions and is only used for ARC applications as a non-leaker in the probability of burst correlation. Tube R31C46 was not leak or burst tested and since either leak or no leak cannot be assured for this indication, it is not used for ARC applications. The two Unit-1 freespan burst pressures are used as typical undegraded or NDD burst pressures in the burst correlation to help anchor one end of the burst correlation.

4.5 Evaluation of Plant L Pulled Tubes

Eight tubes and 24 intersections were pulled from Plant L in 1991. Twenty-three intersections were destructively examined and 21 intersections were burst tested. An evaluation of these pulled tubes with emphasis on the NDE data is documented in Revision 0, Volume 1 of this report. Table 4-5 summarizes the NDE and destructive examination results for the Plant L tubes.

Statistical analyses indicate that four of the indications (R8C69-1 and 2, R12C70-1, R29C70-2) are potential low burst pressure outliers in the burst correlation with R8C69, TSP-1 being the lowest potential outlier in the current database. Appendix C provides a discussion of crack morphologies for ARC applications including the influence of morphology and ligaments on bobbin voltage response. It is concluded in Appendix C, using the Plant L potential outliers as examples, that the presence of uncorroded ligaments between microcracks is the principal contributor to outlier behavior in the burst/voltage correlation in the voltage range less than about volts. This conclusion applies to the Plant L potential outliers. It is also shown in Appendix C that burst capability is determined by the most limiting single macrocrack and is essentially independent of the more detailed crack morphology such as the presence of ligaments or cellular patches. Since the Plant L pulled tubes with remaining ligaments are a typical low voltage morphology and are low burst outliers (non-conservative), all indications of Table 4-5 are retained in the burst correlation. None of the indications leaked when pressurized to SLB conditions so they are not used in the leak rate correlation but are included as non-leakers in the probability of leakage correlation.

4.6 Evaluation of Plant D Pulled Tubes

Plant D was one of the first domestic plants to identify ODSCC at TSPs based on pulled tube exams in the 1983 to 1985 time frame. Tubes with bobbin indications analyzed to ARC eddy current analysis guidelines (bobbin reevaluation) are given in Table 4-6. Three indications on tube R7C38 were leak tested by pressurization and burst tested with results given in the table. The remaining 1984 to 1985 tubes were destructively examined without burst testing. The R7C38 burst results are included in the burst correlation and all Plant D-2 indications of the table are inferred as non-leakers in the probability of leakage correlation.

In 1992, 3 tubes and 8 intersections were pulled from Plant D-1 in direct support of ARC applications. The NDE, leak and burst test results for these indications are given in Table 4-6. All indications were burst tested and two were leak tested. The remaining indications can be inferred as non-leakers based on maximum crack depths. One indication was not detected and found to have a maximum crack depth of . This indication is included as an NDD in the burst correlation to support the very low voltage trend for the correlation. All five burst results for bobbin indications were identified by statistical analyses as high burst outliers in the burst correlation. These indications have high bobbin voltages for the relatively shallow depths (maximum of). As discussed in Appendix C, these indications have few remaining uncorroded ligaments which result in unusually high voltages for shallow indications. Plant D has implemented primary pressure and temperature reductions to reduce crack initiation and growth. Growth rates are the lowest for plants evaluated to date. It is believed that the low growth rates tend to cause corrosion of remaining ligaments between microcracks without significant growth in depth. Given the low growth rates and high bobbin voltages for the Plant D-1 tubes, the voltages are atypical of the dominant database for ARC application. For this reason, the burst results are not included in the ARC database for burst or leakage.

4.7 Evaluation of Plant P-1 Pulled Tubes

Two tubes and six intersections were removed from Plant P-1. Five intersections were destructively examined. The results are summarized in Table 4-7. Three indications were not reported in the field analysis while two of the three indications were identified by reevaluation applying guidelines for ARC applications. Data is not available for cross-calibration of the field ASME standards to the reference laboratory standard. Crack morphologies were found to be dominant axial indications with significant cellular involvement.

Tube R11C48, TSP 1 was burst inside the TSP so that the burst test result is not applicable for ARC applications. The two burst results for R16C60 are included in the burst database. The four indications with reevaluated bobbin voltages are included as non-leakers in the probability of leakage correlation.

4.8 Evaluation of Plant J-1 Pulled Tubes

As noted in Table 4-1, French pulled tube data are available for 13 intersections with known voltages and maximum crack depths. Data on 4 tubes and 8 intersections are available from Plant J-1. In general, burst tests in France are performed with the indication within a simulated support plate and the data are not applicable to domestic ARC applications. One burst test (R5C28, TSP 2) was performed in free span without a TSP. Six leak tests were performed for which 2 had quantified leak rates, 3 were non-leakers and 1 had leakage but not quantified. The Plant J-1 data for which leak and/or burst tests were performed are summarized in Table 4-8.

The leak tests were performed at room temperature using demineralized water. No repeat measurements were made during the leak rate tests. The leak rate for R8C74, TSP1 at SLB conditions ($\Delta P =$ psi) is smaller than for R22C26 even though the leak rate at normal operation was higher and the voltage for R8C74 is higher. A possible explanation, based on EdF observations from the destructive exam, is that R22C26 had more short throughwall indications than R8C74. The large increase in the leak rate between normal operating and SLB conditions for R22C26 indicates that ligament tearing was likely significant at higher ΔP s for this specimen. It is not clear whether testing at temperature would have resulted in a higher leak rate due to ligament tearing for R8C74. However, the low leak rate at the high voltage of R8C74 does not appear to be prototypic and is not recommended for incorporation in the ARC database. The burst pressure for R5C28, TSP2 and the SLB leak rate for R22C26, TSP1 are included in the burst and leak rate correlations, respectively. All indications are included in the probability of leakage correlation with R9C22, TSPs 1 and 2 inferred as a leaker and non-leaker, respectively.

Table 4-8 includes five indications for which only bobbin voltages and maximum depths from destructive exams have been reported. These results are included as inferred non-leakers in the probability of leakage correlation.

4.9 Evaluation of Plant F Pulled Tubes

Three tubes with 5 intersections were pulled from Plant F in 1993. These tubes were removed from the cold leg and represent the only cold leg tubes pulled for ODS/CC at TSPs. Table 4-9 summarizes the NDE and destructive examination data. The bobbin voltages from the field and laboratory reevaluation of the field data are in reasonable agreement. The TSP intersections were distorted from tube pulling operations such that post-pull bobbin voltages are not considered to be reliable and are not given in Table 4-9. The destructive examination results show very shallow indications with maximum depths between and and average depths of . There are small differences in depths between the bobbin NDD

indication at R13C42, TSP2 and the other indications having up to volt indications. The NDD indication has the shorter crack length of inch, compared to inch for the other indications. Since the indications had very shallow depths by NDE examination, leak tests were not performed. The indications can be inferred as non-leakers for probability of leakage considerations.

All five burst pressures are in the range of psi. Burst tests of undegraded free span tube sections were in the range of psi. Thus, the burst pressures are negligibly affected by the shallow indications. As given in Table 4-2, the tensile properties for these tubes are relatively low, which is consistent with the relatively low undegraded burst pressures. When normalized to $\sigma_y + \sigma_u =$ ksi, the burst pressures are about psi, which is consistent with undegraded tubing.

The bobbin voltages for the Plant F pulled tubes are very high for the shallow indications with high burst pressures. These indications were identified as high outliers in the burst pressure versus voltage correlation based on statistical analyses for outliers. None of the burst cracks had any remaining uncorroded ligaments. As discussed in Section 4.6 and in Section C.5 of Appendix C, the absence of uncorroded ligaments in shallow cracks leads to high voltage responses compared to the more common presence of ligaments in shallow cracks. This behavior is similar to that found for Plant D-1. Like Plant D-1, Plant F has been found to have low growth rates. This may be due to the fact that the Plant F tubes were pulled from the cold leg. The high voltages and high burst pressures of the Plant F tubes represent, like Plant D-1, a conservative departure from the remaining pulled tube and model boiler database. This is due to differences in crack morphology (no ligaments in shallow cracks.). Inclusion of the Plant F tubes in the burst correlation would raise the mean and the standard deviation for the correlation in a manner not representative of most pulled tube and model boiler specimens. Due to the atypical crack morphology and associated high voltages, the Plant F burst pressures and leakage data are excluded from the correlation database. The ARC repair limits developed without including the Plant F results can be conservatively applied to Plant F.

4.10 Evaluation of Plant W-1 Pulled Tubes

One tube (R6C58) with two intersections was removed from Plant W-1 in 1993. Table 4-10 summarizes the NDE and destructive examination data for this tube. No significant differences were found for the bobbin voltages between the field evaluation and laboratory reevaluation of the field data. Cross-calibration of the field ASME calibration standard to the reference laboratory standard was not performed. Post-pull bobbin volts were only slightly increased above pre-pull values, while RPC volts increased by about . The field and laboratory RPC crack indications were well rounded, which is suggestive of cellular patches as were found in the destructive exam (see Section 2). The second TSP indication was noisy, with a long patch discernable in the data.

The first TSP indication was leak tested and found to have no leakage up to a pressure differential of psi. Both indications were burst test with the results given in the table. Tensile properties were obtained from the pulled tube with results given in Table 4-2. Statistical analyses for outliers would indicate that the first TSP indication is a somewhat low burst pressure outlier. The burst pressure of psi is consistent with expectations for a crack of average depth. The burst crack opening was inch long, indicating significant tearing for the burst. The measured burst pressure from an undegraded free span section of the tube was psi, which is also consistent with the tensile properties of this tube. Thus, there is no basis to question the adequacy of the burst test and no indication that the cellular morphology influenced the burst pressure. Thus, it is expected that the bobbin voltage is lower than typical for the crack size. However, this indication had no remaining uncorroded ligaments in the burst crack face, whereas remaining ligaments are the most common cause for lower than expected voltages. There is no identifiable cause for the potential outlier, and both of the Plant W-1 burst data points are included in the burst correlation database.

4.11 Pulled Tubes With Axial Indications Extending Outside the TSP

Seven pulled tube indications from four plants have been identified to have axial indications extending outside the TSP. These are the only reported indications from more than 150 TSP intersections for which data has been reviewed. The seven indications are described in Appendix C. Overall, the pulled tube exams show that the indications outside the TSP are intermittent and generally result from additional initiation sites. There is no evidence that crack growth from indications within the TSP leads to crack extension outside the TSP.

4.12 Burst Pressures for Indications Burst Inside the TSP

NRC Regulatory Guide 1.121 guidelines indicate that tube repair limits, under normal operating conditions, should maintain a burst capability of three times normal operating pressure differential. Under normal operating conditions, ODSCC at TSPs is contained within the TSP and potential burst is constrained by the TSP. Thus burst pressures for indications burst inside the TSP are of interest for comparisons with the regulatory guide. Pulled tube burst test results with TSP constraint are given in Table 4-11. These results indicate burst capability with TSP constraint well in excess of regulatory guidance.

4.13 Summary of Pulled Tube Results

Table 4-12 summarizes the pulled tube burst and leak rate measurement results. Data not included in burst and leak rate correlations are indicated as NP (non-prototypic) or NR (not reliable). Bobbin voltages given in the table for ARC applications are based on laboratory reevaluation of the field eddy current data tapes. This assures that bobbin voltages are

evaluated to ARC analysis guidelines. Differences between analysts are accounted for in eddy current uncertainties for ARC applications. The leak rates and burst pressures in Table 4-12 are as-measured. Leak rates are adjusted to reference conditions in Appendix B and summarized in Section 6.2. Burst pressures for ARC correlations are adjusted to a reference flow stress using the material properties of Table 4-2. Adjusted burst pressures are given in Section 6.2.

Table 4-12 does not include all pulled tube data for the probability of leakage correlation. Additional data for this correlation are given in Tables 4-4 to 4-8 for indications having leakage inferred from the crack morphology. An additional data point included in probability of leakage was obtained from Plant M-1 which had a bobbin voltage of volts, an IGA crack morphology and an inferred no leakage based on a destructive exam maximum depth of

The pulled tube database showing bobbin voltages as a function of maximum crack depth from destructive exam is shown graphically in Figure 4-1. The data show a broad trend for voltage to increase with depth. The smallest voltage found for a throughwall crack in the current 7/8 inch diameter data is volts.

Appendix C provides an assessment of crack morphologies for ARC applications. It is concluded that all crack morphologies found in pulled tubes for indications at non-dented TSPs are acceptable for ARC applications. None of the data suggests any need to limit morphology variations for ARC. Comparisons of measured and predicted burst pressures show that burst capability is dominated by the length and depth profile of the most limiting macrocrack and is minimally influenced by morphology and the spread in the burst correlation (and to a lesser extent, the leak rate correlation) results from morphology influence on voltage. In the lower voltage range (volts), voltage response is reduced by the typical uncorroded ligaments between microcracks forming the limiting macrocrack.

Table 4-1

Number of Pulled Tubes with NDE and Destructive Exam Data

Table 4-2

Tensile Properties for Model Boiler and Pulled Tubes
(7/8" Diameter)

Table 4-2 Continuation

Table 4-3

Field Experience: Suspected Tube Leakage for ODS/CC at TSPs⁽¹⁾

Table 4 - 4

Plant A Pulled Tube Results

Table 4 - 5
Plant L Pulled Tube Results

Table 4 - 6
Plant D Pulled Tube Results

Table 4 - 7

Plant P - 1 Pulled Tube Results

Table 4-8
Plant J-1 Pulled Tube Leak Rate and Burst Test Data

Table 4-9
Plant F Pulled Tube Results

Table 4 - 10

Plant W - 1 Pulled Tube Results

Table 4 - 11

Pulled Tube Burst Capability for Indications Within TSP

Table 4 - 12: Pulled Tube (7/8" Diameter) Leak Rate and Burst Pressure Measurements

Table 4 - 12: Pulled Tube (7/8" Diameter) Leak Rate and Burst Pressure Measurements

Figure 4-1: Bobbin Coil Voltage vs. Maximum Examination Depth
7/8" Pulled Tubes Data, Destructive Examination

5.0 Laboratory Specimen Preparation and Testing

5.1 Model Boiler Specimens

The Forest Hills Single Tube Model Boiler test facility consists of thirteen pressure vessels in which a forced flow primary system transfers heat to a natural circulation secondary system. Test specimens are placed around the heat transfer tube to simulate steam generator tube support plates. One to six tube support plate crevice assemblies are typically included in a given test. A schematic of the test facility is presented in figure 5-1, and typical thermal and hydraulic specifications are presented in table 5-1. As indicated in the table, these specifications are representative of those in a pressurized water reactor steam generator.

Six series of Single Tube Model Boiler tests have been performed to provide test pieces having ODS/SCC for subsequent nondestructive examination, leak rate measurements, and destructive examination. The first series consisted of 19 archive crevice assemblies which were produced in previous Westinghouse-funded testing; the second and third series each consisted of eight crevice assemblies; the fourth series contained 45 crevice assemblies, while the fifth and sixth each contained eight assemblies. The later test series were performed to provide additional specimens, with an emphasis on producing specimens having lower voltage eddy current signals. Series 6 tests attempted to promote intergranular attack (IGA), as well as stress corrosion cracking.

Series 1 Tests: Of the 19 archive crevice assemblies which comprised the Series 1 tests, several had no detectable cracks or were not used due to having voltages which were larger than those observed in pulled tubes. The archive test pieces used for this program are summarized in table 5-2. The test pieces are listed by their tube designation and their location on the tube. The sludge type refers to the manner in which sludge was placed in the tube support plate crevices. Chemically consolidated sludge is formed by baking a mixture of sodium hydroxide, sodium silicate and sodium phosphate with the sludge; mechanically consolidated sludge is formed by hydraulically pressing the sludge into the tube support plate, drilling a hole in the sludge, and sliding the tube through the hole; the fritted design uses an Inconel sinter at each end of the crevice to hold the sludge in place. The test containing an eccentrically mounted tube support plate, in which the sludge was removed from the crevice, was used to simulate chemical cleaning. All tests utilized simulated plant sludge, consisting of approximately

The cracks were produced in what is termed the reference cracking chemistry, consisting of either a _____ solution in the makeup tank. Because of hideout in the crevices, the boiler concentration is typically about _____ of the makeup tank concentration. Hydrazine and ammonia are also added to the makeup tank for oxygen and Ph control, respectively.

The tubing used for the tests was taken from Heat 2675, except for specimens 500, 509 and 510 which were taken from Heat 3244. This heat of mill annealed Alloy 600 was fabricated by Westinghouse and has been used extensively in other stress corrosion cracking programs. The tubing has a 0.875 inch outside diameter.

Series 2 Tests: The initial program test pieces consisted of eight crevice stimulants which were mounted on two tubes. These tests were specified to produce rapid throughwall cracking, so that the reference cracking chemistry was utilized. Heat 2675 was also used for these tests. One test utilized chemically consolidated simulated plant sludge (tube 543), while the other used mechanically consolidated sludge (tube 542). The sludge filled the entire crevice volume. Primary to secondary leakage was noted in the chemically consolidated test after days of boiler operation, and in the mechanically consolidated test after days of operation. During the subsequent nondestructive examination (NDE), indications were identified adjacent to the Teflon collars used to support the tube support plates, as well as within the support plates. The bobbin probe voltages were found to be higher than those typically encountered in plant eddy current examinations. As a consequence, subsequent tests were designed to produce smaller cracks.

Series 3 Tests: Since the NDE of the archive and Series 2 test pieces produced higher voltages than are measured in steam generator tube support plate crevices, the sludge configuration of the Series 3 tests was modified to produce shorter cracks. Two tests were specified, with each containing four test specimens. Both tests utilized chemically consolidated sludge, with the sludge occupying a arc and inch height of the tube support plate crevice. As in the Series 1 tests, Westinghouse heat 2675 was used for the tubing.

Tube 557 utilized simulated plant sludge and was treated with the reference cracking chemistry, in order to produce accelerated SCC. Tube 558 utilized chromium oxide for crevice packing and was treated with the cracking chemistry. Previous testing has found that using chromium oxide rather than simulated plant sludge promotes IGA rather than SCC. It was believed that field experience with IGA produces lower bobbin probe voltages than does SCC. The chemistry was specified because it was hypothesized that it would produce less grain boundary corrosion, and therefore lower voltages.

Through wall cracking of tube 557 was produced after days of operation. NDE of the tube indicated the voltages to be generally lower than in the previous tests, but still well above what is typically found in the field in TSP crevices.

Operation of tube 558 continued with the chemistry for days, at which time the specification was changed to the chemistry in order to accelerate the corrosion rate. The test was then operated for an additional days, at which time a primary to secondary leak occurred. Eddy current inspection identified a throughwall crack at the bottom tube support plate elevation, with the crack producing a volt signal and a indicated depth.

The voltage is typical of field indications of throughwall cracks, while the indicated depth is shallower than what is typically found in the field. Following inspection, the remaining three tube support assemblies were returned to test. Testing continued for an additional days, extending beyond the scheduled program completion date.

Although not originally included in the Series 3 tests, one test piece produced as part of EPRI Program S408-06, "Alloy 690 Qualification: Corrosion Under Prototypic Heat Flux and Temperature Conditions", was subsequently transferred to this program. Test piece 555-3 utilized mill annealed Alloy 600 tubing from heat 2675, and contained a cylindrical hole tube support plate crevice. As in some of the Series 1 tests, the crevice was filled with simulated plant sludge, which was held in place with porous Inconel frits located at both ends of the crevice. The test piece developed a through wall crack following days of operation with the cracking chemistry. Test piece 547-1, also from Heat 2675, was prepared similarly to 555-3 and obtained from another Westinghouse program.

Series 4 Tests: This test series was undertaken after it was found that the test specimens produced in doped steam environments exhibited very low voltages and high leak rates compared to those found in tests of model boiler specimens and tubes pulled from the field. The high leak rates of the specimens produced in doped steam were attributed to the plastic deformation of the tubing required to obtain accelerated corrosion. Consequently, the Series 4 tests were intended to produce both bobbin probe voltages and leak rates representative of those expected to be found in the field.

The Series 4 tests contained 45 specimens, mounted on eight tubes. 23 of the specimen collars were fabricated from Teflon, while the remaining 22 were fabricated from carbon steel. Teflon collars were utilized because the cracks located beneath the Teflon collars in the Series 2 tests typically produced lower bobbin probe voltages than did the cracks located adjacent to the collars.

Unlike the Series 2 and 3 tests, the Series 4 tests used tubes supplied to Westinghouse by the EPRI NDE Center. Tubing Heat 96834, lot 6, was originally fabricated by another NSSS vendor, and is the same as was used in the doped steam testing (see Section 5.2). The heat of material was changed because the doped steam testing found that this heat produced more accelerated corrosion than did the Westinghouse heat.

The design of the test specimens was also modified in order to reduce the magnitude of the eddy current voltages. These modifications are outlined in table 5-3. The specimens in Series 4, Test 1 were configured to fit snugly around the tube (as did the Teflon collars in the Series 1 tests), but the height of the collars was varied between inch. The expectation is that the shorter collars should limit the length of the cracks which can be produced.

The inside face of the specimens in Series 4, Test 2 were machined to produce a grid pattern to limit the crevice area between the tube and the collar. Six holes were first drilled around the periphery of the inside face of the specimen, so that the crevice would have an approximate arc width. Two rings were milled on the face of three of the specimens. The rings had a width of inch, so that the face was divided into three contact regions, with the outer regions having a inch width and the central region having a inch width. A helical pattern was machined into the face of the remaining three specimens, with the width of the helix being inch and the pitch of the helix being inch.

The specimens in Series 4, Test 3 all had a 0.75 inch height, but the diametral gap width was varied between a snug fit (as in Series 4, Test 1), a -mil gap, and a -mil gap. The gap width was varied because previous testing has found that the gap width affects the rate and location of corrosion.

Tests 4 and 5 of Series 4 both utilized chemically consolidated simulated plant sludge located adjacent to carbon steel tube support specimens. Two sets of specimens having thicknesses of inch were used in each test. The sludge was consolidated over a arc width within the crevice. The inch specimens contained one sludge region, which occupied essentially the full thickness of a specimen; the inch specimens contained two sludge regions, separated by a -mil wide band at the center; the inch specimens contained three sludge regions, separated by two bands.

Test 6 of Series 4 contained carbon steel specimens having the same range of thicknesses as in Tests 4 and 5. Instead of using simulated plant sludge, however, the crevices remained empty, with the specimens being held in place with porous Inconel sinters located at each end of the crevice. This design has been used to produce accelerated intergranular corrosion in previous tests.

The reference cracking chemistry was specified for use in Tests 1 through 6 of Series 4. Because of concern that this specification may produce excessive grain boundary corrosion and therefore high bobbin probe voltages, two additional tests (7 and 8) were specified to utilize the chemistry. Test 7 of Series 4 utilized five Teflon specimens, while Test 8 utilized four carbon steel specimens. The specimens utilize a range of designs selected from Tests 1 through 6 of Series 4.

The eight Series 4 tests accumulated between days of operation, depending upon the test. Throughwall cracks had been produced in five test pieces, with a few additional test pieces containing partial throughwall cracks. The designs of the test specimens having throughwall cracks are presented in table 5-4. As indicated in the table, three of the throughwall cracks were produced adjacent to Teflon stimulants in Test 3, while the other two throughwall cracks were produced adjacent to carbon steel stimulants.

The only common feature of the crevice configurations which produced the cracks is that the crevice length was always inch, perhaps suggesting that the shorter crevices could not produce sufficient superheat to promote accelerated corrosion.

Series 5 Tests: Two additional tests were conducted when it became apparent that accelerated corrosion was not being produced in Series 4 tests. The test specifications are summarized in table 5-5. Both tests utilized tubing from heat 2675, the same heat used in the first three series, rather than heat 96834, which had been used in Series 4. Test 575 of Series 5 contained four tube support stimulants having the same fritted design used in the Series 1 tests. The test was conducted because the test piece had been assembled for a previous program, but had not been used. Since this design was known to produce accelerated corrosion, it was hoped that the test could also provide additional crevice assemblies having small indications. While throughwall cracking was produced after days of boiler operation, the associated eddy current signals were on the order of volts, so that no further evaluation of the crevice assemblies was performed.

Test 576 of Series 5 was configured to produce small cracks, as was the intention of the Series 4 tests, while maintaining local crevice superheats in the same region as in the tests which produced accelerated corrosion. The crevices contained two sludge regions: a larger outer region of chromium oxide and a smaller inner region of simulated plant sludge. The expectation was that the cracking would be confined to the inner region, while the outer region would increase the superheat to values comparable to those in the early tests. Two of the crevice assemblies were specified to have the simulated plant sludge occupying the center of the top half of the chromium oxide region, while the other two crevice assemblies were specified to have the simulated plant sludge centered in the chromium oxide. In both cases, the inner region had a width of inch and a height of inch.

The test operated for days with the reference cracking chemistry, plus an additional days with the chemistry, when it was shut down because of a primary to secondary leak. Subsequent eddy current evaluation identified indications at two locations. Both locations correspond to crevice configurations in which the simulated plant sludge was centered both axially and circumferentially with respect to the chromium oxide. An RPC evaluation identified three cracks; two were in the simulated sludge, while the third was in the chromium oxide. These results suggest that the two-region sludge configuration is a potential means of producing smaller cracks in model boiler specimens.

Series 6 Tests: Three model boiler tests were conducted in an effort to achieve accelerated intergranular corrosion. The test pieces were included in the program after through wall corrosion was obtained in two of the tests. The test specimens which underwent leak and burst testing are listed in table 5-6. Modifications made to the test specifications to promote intergranular corrosion included using mechanically consolidated chromic oxide sludge (i.e., a nonoxidizing sludge), increasing the secondary pressure, and increasing the bulk concentration. These modifications were intended to reduce tubing stresses and promote uniform corrodant accumulation within the crevices.

5.2 Doped Steam Specimens

Axial stress corrosion cracks and crack networks were produced in 30 mill-annealed Alloy 600 tubes through exposure to a doped steam environment. The steam was produced from water containing ppm each of chloride, fluoride, sulfate and nitrate anions as salts of sodium. The steam pressure was psi at a temperature of F. Individual specimens were eight inches in length. Stressing was accomplished by clamping the tube at mid length between two flat steel plates, as shown in figure 5-2. Ovalization of the tube resulted in outer fiber tensile yielding on the OD surface of the tube at the maximum diameter. The tube ends were sealed to permit internal pressurization of the tube during the autoclave exposure. The OD surface of the clamped tube was exposed to the psi doped steam environment in a one gallon autoclave. Nitrogen gas was used to pressurize the inside of the tube to psi producing a differential pressure across the tube wall of psi. The development of throughwall cracking was detected by a drop in the internal pressure of the tube.

Table 5-7 summarizes the specimens tested in the doped steam environment. Two heats of mill annealed Alloy 600 tubing were used, Heat 2675 and Heat 96834L. The width of the clamp in contact with the tube was typically inch but larger clamp widths were also used in an attempt to vary the crack morphology. All of the tube displacements were sufficient to cause outer fiber yielding. These displacements ranged from inch. In general, the smaller displacements resulted in shorter crack lengths and an increase in the test exposure time. The eddy current voltages listed in Table 5-7 are preliminary values used to help decide the disposition of the tube. The crack lengths shown in Table 5-7 are from optical measurements on the tube OD surface obtained at low magnification and may differ significantly from destructive examinations. Some attempt to control the length of crack initiation sites was made on the last 7 specimens listed in Table 5-7. Selected portions of these specimens were grit blasted. This procedure had no discernible effect on crack initiation.

5.3 Fatigue Precracked Specimens

Throughwall axial fatigue precracks were developed in 12 mill annealed Alloy 600 tubes by cyclic internal pressurization. A starter flaw was spark machined through the wall of the 0.050 inch thick by 0.875 inch diameter tubing with a length of inch. Cyclic internal pressurization then was used to grow the crack throughwall. A soft plastic bladder seal was then inserted in the tube and cracks up to inch in length were grown by a fatigue process. The pressure was adjusted during fatigue precracking to maintain the maximum applied stress intensity factor below $\text{ksi}\sqrt{\text{in.}}$. The maximum plastic blunting of the crack tip was thus kept below inch. Table 5-8 lists the fatigue precracked specimens, crack lengths and number of cycles. The fatigue precracked samples have well characterized leak rates from previous evaluations, although the leak rates are large compared to those for ODSCC cracks. These samples were used in studies of the effect of denting at tube support plate intersections on leak rates through cracked tubes.

5.4 Chemically Dented Tubes

Fatigue precracked tubes and tubes with stress corrosion cracks were used to simulate cracked tubes in tube support plates which are also dented. Carbon steel collars were used to simulate tube support plates. These collars were drilled with the nominal clearance hole for 0.875 inch diameter tubing. The collars were then packed with magnetite using a hydraulic press. The pressed magnetite was drilled out to a tight fit hole for insertion of a precracked tube. The final configuration was a carbon steel collar with an inside diametral clearance of _____ inch, a pressed _____ inch layer of magnetite and then the tube wall. The ends of these specimens were sealed and the specimens were exposed to a _____ M cupric chloride solution in an autoclave at _____ F.

Corrosion of the carbon steel and a smaller reaction layer with the Alloy 600 tubing resulted in corrosion products which tightly packed the tube-tube support plate crevice and led to a small amount of denting of the tube. Table 5-9 lists the dented specimens, the eddy current dent voltage and the average estimated radial dent size.

A section through the tube and collar of specimen Trial-1 is shown in figure 5-3. The packed magnetite and the corrosion products in the crevice are clearly evident. A scanning electron photograph of the polished section in figure 5-3 shows several layers of corrosion products along with the starting layer of packed magnetite. The EDS nickel and iron maps of figure 5-4 show that the corrosion product adjacent to the Alloy 600 tube is enriched in nickel and somewhat depleted in iron. The corrosion product adjacent to the carbon steel collar appears to have the same iron content as the packed magnetite layer. The corrosion product layers in general appear to be relatively dense and any leakage path would be highly tortuous.

5.5 Crack Morphologies

Plugging criteria which are partially based upon eddy current characterization, leak rate and burst strength testing of laboratory specimens depend upon a reasonable simulation of actual service produced cracks. The crack morphologies of service tubes, doped steam test specimens and model boiler test specimens are presented in this section. An intergranular mode of cracking is common to cracks produced in these three environments. Figure 5-5 illustrates this fact with scanning electron fractographs. A further illustration of intergranular cracking is provided by the metallographic details shown in figure 5-6.

Stress corrosion cracking patterns on the OD of Alloy 600 tubes at tube support plate intersections range from a few to many axial cracks distributed around the circumference of the tube. The model boiler test specimens also show this characteristic. Figure 5-7 shows several arrays of cracks and a larger single crack. The cracks in the doped steam specimens tend to be either a single axial network or axial cracks _____ degrees apart. This is due to the nature of loading of the doped steam specimens. Clamping of the tube leads to a _____ degree symmetry of stresses, bending across the wall thickness and outer fiber bending stresses beyond the yield point.

In model boiler specimens, as in actual tube support plate intersections, the stresses are uniform around the circumference of the tube and the occurrence of single or multiple axial cracks is controlled by the crevice conditions. The differential pressure hoop stress is relatively low, about ksi. Hence the model boiler specimens experience essentially prototypic loading while the doped steam specimens experience stresses far beyond actual service conditions. The doped steam environment is substantially less aggressive than that produced in the model boiler tests and thus clamping loads are required in addition to the pressure stress to produce cracking in reasonable lengths of time. The high stress clamped condition of the doped steam specimens led to a higher degree of throughwall cracking for a given total axial crack network length and hence higher leak rates at a given eddy current bobbin coil voltage. Another complicating factor is the fact that relaxation of the throughwall bending stresses when the clamping fixture is removed can lead to contact across the faces of the crack. This would provide an eddy current path and reduce the bobbin coil voltage relative to a crack with non-contacting faces, as in the model boiler specimens. The above considerations indicate that the clamped test condition of the doped steam specimens produced non-prototypic stress corrosion cracks, particularly as they relate to any correlation between bobbin coil voltage, leak rate and burst strength. Therefore, only the model boiler specimen test results were added to the data base used to develop tube plugging criteria.

5.6 Nondestructive Examination (NDE) Results

The model boiler specimens were eddy current tested in the laboratory using both the bobbin coil probe and the RPC probe. The bobbin coil voltages were measured in accordance with the analysis guidelines used for the EPRI ARC program. In the case of the 7/8-inch diameter tubing, the bobbin coil results reported here are for the kHz mix frequency. The reference calibration was performed with the holes in the ASME standard set to volts in the differential mix channel. The RPC test results are for the kHz frequency with the voltage normalization of volts for the inch long through-wall EDM (electric discharge machining) slot in the ASME calibration standard. Table 5-10 presents a summary of the NDE data for the model boiler specimens. The NDE data of table 5-10 are obtained as received from the model boilers with TSPs in place and packed crevices. A few cases are given for which the NDE measurements were reported following a leak test at normal operating conditions and after removal of the packed crevice condition to obtain an open crevice. In these cases, the force required to remove the TSPs is expected to have changed the crack morphology, such as by tearing ligaments, to result in higher bobbin voltages for the subsequent open crevice measurements. The 7/8-inch tubing analysis guidelines used in the evaluation of the laboratory specimens are consistent with the field 7/8" tube inspection analysis guidelines.

5.7 Leak and Burst Test Objectives

The objective of the leak rate tests is to determine the relationship between eddy current characteristics and the leak rates of tubes with stress corrosion cracks. Leak rates at normal operating pressure differentials and under steam line break conditions are both of interest, since leakage limits are imposed under both circumstances.

The SLB leak rate data are used to develop a formulation between leak rate and bobbin coil voltage.

Crevice condition is another important factor. Tightly packed or dented crevices are expected to impede leakage through cracked tubes. Since denting is readily detectable by non destructive means while crevice gaps cannot be readily assessed, the emphasis is placed upon open crevices and dented crevices as the limiting cases.

Given the assumption that significant support plate displacements cannot be excluded under accident conditions, burst tests of tubes with stress corrosion cracks are conducted in the free span condition and burst pressure is correlated with bobbin coil voltage. This burst pressure correlation is then applied to determine the voltage amplitude that satisfies the guidelines of Reg. Guide 1.121 for tube burst margins.

5.8 Leak Test Procedure

Leak testing of cracked tubes is accomplished as follows. The ends of the tube are plug welded. One end has a fitting for a supply of lithiated (ppm Li), borated (ppm B) and hydrogenated (psia) water to the tube inner diameter. The specimen is placed in an autoclave and brought to a temperature of and a pressure of . The pressure on the outer diameter is brought to psi. A back pressure regulator on the secondary side maintains the psi pressure. Any leakage from the primary side of the tube tends to increase the secondary pressure because of the superheated conditions. The back pressure regulator then opens, the fluid is released, condensed, collected and measured as a function of time. This provides the measured leak rate. The cooling coil is located prior to the back pressure regulator to prevent overheating and to provide good pressure control. Typical leakage duration is one hour unless leak rate is excessive and overheating of the back pressure regulator occurs. Pressure is controlled on the primary side of the tube by continuous pumping against another back pressure regulator set at psi. The bypass fluid from this regulator is returned to the makeup tank.

To simulate steam line break conditions the primary pressure is increased to psi by a simple adjustment of the back pressure regulator and secondary side is vented within one to three minutes to a pressure of psi. The pressure differential across the tube is thus psi. Temperature fluctuations settle out in several minutes and the leakage test period lasts for approximately minutes.

5.9 Leak Test Results

A summary of leak test results is provided in table 5-11. The first series of leak rate tests were conducted at the normal operating pressure differential. Some of the model boiler specimens had tightly packed crevices as a result of corrosion product buildup. These specimens were tested as is. Following this first series of leak rate tests, the welded end plugs were cut from the leak specimens. Because of the crack location and short length of some specimens additional leak rate testing could not be performed.

Specimens with tight collars were subjected to extensive eddy current testing. This required removal of the tight collars to obtain data comparing packed and open crevice eddy current response. Hence all repeat testing of the first series of test specimens was performed under open crevice conditions. Repeat testing led to higher leak rates either as a consequence of the open versus packed crevices, handling or forceful removal of tight collars. Only in one case did a non-leaker become converted into a leaker as a result of retesting. This case, 533-4, is one of forceful removal of a tight collar.

From table 5-11, tight crevices are seen to be sometimes of benefit in reducing leak rates. Specimen 542-4 had a very high eddy current voltage and a low leak rate of while specimen 543-2 had a high voltage and a leak rate of . The four other tight crevice specimens were non-leakers. Three of these remained non-leakers after removal of the tight collars. Damage during removal of the tight collar is suspected as the reason the fourth non-leaker became a leaker. Tight crevices can be of benefit in reducing leak rate but cannot be relied upon. Further, pending future developments, eddy current techniques have not been shown to be able to clearly distinguish between open and tight crevices, although the presence of magnetite from TSP corrosion can often be detected in the crevice and can be expected to be associated with tight crevices.

Eddy current inspection techniques are very sensitive to denting at tube support plate intersections. Dents of a fraction of a mil are easily detectable. Specimens with large through wall cracks which were then dented to less than one mil have not leaked significantly either at operating pressure or under steam line break conditions. A tight through wall fatigue crack inch in length will leak at more than the typical tech spec limit of 0.35 gpm. From table 5-11 it is evident that a small dent has turned such a cracked tube into a non-leaker. Only one case of small leakage even at SLB conditions at a dent size less than mil was found for the eleven tested conditions of incipient denting and dented tubes.

The data of table 5-11 that are used for ARC development are given in table 5-12. All bobbin voltages applied are obtained prior to removal of the TSPs, i.e., for the tight crevice condition. The crevice condition given in table 5-11 applies to the condition for the leak rate tests and not for the voltage measurement except where both tight and open crevice voltages are given. All leak rates of table 5-12 are for open crevice conditions.

5.10 Burst Test Procedure

Given the assumption that significant support plate displacements cannot be excluded under accident conditions, burst tests of tubes with stress corrosion cracks are conducted in the free span condition and burst pressure is correlated with bobbin coil voltage. This burst pressure correlation is then applied to determine the voltage amplitude that satisfies the guidelines of Reg. Guide 1.121 for tube burst margins.

Burst tests were conducted using an air driven differential piston water pump at room temperature. Pressure was recorded as a function of time on an X-Y plotter. Sealing was accomplished by use of a soft plastic bladder.

Burst tests of tubes with stress corrosion cracks were done in the free span condition. No foil reinforcement of the sealing bladders was used since the crack location which was to dominate the burst behavior was not always readily apparent. Some of the maximum openings developed during burst testing were not sufficient to cause extensive crack tearing and thus represent lower bounds to the burst pressures. The openings were large enough in all cases to lead to large leakage.

5.11 Burst Test Results

Burst test results are summarized in table 5-11. Figure 5-8 illustrates a plot of burst pressure versus bobbin coil voltage for specimens from model boiler and pulled tube tests which are considered reasonably representative of the range of field observations of ODSCC of tubes at tube support plate intersections. Note that some of the burst data points are lower bound estimates since extensive crack tearing did not develop. In these cases the crack openings were large enough to cause large leakage events in service. From figure 5-8 it is seen that burst pressures remain above about psi even for voltage up to volts. As discussed later, reasonable limits on bobbin coil voltage contributes to maintenance of required burst pressure margins with respect to both operating and accident pressure differentials.

The burst test data used for ARC applications are given in table 5-12. As noted previously, the bobbin voltages used to correlate with burst pressure were obtained with the TSPs present and with packed crevices as obtained from the model boilers.

5.12 Destructive Examination of Laboratory Specimens

The objective of this task was to characterize the size, shape, and morphology of the laboratory created corrosion in alloy 600 tube specimens which have been leak rate and burst tested. Examination methods include visual examinations, macrophotography, light microscopy and/or SEM (scanning electron microscopy) examinations, SEM fractography, and metallography. The crack morphology is also to be compared generally to the corrosion morphology observed in tubes pulled from operating power plant steam generators. Appendix A provides a description of the results of destructive examinations performed on the 7/8-inch laboratory tube specimens. Table 5-12 provides measured crack lengths for the burst cracks from the destructive examinations.

5.13 Comparison with Pulled Tube Crack Morphology

Section 3.0 of this report described the crack morphology observed on tubes pulled from operating steam generators. Most of the support plate cracking was OD origin, intergranular stress corrosion cracking that was axially orientated. Most cracks had minimal IGA features in addition to the overall stress corrosion features. Even when the IGA was present in significant amounts, it usually did not dominate over the overall SCC morphology. Large macrocracks were composed of numerous short microcracks (typically inch long) separated by ledges or ligaments.

The ledges could have either intergranular or dimple rupture features depending on whether or not the microcracks had grown together during plant operation.

The laboratory-generated corrosion cracks are observed to have the same basic features as the support plate crevice corrosion from pulled tubes. The laboratory specimens frequently had somewhat lower crack densities, but individual cracks usually had similar IGA aspects. The laboratory specimens possibly had even less of a tendency to develop IGA components to the overall stress corrosion crack features. The observed differences in corrosion morphology between the model boiler specimens and the pulled tubes is believed to be insignificant.

5.14 Review of Model Boiler Data for Acceptability

Based on potential outlier behavior in the burst and leak rate correlations, specimen voltage, leak rate and burst test data were reviewed to assess acceptability of the measurements. The methodology for these analyses is discussed in Sections 6, 7 and Appendix D. The assessments performed on specimens identified as potential outliers are summarized below.

Specimen 543-1, 543-2 SLB Leak Rates

In the initial leak rate tests of this program, the capability of the leak rate facility was limited to about ℓ/hr . The measured leak rates for specimens 543-1 and 543-2 were at the limit of the facility and thus cannot be considered to be reliable measurements. These data points are not included in the database for leak rate correlations. The next largest leak rate measured in the initial program was ℓ/hr for specimen 557-2. This measurement is below the expected facility limit and the measurement is reasonably consistent with the overall database.

Specimen 525-1 and 535-1 Voltage

Specimens 525-1 and 535-1 were Series 1 pieces taken from archive model boiler tubes and were not prepared specifically for this program. Upon review at the bobbin date (Figure 5-9), nearly horizontal responses were found in addition to the flaw signals. These responses were found to be due to circumferential welds made near the flaw to extend the tube length. Weld and heat affected zones affect the magnetic properties of the tubing and influence the voltage calibration. Consequently, the bobbin voltage responses for these indications cannot be considered to be reliable and are excluded from the database. It is expected that the RPC voltages are insignificantly affected by heated zones that, like the model boiler specimens, are approximately uniform in the circumferential direction of probe rotation.

The SLB leak rate for Specimen 535-1 was found to be less than that measured at normal operating pressure differentials. This could only occur by deposits plugging the crack or a measurement error. Thus the SLB leak rate for this specimen is also not reliable.

Specimen 542-4 SLB Leak Rate

The SLB leak rate of ℓ/hr for specimen 542-4 is exceedingly small for a bobbin voltage of volts prior to TSP removal and volts after TSP removal. This increase in voltage upon TSP removal indicates ligament damage that would be expected to result in increased leakage. The SLB leak rate is also only $\text{higher than the normal operating leak rate}$. Consequently, the SLB leak rate measurement for 542-4 is suspect with potential measurement error (initial leak rate test facility as used for 543-1, -2) or plugging of the cracks occurred during the measurements and this data point should not be used in the leakage correlations.

Specimen 568-4 Voltage

Specimen 568-4 was found to have an RPC crack length of inch (Table 5-10) which is expected to have resulted from slipping of the collar during the model boiler preparation of the specimen (see Table 5-4). The RPC trace for this specimen is shown in Figure 5-10. Following burst testing of this specimen, the burst crack length was found to be inch long. The remainder of the implied RPC crack length of Figure 5-10 did not open during the burst test. It is expected that the RPC crack length of inch is comprised of the burst crack and a second shallow crack aligned with the burst crack. RPC resolution was not adequate to separately resolve the two cracks. The second crack was not destructively examined.

It is judged that the bobbin voltage is unexpectedly high for the burst crack due to the overall crack extent of inches . However, the second shallow crack is a conservative representation of a few pulled tubes which were found to have shallow cracks extending outside the TSP. The pulled tube cracks outside the TSP were too shallow to be detected by eddy current, while specimen 568-4 was detectable which implies deeper penetration than the pulled tubes. Due to the general similarity of the specimen 568-4 morphology to the pulled tubes with crack extent outside the TSP, this model boiler specimen is retained in the database. The higher than expected voltage for this specimen does lead to potential outlier behavior based on the statistical analyses for outliers.

Specimen 576-4 Bobbin Voltage and SLB Leak Rate

Specimen 576-4 is a high leakage outlier in the SLB leak rate correlation. The bobbin voltage of volts is particularly low for the crack length with a inch throughwall length. The bobbin coil inspection results show a well defined flaw with no analysis error. The RPC response shows a single crack.

The destructive examination of this specimen found no remaining ductile ligaments in the crack face. In general, the loss of all ligaments tends to lead to higher than typical voltages while specimen 576-4 had a lower than expected voltage.

It is judged that the high SLB leakage results from a smoother or less tortuous crack than typical ODSCC, which leads to reduced friction. It is feasible that the smoother crack face may lead to increased contact across the crack face with a resulting voltage decrease. These crack features are reasonably within expected crack behavior and there would be no acceptable justification to exclude this specimen from the ARC database. In either case, non-conservative outliers would not be excluded from the database unless there was a known measurement error.

Specimen 605-2 SLB Leak Rate

The SLB leak rate of liter/hr for specimen 605-2 is very low for the throughwall crack length of inch. The leak rate, however, shows an increase of a factor of between normal operating and SLB conditions, which is within expected behavior. The bobbin voltage of volts is high for the burst crack length, although the high voltage is attributable to three closely spaced (overlapping in RPC response) axial cracks at comparable RPC amplitudes. This crack morphology is within the range of that found in pulled tubes and the bobbin voltage is reasonable for the overall crack morphology. The SLB leak rate measurement was reviewed and found to have no apparent measurement error. The low SLB leak rate could be the result of irregularities or tortuosity on the crack face. Thus, there is no apparent basis to exclude this specimen from the ARC database.

Based on the above assessments of potential outliers identified by statistical analyses, the following data points have been found necessary to exclude from the ARC database: bobbin voltage measurements for specimens 525-1 and 535-1 and the SLB leak rate measurements for specimens 535-1, 542-4, 543-1 (also normal operating leak rate) and 543-2. These data points are indicated as N.R. (not reliable) in the model boiler test data summary of Table 5-12.

5.15 Burst Testing of IGA Specimens

Paragraph 3.3 addresses IGA detectability of laboratory prepared specimens about inches in length with uniform IGA depths and no cracking. Figure 3-9 shows bobbin coil voltage amplitudes for these specimens. The IGA specimens from figure 3-9b with depths of and in non-sensitized, 7/8 inch OD tubing were burst tested to compare the voltage vs. burst characteristics of IGA to that of the available data base (see table 6-1, figure 6-1). In addition, a 3/4 inch diameter, sensitized specimen of figure 3-9a with deep uniform IGA was burst tested. These specimens had IGA from one end of the tube to the other and hence differential bobbin coil measurements could not be made. As noted in figure 3-9, the bobbin amplitudes were measured in the absolute mode. It is expected that for uniform step change in depth, the peak to peak differential voltages would be a factor of higher than the

absolute voltages which are typical of single peak amplitudes. Thus using the absolute amplitudes of the specimens appears to be a conservative representation of the differential amplitudes. However, due to the associated uncertainty on the voltage amplitudes, the burst results for these specimens are provided for information only. The burst test results from the IGA specimens are not included in the voltage/burst correlation discussed in paragraph 6.1.

5.16 Pull Force Tests and Results

The axial force needed to move a tube past a dented tube-tube support plate intersection was evaluated by tests at room temperature. Both pull and push tests were conducted. The two specimens with the highest dent levels, FAT-2 and FAT-3, were used in these tests.

In the pull tests, pull forces were applied to one end of the tube while holding the support plate fixed. First, a solid plug was welded to one end of the specimen. The plug was then drilled and tapped to accommodate a threaded pull rod. The tube with the pull rod was passed through a hole in the crosshead of an Instron test machine. The hole was sized to allow passage of the tube, but not the simulated support plate. Force was applied so as to separate the pull rod and tube from the support plate simulant. The load versus crosshead movement was recorded. Because of the very high stiffness of the crosshead, the recorded displacement corresponded to the movement of the tube past the dented support plate simulant.

Other intersections with significantly less denting and hence much lower friction forces were tested by pushing the tube past the collar. In this case, the collar (support plate simulant) was supported by a cylindrical section of pipe and the test machine crosshead pushed one end of the tube past the collar. Again, load versus displacement was recorded to determine the friction force.

The results of these tests are displayed in table 5-11. The specimens with the highest dent levels required pull forces in excess of lbs to separate the tube from the support plate simulant. In the other, less dented specimens, the push forces required varied from lbs.

5.17 Burst Tests in Quatrefoil and Eggcrate TSP Designs

In order to quantify the potential for the presence of quatrefoil and eggcrate type tube supports to elevate the burst strength of tubes with ODS/CC located within the confines of the supports, a series of burst tests were performed with prototypic support conditions. The burst tests were performed using an air-driven differential piston water pump at room temperature. In order to pressurize the tube specimens with the through-wall slits they were internally sealed with a soft plastic bladder. To prevent extrusion of the bladder prior to bursting of the tube, the bladder was reinforced at the location of the slit with a thick by wide brass foil shim. The length of the shims were such that they extended beyond the ends of the slits by .

The restraint conditions for the testing consisted of quatrefoil holes in thick

support plate sections and eggcrate type supports. The slits were oriented to provide for maximum opening of the flanks prior to contact with the supporting structure. For each support type two orientations were tested. For the quatrefoil supports the slits were oriented facing the cutout spaces and facing the lands. For the eggcrate type supports, tests were conducted with the slits facing the acute angle of the slats intersections, and facing the obtuse angle of the slats intersections.

The burst test results are summarized in Table 5-12. A comparison of the results with the database obtained from the testing of free-span slits is shown on Figure 5-11. In order to compare results from various tubing sizes, a normalized burst pressure, P_{bar} , is plotted versus a normalized crack length, λ . The normalized burst pressure is calculated as

$$(5.1)$$

where P_B is the measured burst pressure, r_m is the mean radius of the tube, t is the thickness of the tube, S_Y is the yield strength of the tube and S_U is the ultimate tensile strength of the tube material. The normalized burst pressure is simply the ratio of the maximum elastic Tresca stress intensity in the tube wall (considering a linear distribution of the radial stress) to twice the flow stress of the material. The normalized crack length is calculated as

$$(5.2)$$

where a is the total slit or crack length. Thus, for 3/4" OD tubes with a 0.043" wall thickness λ is times the crack length in inches, e.g., for $\lambda =$

The results of the testing indicate that the presence of quatrefoil and eggcrate supports elevates the burst pressure slightly for longer crack lengths, in 3/4" diameter tubes. Examination of the test specimens revealed that crack tearing may be prevented depending on the orientation of the crack. However, this cannot be relied upon since significant crack tearing was often observed. The presence of the support from both configurations does restrict lateral motion of the crack flanks such that the crack opening area is less than the cross-section area of the tubes. Thus, the quatrefoil and eggcrate supports could be expected to prevent leakage similar to a full unrestricted tube burst, but would not be expected to prevent a large leakage event.

5.18 Model Boiler Database Summary

As described in the above subsections, model boiler specimens have been fabricated and tested to augment the pulled tube database at support plate intersections. Thirty-six laboratory specimens have been prepared using 7/8-inch OD tubing. The specimens were subjected to eddy current examination. Degradation at simulated tube support plate intersections have

ranged from volts in bobbin coil amplitude. These specimens have been burst tested, with the results displayed in table 5-12. All specimens were also been leak tested. Further, several of the samples were destructively examined to determine degradation characteristics and crack morphology. The maximum and through wall crack length data obtained for many of these specimens from the destructive examinations are also listed in table 5-12. All bobbin voltages given in Table 5-12 were obtained with packed TSP crevices as received from the model boilers prior to removal of the TSPs. The model boiler database is combined with the pulled tube database and the total used for determining leak rate and burst correlations.

Table 5-1

MODEL BOILER THERMAL AND HYDRAULIC SPECIFICATIONS

Table 5-2

MODEL BOILER TEST SPECIMEN SUMMARY FOR SERIES 1, 2, AND 3
7/8" Diameter Tubing

Table 5-3

SUMMARY OF SERIES 4 TEST SPECIFICATIONS

Table 5-4

SUMMARY OF SERIES 4 TEST PIECES HAVING EDDY CURRENT SIGNALS
7/8" Diameter Tubing

Table 5-5

SERIES 5 TEST SPECIMENS

Table 5-6

SERIES 6 TEST SPECIMENS

Table 5-7

Summary of SCC Behavior in Doped Steam at

Table 5-8

Fatigue Precracked Specimens

Table 5-9

Summary of Dented Specimens

Table 5-10
Laboratory Specimen NDE Summary⁽¹⁾

Table 5-10 (continued)

Laboratory Specimen NDE Summary⁽¹⁾

Table 5-10 (continued)

Laboratory Specimen NDE Summary⁽¹⁾

Table 5-10 (continued)

Laboratory Specimen NDE Summary⁽¹⁾

Table 5-11

Summary of Leak and Burst Test Results

**Table 5-13: Burst Tests Results for Tubes Tested with Supports
7/8" & 3/4" OD Alloy 600 SG Tubes in Quatrefoil and Eggcrate Supports**

Figure 5-1. Schematic of Model Boiler Facility

Figure 5 -2. Clamped Specimen Used For Doped Steam Test

Figure 5-3. Section Through a Dented Tube Support Plate Intersection

Figure 5-4. EDS Elemental Maps Across a Dented Crevice; Speciment Trial-1

Figure 5-5. SEM Fractographs of Cracks in Doped Steam Specimen,
Model Boiler Specimen and Service Tube

Figure 5-6. Metallograph of Cracked Specimens

Figure 5-7. Cracks in Model Boiler Specimens

Figure 5-8

Burst Test Results Versus Bobbin Coil Voltage

Figure 5-9. Bobbin Data for Model Boiler Specimen 535-1

Figure 5-10. RPC Trace for Model Boiler Specimen 568-4

Figure 5-11. Burst Pressure Correlation With Bobbin Voltage -
IGA Specimen Burst Test Results Included

Figure 5-12: Normalized Burst Pressure vs Normalized Crack Length
3/4" & 7/8" OD Alloy 600 SG Tubes

6.0 Burst Pressure Correlation

6.1 Introduction

This section utilizes the model boiler (Section 5) and pulled tube (Section 4) data to develop a correlation of burst pressure vs. bobbin voltage. An enhanced statistical procedure was implemented as described below and in Appendix D. The methodology has been reviewed and accepted by the EPRI Committee for Alternate Repair Limits for ODS/CC at TSP's, and an independent EPRI consultant. All normalization of eddy current data has been reviewed and has been accepted by the EPRI Committee. Thus the data, methodology, and correlation provided in this section provide confidence in the results.

6.2 Data Base for Burst Pressure Correlation (7/8 Inch Tubing)

The database used for the development of the burst correlation (burst pressure vs bobbin coil voltage amplitude) for 7/8 inch diameter tubing is derived from model boiler specimens and pulled tubes. All of the data were derived from Alloy 600 tubing with 7/8 inch OD and 0.050 inch nominal wall thickness. The model boiler test results for 7/8 inch tubing are described in detail in Section 5. All bobbin coil measurements on model boiler specimens are reported from the _____ kHz mix frequency with the _____ holes in the reference ASME standard normalized to _____ volts.

The pulled tube data included in the database are obtained from Plants A-2, D-1, D-2, J-1, L, F, P-1 and W. Except for Plant J-1, the bobbin voltages for Plants A-2, D-1, D-2, L, and P-1 were field measured prior to the tube pulls at a frequency mix the same as the model boiler specimens. The bobbin data from Plant J-1 pulled tubes were measured at _____ kHz using the French NDE procedures. This data has been normalized to correspond to the ARC database using the process described in Section 6.6. The pulled tube results are described in Section 4.

The burst pressures of all the room temperature data are normalized to a reference flow stress of _____ ksi to provide a consistent data base. This value is close to the _____ ksi mean flow stress for the mill annealed Alloy 600 tubing at room temperature. The resulting burst pressure database is summarized in table 6-1 for both the model boiler specimens and the pulled tubes. The database includes 32 model boiler specimens and 37 pulled tube intersections.

6.3 Burst Pressure vs. Voltage Correlation

The bobbin coil voltage amplitude and burst pressure data of Table 6-1 were used to determine a correlation between burst pressure and bobbin voltage amplitude. This is not to say that a "formal" functional relationship, in the sense of one variable being dependent on the other, exists between the variables since the burst pressure is not caused by the bobbin voltage and vice versa. The burst pressure and bobbin voltage variables considered are mainly functions of a third variable, i.e., the crack morphology. While the variation in crack morphologies is essentially infinite, suitable descriptions can be effected based on the depth, average depth, profile description, etc.

However, the characterization of the morphology is not essential to this analysis since a relationship is being independently established between two offspring variables. Although the correlation analysis does not establish a causal relationship between the variables, it does, however, establish a "working" relationship that can be employed for the prediction of one variable from the other. The data considered are shown on Figure 6-1 along with the results of the correlation analysis discussed in subsequent sections.

The analysis performed considered the scale factors for the coordinate system to be employed, i.e., logarithmic versus linear, the detection and treatment of outliers, the order of the regression equation, the potential for measurement errors in the variables, and the evaluation of the residuals following the development of a relation by least squares regression analysis.

In summary, it was concluded that the a linear, first order relation for the burst pressure as a function of the common logarithm (log) of the bobbin amplitude voltage is appropriate and sufficient. For the relationship it was determined that a bobbin voltage value of V could be ascribed to the burst data where degradation was not detected, i.e., no detectable degradation (NDD). This is necessary to include NDD specimens in the database since the burst pressure should be a continuous function to the point of no existing degradation. The correlation coefficient from the regression analysis was found to be significant at a level. Analysis of the residuals from the regression analysis indicated that they are normally distributed, thus verifying the assumption of normality inherent in the use of least squares regression.

6.3.1 Selection of Coordinate System

In order to establish a correlating relationship between the pairs of variables, but expected to have independent variances, the method of least squares (LS) curve fitting was employed. The simplest functional form is a linear relationship of the type

(6.1)

where the variables x and y may be linear or logarithmic independently, and the coefficients of the relation, a_0 and a_1 are to be determined from the analysis. In addition, the choice of the regressor variable is not pre-determined. Both variables are assumed to be subject to random fluctuations which are normally distributed about the mean of the variable or the logarithm of the variable with a mean of zero and some unknown, but reasonable variance. It is also assumed that this variance is constant, or uniform, over the range of interest of the variables. In practice this may not be the case, however, any non-uniformity present would not be expected to significantly affect the analysis outcome, and can be tested at the conclusion of the analysis.

Analyses were performed to determine the optimum nature of the variable scales, i.e., linear versus logarithmic, and the appropriate selection of the regressor variable. It was concluded that the most meaningful correlation could be achieved by considering the log of the voltage as

the regressor and the burst pressure as the response. Thus, the functional form of the correlation is

$$(6.2)$$

where P_B is the burst pressure and V is the bobbin voltage amplitude. The basis for selection of the form of the variables was based on performing least squares regression analysis on each possible combination and examining the square of the correlation coefficient for each case. The selection of the regressor variable does not affect the calculation of the index if the

Index of Determination, r^2 , for Various Selections of Coordinate Scales		
	<i>Pressure</i>	<i>Log(Pressure)</i>
<i>Volts</i>		
<i>Log(Volts)</i>		

calculations are performed on the transformed data. The results of the calculations are shown in the above table. The results clearly show an advantage for treating the voltage on a logarithmic scale and the burst pressure on a linear scale.

It is noted that the data contain some results for specimens in which there was no detectable degradation (NDD) from the non-destructive examination. The inclusion of this data is necessary in order to predict burst pressures for very low bobbin amplitude response tubes. Two methods were considered for inclusion of the data in the analysis. The first method consists simply of assigning a low bobbin voltage amplitude, V_{NDD} , to the data. This was done for the determination of the best choice of scales for the coordinates of the plot. The value assigned to V_{NDD} was . The second method consists of modifying the prediction model to include a voltage offset variable to be determined from the data, i.e., the prediction equation becomes

$$(6.3)$$

where V_0 is the additional parameter to be determined from the data. Since the equation is now non-linear in the parameters the application of least squares techniques is not appropriate. However, if an assumed value is assigned to the offset term the equation is once again linear and LS can be applied to find the values for the other two coefficients. Analysis was performed which determined that using a value of $V_0 =$ resulted in a maximum index of determination of for LS fit of the remaining parameters. This is slightly better than the value of reported above for determining the best selection of the coordinate scales. The improvement is judged to be too small to justify the added complication of including a voltage offset in the prediction model to account for the NDD specimens.

Additional analysis was performed which determined that assigning a value of V_{NDD} to V_{NDD} would increase the index of determination to R^2 , which is greater than the maximum achieved using an offset value. However, this improvement is significant only in the third decimal place. Similar analyses performed for 3/4" tube data resulted in a "best" V_{NDD} value on the order of amplitude values present in the data. The use of such a value would thus be inappropriate as an assigned value for NDD specimens. It was thus concluded that the use of a value of V_{NDD} was appropriate.

An additional consideration for the analysis of the data was to increase the order of the prediction equation. This would allow for the assignment of a lower value for the NDD specimens. Under this consideration the model would be

(6.4)

The index of determination for this type of model was found to be R^2 . Although this is a slight improvement over the 1st order model, the curve was found to be concave upward and judged to be inappropriate. Thus, the introduction of a second order term was concluded to provide no improvement in the model. To examine the effect of changing the direction of the regression, a first order linear fit was also performed relating the logarithm of the bobbin amplitude to the burst pressure, usually termed an "inverse" regression. The inverse regression curve did not adequately relate to the burst behavior for low voltages, and it was concluded that the inverse regression did not provide additional useful information beyond the conventional regression curve. Based on the above considerations it was concluded that the linear (in the coefficients), first order model was appropriate for the analysis.

6.3.2 Regression Analysis for the Identification of Outliers

The burst pressure data were analyzed to identify any potential outlying data points. The analysis was performed using the robust regression technique based on minimizing the median of the squares of the residuals. The method, known as the least median of squares method, is described in Appendix D.

The potential outlier analyses were performed in two steps. An initial evaluation was performed to identify potential outliers for further evaluation of the test data. This process led to identification of unreliable and atypical data as described in the evaluations reported in Sections 4 and 5. After exclusion of the unreliable data from the database, the analysis for potential outliers was repeated with the results discussed in the following paragraph.

Five (5) burst data points were identified as potential outliers. These had residual to scale ratios from the median regression ranging from R_{res}/S with respective probabilities of occurrence of P . Examination of the test program information and specimens did not indicate that the results should be removed from the database, thus, the data were retained for the analysis. Confirmation of the outlying nature of the burst pressure results for these specimens is only indicated for one of the data points, i.e., that with the largest residual to scale ratio, from the plot of the residuals relative to the predicted burst pressures and from the cumulative probability plot of the sorted residuals (Figure 6-3, discussed later).

6.3.3 Error-in-Variables Analysis

A general assumption in performing a least squares regression analysis to establish a correlating relationship is that both of the variables, burst pressure and bobbin voltage in this case, are subject to random fluctuations about their respective mean values (or their respective log mean values). If there are significant uncertainties in the measurement of one or both of the variables the slope of the LS correlation line will be biased. A discussion of regression when errors are present in the independent variable is provided in Appendix D. In essence, the regression performed always underestimates the absolute value of the slope of the true relation, if one exists. A Wald-Bartlett evaluation of the data was performed, and it was concluded that the presence of measurement error would not have a significant effect on the slope of the correlation line. It is noted that the Wald-Bartlett technique relies on being able to sort the data in the order of the real x variable. The application here is based on sorting on the observed, i.e., X , variable. Thus, the application is for the purposes of determining whether or not gross measurement errors are likely to be present, not for the determination of an improved estimate of the slope. The later analysis of the residuals demonstrates that the conventional regression curve is adequate for this evaluation.

Since the omission of correction for measurement error results in an under prediction of the magnitude of the slope of the correlation and the slope is negative, predicted burst pressures for voltages below the centroid of the data will be slightly less than predictions based on consideration of the measurement error. For voltage values greater than the centroid of the data the correlation slightly over predicts the burst pressure.

6.3.4 Burst Pressure Correlation for 7/8 Inch Diameter Tubing

The final fit of the data is shown on Figure 6-1. The correlation line is given by

(6.5)

where the burst pressure is measured in ksi and the bobbin amplitude is in volts. As noted previously, the index of determination for this regression was $r^2 = 0.85$, thus the correlation coefficient is $r = 0.92$. The estimated standard deviation of the residuals, i.e., the error of the estimate, s_p , of the burst pressure was 0.5 ksi. Based on an F test of the mean square of the regression to the mean square of the residuals, the regression is significant at a 0.05 level. This simply means that if the burst pressure was truly uncorrelated to the bobbin amplitude the observed correlation would be expected to occur with a probability of 0.05.

A one-sided simultaneous confidence bound, corresponding to a two-sided band, was calculated for the mean burst pressure, P_i , corresponding to a specific voltage, V_i , per the following equation:

(6.6)

where n is the total number of data points used, and F_{α} is the Fisher's F-distribution value corresponding to an upper tail area of α . In addition, a one-sided prediction band for individual values of the burst pressure, P_i , as a function of voltage was also calculated per the following equation:

(6.7)

where t_{α} is the Student's t-distribution value corresponding to an upper tail area of α . Since the burst tests were performed at room temperature (RT) conditions, the prediction bound was further reduced to a level corresponding the lower tolerance limit (LTL) for the material properties of the tubes. This was done by multiplying the predicted burst pressure by the ratio of the LTL limit of flow stress at the reference, or normalized, value of the RT flow stress used in the analysis. The results of this adjustment are also shown on Figure 6-1. A second order fit of bobbin amplitude to differential pressure for the prediction curve as adjusted by the LTL material flow stress was performed for the purpose of determining lower bound voltage amplitudes as a function of the applied pressure differential, resulting in the following equation,

(6.8)

Using this result the voltage amplitude corresponding to a differential pressure of 1000 ksi would be 1000, and the amplitude corresponding to a differential pressure of 1000 ksi would be 1000.

6.3.5 Analysis of Residuals

The results of the analysis of the residuals specific to the burst data for 7/8" tubes is provided on Figures 6-2 through 6-4. The types of analysis of the residuals performed is described in Appendix D. The initial analysis consisted of plotting the residual burst pressure values against the regression (predicted) burst pressure values. Since these are not expected to be correlated the scatter plot should exhibit non-descript characteristics. An examination of the data plotted on Figure 6-2 does verify that a correlation does not exist between the residual values and the predicted values, and that the variance of the residuals is uniform. The data also support the limitation of the regression equation to 1st order.

Figure 6-3 shows the cumulative probability of the ordered residuals versus the ordered residual values. If the residuals are normally distributed with a mean of zero they should plot as a straight line with the zero value of the residual burst pressure at the 50 percent value. Examination of Figure 6-3 verifies that the amplitudes do plot as an approximate straight line with a mean value of 0. The conclusion of the examination of the residuals is that the assumptions inherent in the least squares analysis are verified. Figure 6-4 depicts an alternate way of looking at the same information. For this plot the actual cumulative probabilities of the residuals are plotted against the expected cumulative probabilities. For the entire range the actual values reasonably approximate the expected values.

The data identified as potential outliers, but included in the analysis were also included on the plots. For the scatter plot only one data point appears to be significantly outlying, however, it does not necessarily violate the non-descript nature of the plot. On the cumulative probability plot one potentially significant outlying data point is located at the lower left corner of the plot. The potential outlying data point is Plant L, R8C69, TSP-1, which indicates the lowest outlying burst behavior on Figure 6-1. However, most of the departure from linearity is expected in the extremes, thus the location of the data point is a basis for further examination, but not elimination.

Table 6-1
7/8-Inch Diameter Pulled and Model Boiler Tube Leak Rate
and Burst Pressure Measurements

Table 6-1 (continued)

Table 6-2
Summary of Data for High, Low and Nominal Burst Pressure Specimens

Figure 6-1: Burst Pressure vs. Bobbin Amplitude
7/8" ± 0.050" Alloy 600 SG Tubes, Model Boiler & Field Data

Figure 6-2: Burst Pressure vs. Bobbin Amplitude
7/8" x 0.050" Alloy 600 SG Tubes, Model Boiler & Field Data

Figure 6-3: Burst Pressure vs. Bobbin Amplitude
7/8" x 0.050" Alloy 600 SG Tubes, Model Boiler & Field Data

Figure 6-4: Burst Pressure vs. Bobbin Amplitude
7/8" x 0.050" Alloy 600 SG Tubes, Model Boiler & Field Data

7.0 SLB Leak Rate Correlation

7.1 Introduction

This section uses the model boiler (Section 5) and pulled tube (Section 4) data to develop a correlation of SLB leak rate (primary to secondary leak rate under steam line break conditions) vs bobbin voltage. An enhanced statistical procedure was implemented as described below. All renormalization of eddy current data has been reviewed in detail and resolved by the EPRI APC Committee. Data from non-leaking tubes are not included in the leak rate correlation. However, a separate correlation has been developed for probability of leakage using all available data from 7/8 inch tubing, as described in Section 7.4 below.

The developed probability of leakage (Section 7.4) as a function of voltage provides a statistically based estimate of the leakage threshold. Alternate leakage threshold assessments are given in Section 7.3 to estimate a threshold for significant leakage. To assess trends expected for leak rate vs. voltage correlations, a combination of analytical calculations of leakage as a function of crack length and field crack length vs. voltage data are presented in Section 7.5. These trend analyses help to guide selection of the bounding leak rate correlation in Section 7.6.

7.2 Database for SLB Leak Rate Correlation

The database used for the development of the SLB leak rate correlation (primary to secondary leak rate under SLB conditions vs bobbin coil voltage amplitude) for 7/8 inch diameter tubing is derived from model boiler specimens and pulled tubes. All of the data were derived from Alloy 600 tubing with 7/8 inch OD and 0.050 inch nominal wall thickness. The model boiler test results for 7/8 inch tubing are described in detail in Section 5. All bobbin coil measurements on model boiler specimens were reported from the _____ kHz mix frequency with the _____ holes in the reference ASME standard normalized to _____ volts.

The pulled tube data in the database that had leakage are obtained from Plants A-2 and J-1. The bobbin data from Plant J-1 pulled tubes were renormalized to the ARC _____ kHz mix as described in Section 4. The data used for renormalization include cross-calibration of ASME standards to the reference laboratory standard. This process involved significant and detailed efforts by two independent parties (Laborelec and Westinghouse) and review by the EPRI ARC Committee such that there is acceptable uncertainty in the renormalization procedure. The pulled tube results are described in Section 4.

The SLB leak rate data are normalized to primary pressures of _____ and _____ psia and to the secondary side pressure of _____ at operating temperature. Renormalization from the measured leak rate conditions for SLB leak rates is developed in Appendix B. The resulting SLB leak rate database is summarized in Table 6-1 for both the model boiler specimens and the pulled tubes. The development of these data and the assessments for non-reliable data are given in Section 4 for the pulled tubes and Section 5 for the model boiler specimens. Data from non-leaking tubes are not included in the leak rate correlation. The resulting leak rate database includes 20 model boiler specimens and 3 pulled tube intersections.

7.3 Leak Rate Threshold Assessment

As a crack is initiated and grows to a certain size (in depth and length) it becomes detectable through eddy current inspection. Such a crack indication would have a signal amplitude associated with it. As the crack grows, so does its signal amplitude. When the crack becomes through-wall, it would have a significant voltage amplitude signal. Although extremely short cracks may be construed to have small amplitudes, in practice, a through-wall corrosion crack will have some minimum signal amplitude. It is not known explicitly what minimum voltage amplitude may be associated with such a crack.

In order for a crack to result in leakage across the tube wall, the crack must be through-wall or long and nearly () through-wall such that break through can occur at SLB conditions. Further, for an OD initiated through-wall crack to leak, it must have some minimum length at the tube ID. The estimated bobbin voltage threshold for leakage based on through-wall crack length considerations is discussed in Section 7.3.4. A voltage threshold for leakage is also supported by the scarcity of leak rate test results for bobbin coil amplitudes below volts. Thus it may be concluded that there would be an eddy current voltage threshold below which corrosion cracks would not cause leakage. A voltage threshold for SLB leakage is assessed below from the body of available data.

7.3.1 Threshold Based on Destructive Exam Depth of Pulled Tubes

Figure 7-1 is a plot of bobbin voltage versus maximum depth of cracks in pulled tubes from operating steam generators with 7/8 inch diameter Alloy 600 tubing. Due to the differences in crack morphology among the various pulled tube specimens, the plotted data is scattered as expected. However, an increasing trend between bobbin voltage and maximum through-wall depth from destructive examination is visible. On the semi-log plot, a linear relationship between the voltage and destructive examination depth is broadly indicated. Figure 7-1 shows a regression fit to the data for depths . This regression fit can then be extrapolated to depth to estimate the expected voltage for a crack just penetrating through-wall. The best estimate voltage for a through-wall indication is about volts and the lower confidence on the mean regression line is about volts. All of the data for through-wall cracks fall above this voltage as may be noted in Figure 7-1. Since a crack must be through-wall to cause leakage, it follows that the minimum bobbin voltage threshold for leakage in 7/8 inch tubing is expected to be about volts.

Figure 7-2 is a similar plot for pulled tubes of 3/4 inch diameter. A trend similar to the 7/8 inch data may be observed. The data is scattered and a linear relationship on the semi-log plot is displayed. Extrapolation of a regression fit of the partial depth cracks suggests a bobbin amplitude of about volts for a crack in 3/4 inch diameter tubing to reach through-wall depth. Again almost all of the pulled tube data from through-wall cracks lie above this value (higher voltage amplitudes than volts).

7.3.2 Threshold Based on Leakage Data

A considerable amount of data exists on the leak rate of ODSCC flaws in pulled tubes and model boiler specimens. This database includes both 3/4 inch and 7/8 inch diameter tubing. The database used for this analysis consisted of 77 model boiler specimens and 109 pulled tube intersections.

The data from 7/8 inch tubing is reported from the _____ kHz differential mix with the holes in the ASME standard normalized to _____ volts in the mix. Similarly, the 3/4 inch tubing data is normalized to _____ volts for the _____ holes in the ASME standard at the _____ kHz differential mix.

In order to combine the data from the 7/8 inch and 3/4 inch specimens, a conversion factor equal to the square of the diameter ratios is applied. This factor results from the fact that the ASME standard hole size is the same for 3/4 and 7/8 inch tubing. Thus, to convert the 3/4 inch data to the same basis as the 7/8 inch data, the voltage amplitudes from the 3/4 inch data (at _____ kHz) were multiplied by the factor 1.36. The results were then combined with the 7/8 inch database.

The leak rates were, for most (150 of 186) cases, the direct result of measurements in the laboratory under SLB conditions. For the other (36) cases, laboratory data on leak rate measurement was not available and the likelihood of leakage was inferred from crack morphology (through-wall depth and length) obtained from destructive examination.

The data was classified into leaking and nonleaking specimens. A frequency distribution of voltage amplitudes (corresponding to the 7/8 inch data normalization) in each classification was determined. This is shown in Figure 7-3 as a stacked bar chart. The number of leaking specimens in each voltage range out of the total number in that range is also shown at the top of each bar in the figure.

The ratio of the number of leaking specimens in a voltage range (bin) to the total number of specimens in the bin was calculated from the above frequency distribution of voltage amplitudes. This result, probability of leakage, within each voltage range is plotted as a bar chart in Figure 7-4.

The above results (Figures 7-3 and 7-4) were developed using data from both the 7/8 and 3/4 inch diameter tubing. If the 3/4 inch data is excluded and only the SLB leak rate data from 7/8 inch tubing is used, the results are not changed significantly. This is displayed in Figures 7-5 and 7-6.

For the 7/8 inch tubes, the data supports no leakage under SLB conditions for indications up to _____ volts and a low probability of leakage between _____ and _____ volts.

7.3.3 Threshold Based on Bobbin Voltages of Non-leaking Specimens

The voltage threshold for SLB leakage is derived using data from non-leaking specimens. All available data for corrosion cracks with through-wall or near through-wall indications is used in this evaluation. Specimens with crack depths greater than _____ (from destructive examination) which exhibited no leakage during the leak test are listed in Table 7-1. It may be noted that, in the case of 7/8 inch tubing, these flaws had signal amplitudes in the range of _____ volts. These data suggest an SLB leakage threshold of about _____ volts, although the standard deviation is large which indicates that this estimate may not be reliable.

7.3.4 Threshold Based on Through-wall Crack Length

The threshold for SLB leakage can also be assessed by evaluating the lowest bobbin voltages resulting in leakage at SLB conditions and by evaluating the through-wall crack length generally required for measurable leakage. If the through-wall crack length associated with measurable leakage can be defined, the voltage versus crack length relationships developed in Section 7 of Volume 2 of this report can be used to assess the voltage threshold for leakage. The crack length method for estimating a voltage threshold for leakage provides a more physical insight into the threshold estimate.

The leakage threshold can be assessed by examining crack length data. Table 7-2 shows specimen through-wall crack lengths for no leakage, leakage liter/hr and leakage between and liter/hr. In the case of 7/8 inch diameter tubing, no leakage was found for through-wall cracks up to inch. The smallest through-wall crack length for which even small leakage (liter/hr) is detected is inch. Specimen 535-1 had a inch through-wall corrosion crack (inch total crack length) with a leak rate of liter/hr at SLB conditions. Pulled tube R4C73 from Plant A-2 had a inch through-wall crack (inch total crack length) with a leak rate of l/hr at normal operating conditions and l/hr at SLB conditions. Overall, the data of Table 7-2 indicate that through-wall crack lengths inch are generally required for SLB leakage. The bobbin voltage associated with a through-wall crack length of inch is expected to be volts.

7.3.5 Voltage Threshold Considerations for SLB Leakage (7/8 Inch Tubing)

In the above sections, the SLB leakage threshold was evaluated from different perspectives: voltage indications required for through-wall cracks (volts), voltage threshold from leak rate data (volts), voltages of non-leaking tubes with through-wall and near through-wall degradation (volts), and crack lengths required for leakage (volts). In all cases, the data show that the bobbin amplitude threshold for zero leakage is expected to exceed about volts whereas the threshold for significant leakage (liter/hr or gpm) in a 7/8 inch diameter tube, based on Table 7-2, is about volts.

Based on the above, leakage rates (bobbin volts) should be related to a threshold leak rate. The threshold for zero leakage is expected to exceed volts, while the threshold for meaningful leakage (liter/hr or gpm) is expected to exceed volts. The SLB leak rate methodology and analysis for units with 7/8" OD tubes is intended to be conservatively applied. Therefore, a leakage threshold of volts could be conservatively applied for units with 7/8" OD tubes. That is, all indications above volts have a probability of leakage as developed in Section 7.4 (Figure 7-7) and a leak rate (Figure 7-8) for indications in the range of ARC applications.

The best fit or maximum likelihood estimate for probability of leakage given in Figure 7-7, developed below in Section 7.4, supports a volt leakage threshold. The upper bound of Figure 7-7 shows a low probability of leakage of less than below the volt limit. This lower voltage estimate is inconsistent with the threshold estimates developed above and is judged to result from the limited database in the range of volts. In either case, both the volt probability of leakage at confidence and the SLB leak rate at prediction interval are very low such that a volt threshold could be applied with negligible error in the SLB leak rate.

7.4 Probability of SLB Leakage versus Voltage

The above discussion and the supporting data indicate that even when the voltage amplitude of a corrosion crack exceeds the leakage threshold, there is a likelihood of no leakage. In order to quantify this fact, the probability of SLB leakage as a function of voltage is derived in this section.

7.4.1 Database for Probability of Leakage

The current evaluation of probability of SLB leakage is limited to 7/8 inch diameter tubing. Hence, the database used here is limited to the 7/8 inch specimen results given in Table 7-3 and Figure 7-7. Figure 7-7 includes pulled tube results for which leak or burst tests were not performed. The data set for this analysis consists of a total of 98 pairs of test results for which leak tests were available, or for which it could be verified from destructive examination results that leakage would not occur at a pressure less than or equal to the postulated SLB pressure differential. When leak tests were not performed, the maximum crack depths were evaluated to define the indications as non-leakers or leakers. An example would be for a very small bobbin amplitude wherein a large burst pressure was observed during burst testing, e.g., for a burst pressure test in which no leakage was observed to a pressure in excess of about psi at room temperature for a tube with a material flow stress of ksi. The data base consists of 35 indications from model boiler specimens, and 40 indications from sections of pulled tubes for which SLB leak rates are known from direct measurement. In addition, there are 23 pulled tube specimens for which leak rate tests were not performed and whether or not they would leak was assessed on the basis of crack morphology from destructive examination.

7.4.2 Statistical Evaluation for Leakage Probability

An analysis was performed to establish an algebraic relationship that could be used to predict the probability of leakage during a postulated SLB as a function of bobbin amplitude voltage. Two approaches were considered for the analysis. The procedure for the first approach would be to segregate the results into a series of discrete bobbin amplitude ranges, called bins, based either on the actual bobbin voltage observed or based on the logarithm of the bobbin voltage. This would be followed by the preparation of a cumulative histogram of the results, e.g., Figure 7-4, and the fitting of a smooth polynomial, or a cumulative normal distribution type curve through the results. There are, however, two significant drawbacks associated with this type of an approach. The first drawback is that the shape of the plotted histogram is dependant on the number of subdivisions used to segregate the data range. The second drawback is that there would be no direct way of establishing confidence bounds on the model, although binomial limits could be calculated for each bin.

To consider the second drawback further we note that the probability of leakage must be limited to a range of 0 to 1. A correlating equation to fit the data could be determined by employing the method of least squares (LS) or the principle of maximum likelihood (ML) to estimate the parameters of the equation. If the expression was based on correlating probability as a function of leakage, the upper confidence band for the resulting expression would exceed unity for some voltages. Likewise, for lower voltages the lower confidence band would yield probabilities less than zero.

In general, the criteria for a good estimator are that it be unbiased, consistent, efficient, and sufficient. In general, the parameters of a correlation curve from either LS or ML estimation analysis will satisfy the above requirements if the requirements for performing the analysis are met. However, for the probability of leak data, the estimating curve will not be strictly consistent for a sample size less than infinitely large due to variability inherent in establishing the subdivision size. Thus, while the objections of the second drawback might be overcome by correlating voltage to probability, the requirement for a consistent estimator might not be met. It was therefore decided, that the first analysis approach would not be pursued.

The second approach to the analysis stems from the observation that the data base may be considered as a sample from a dichotomous, or binary, population. This means that the data are categorical and that the number of categories is two, i.e., either no leak or leak. However, for an analysis treating the data in this manner a normal linear correlation model of the type

(7.1)

where $f(\text{volts})$ is either volts or $\log(\text{volts})$, is not appropriate since normal errors, ϵ , do not correspond to a zero (no leak) and one (leak) response. It is appropriate to analyze the data in this situation by non-linear regression analysis to fit a sigmoidal type of response function since the data are dichotomous. The use of the logistic function for the analysis of dichotomous data is standard in many fields, and especially in the health sciences. The function itself is sigmoidal in shape, and is similar to the cumulative normal function, and likewise similar to using a probit model (which is simply a normal function with the deviate axis shifted to avoid dealing with negative values). In principle, any distribution function that has a cumulative area of unity could be fit as the distribution function, a limitless number of possibilities. For example, the cumulative normal distribution already mentioned, the Cauchy distribution, the Poisson distribution, and any number of others. Trying to identify a latent, or physically based, distribution for the probability of leak is considered unrealistic, and is also considered unnecessary. For most purposes the logistic and normal functions will agree closely over the range of interest. The exceptions are the tails of the distributions, where the normal curve approaches its limit more rapidly than the logistic. Thus, relative to the use of the normal distribution the use of the logistic function is conservative. Given its' wide acceptance in multiple fields it was judged that the logistic function would be suitable for use in determining a probability of leak as a function of voltage.

Before actually analyzing the data a decision as to whether the bobbin amplitude or the logarithm of the bobbin amplitude should be used is necessary. Since the logistic distribution function is unbounded, the use of volts would result in a finite probability of leak from non-degraded tubes, and would be zero only for $V=-\infty$. Whereas, using the logarithm of the voltage results in a probability of leak for non-degraded tubes of zero. Clearly, the second situation is more realistic than the first, especially in light of the fact that a voltage threshold is a likely possibility.

Letting P be the probability of leak, and considering a logarithmic scale for volts, V , the logistic expression is

(7.2)

This can be rearranged as

(7.3)

where the logit transform is defined to be

(7.4)

The model considers that there is a binomial probability of leak for each value of the logarithm of the voltage. The objective of the analysis was to find the values of the coefficients, a_0 and a_1 , that best fit the test data.

Since the outcomes of the leakage tests are dichotomous, the binomial distribution, not the normal distribution, describes the distribution of model errors. This means that the variance of the probability of leak is $P(1-P)$, and that the performance of an unweighted LS regression analysis, which assumes constant variance, based on equation (4) would be incorrect. The appropriate method of analysis is based on the principle of maximum likelihood. The application of ML leads to estimates of the equation parameters, i.e., a_0 and a_1 , that are such that the probability of obtaining the observed set of data is a maximum. The results of applying ML to the dichotomous outcome are the likelihood equations,

(7.5)

and

(7.6)

which are to be solved for the coefficients a_0 and a_1 . Here, P_i is a test outcome, and $P(v_i)$ is an expected outcome based on the input value of the voltage using equation (7.2), where $v_i = \log(V_i)$. Since equations (7.5) and (7.6) are non-linear in the coefficients, an iterative solution for the coefficients must be found.

A *macro* for the commercial spreadsheet Excel[®] was written to iteratively solve for the coefficients using weighted LS techniques. The results were compared to the output for the

same data using a commercially available statistics program with logit fitting capability to provide an independent verification of the results. The accepted measure of the goodness of the solution is the deviance,

(7.7)

The deviance is used similar to the residual sum of squares in linear regression analysis and is equal to the error sum of squares (SSE) for linear regression. For the probability of leak evaluation P_i is either zero or one, so equation (7.7) may be written

(7.8)

Both evaluations provided similar deviance values and the final solution obtained was

(7.9)

Asymptotic confidence limits for each individual $\text{logit}(P_i)$ are found as

(7.10)

where α is the associated probability for a two-sided confidence band. The standard error of $\text{logit}(P_i)$ is found for each voltage level as

(7.11)

where V_a is the estimated variance-covariance matrix of the parameter estimates. Letting

(7.12)

the upper and lower one-sided confidence limits are

(7.13)

The upper bound values were calculated for each voltage/leak pair. These results are shown graphically on Figure 7-7.

7.5 General Trends for SLB Leak Rate Correlation

An evaluation has been completed that provides results supporting the recommended correlation methodology employed for SLB leak rate versus bobbin voltage. The evaluation establishes leak rate versus voltage from:

- 1) Formulation of a through-wall (TW) crack length (L) versus voltage (V) correlation from available data using regression analysis ($L=f_1(V)$).
- 2) Calculation of leak rate (Q) as a function of L using the CRACKFLO computer code. Formulate a simplified relationship of Q as a function of L through regression analysis of CRACKFLO predictions ($Q=f_2(L)$).
- 3) Development of a correlation between Q and V from the above. Substitute the formulation $L=f_1(V)$ into $Q=f_2(L)$ to get $Q=f_3(V)$. Compare $Q=f_3(V)$ to the direct correlations.

This evaluation is described in Section 7 of Volume 2 of this report.

7.6 SLB Leak Rate Versus Voltage Correlation

The bobbin coil and leakage data of Table 6-1 were used to determine a correlation between SLB leak rate and bobbin amplitude voltage. This is not to say that a "formal" functional relationship, in the sense of one variable being dependent on the other, exists between the variables since the amount of leakage is not caused by the bobbin voltage and vice versa. Both of the variables considered are really mainly functions of a third variable, namely the crack morphology. While the variation in crack morphologies is essentially infinite, suitable descriptions can be effected based on the depth, average depth, profile description, etc. However, the characterization of the morphology is not essential to this analysis since a relationship is being independently established for two offspring variables. Since both bobbin voltage and leakage are offspring variables the results of the correlation analysis do not establish a formal relationship between the variables, however, the results do establish a "working" relationship that can be employed for the prediction of one variable from the other.

7.6.1 Selection of a Coordinate system

In order to establish a correlating relationship between the two variables, which are paired, but expected to have independent variances, the method of least squares (LS) curve fitting was employed. The simplest functional form is a linear relationship of the type

(7.14)

where the variables x and y may each be considered to be linear or logarithmic. In addition, the choice of the regressor variable is not pre-determined. Both variables are assumed to be subject to random fluctuations which are normally distributed about the mean of the variable, or the logarithm of the variable, with a mean of zero and some unknown, but reasonable variance. It is also assumed that this variance is constant, or uniform, over the range of

interest of the variables. In practice this may not be the case, however, any non-uniformity present would not be expected to significantly affect the analysis outcome, and can be tested at the conclusion of the analysis.

Analyses were performed to determine the optimum nature of the variable scales, i.e., linear versus logarithmic, and the appropriate selection of the regressor variable. It was initially concluded that the most meaningful correlation could be achieved by considering the log of the leak rate as the regressor and the log of the voltage as the predicted variable. Further consideration of the range of interest in making predictions, and comparison with semi-theoretical results (following), led to the conclusion that for a range of less than about 9 volts that the log of the voltage should be considered as the regressor, with the log of the leak rate as the predicted variable. Thus, the functional form of the correlation is

$$(7.15)$$

where Q is the leak rate and V is the bobbin voltage. The final selection of the form of the variable scales was based on performing least squares regression analysis on each possible combination and examining the square of the correlation coefficient for each case.

A summary of the results of the calculations is provided in the following table. Given the results, it is not obvious whether the appropriate choice of axes scales should be linear-linear or log-log. Similar analysis of data for 3/4" diameter tubes yielded results of $r^2 = 0.98$ and $r^2 = 0.99$ for the same respective index of determination values, clearly indicating the choice to be log-log. In addition, independent analyses of the data showed that the distribution of voltages and leak rates independently followed a log-normal distribution. On these bases, analysis based on a log-log relationship is appropriate.

Index of determination, r^2 , for Various Selections of Coordinate Scales		
$\Delta P_{SLB} =$		
Bobbin Amplitude	Leak Rate	
	Linear	Logarithmic
Linear		
Logarithmic		

The number of data points used for the above evaluations was 24 and the number of degrees of freedom (dof) 22. The obtained value of r^2 is significant at a level of $\alpha = 0.05$ based on an F distribution test of the ratio of the mean square of the regression to the mean square of the error. This can also be interpreted as the probability that the log of the leak rate is correlated to the log of the bobbin amplitude. An alternate interpretation is that if the variables are really uncorrelated and the testing was repeated many times, an index of determination

equal to or greater than that obtained from the analyzed data would be expected to occur randomly in only _____ of those tests. Similar analysis of the 3/4" diameter tubes' data resulted in a significance level of _____ with a random probability of occurrence of the level of the observed correlation of only _____. If the variables are truly uncorrelated, then the joint probability of occurrence of the observed correlations would be _____ with an attendant probability that the variables are correlated of _____. The conclusion is that it is very likely that the variables are correlated.

Guidance on the appropriate choice of the regressor variable can be based on the knowledge of the approximate value of the slope of the relationship from CRAKFLO analysis results. Comparisons showed that the slope of a $\log(Q)$ on $\log(V)$ regression line more closely matched the CRAKFLO results bobbin amplitudes _____ volts with an inverse regression matching better for amplitudes _____ volts. The CRAKFLO results indicated the potential for a slope change between about _____ volts. It was initially concluded, therefore, that both regression lines would be calculated, giving the option of selecting the higher of the two for any voltage level as a candidate for the upper bound leakage. Graphical results verified the selection of the regressor and regressed variables as being appropriate in the range of interest. Subsequent discussions with the EPRI Committee for Alternate Repair Limits for ODSCC at TSP's concluded that the voltage range of interest was limited and that only the regression of $\log(Q)$ on $\log(V)$ needed to be considered. The CRAKFLO results are shown on Figure 7-13 associated with the analysis of confidence and prediction bounds (discussed later).

It is noted that the CRAKFLO results also indicated that the leak rate would be expected to decrease dramatically for indications with amplitudes below _____ volts. This is in agreement with the results of the probability of leak analysis.

7.6.2 Correlation Analysis and Identification of Outliers

In order to determine if the parameters of the relationships were being biased by the presence of unduly influential data points, a least median of squares regression analysis was performed on the data set for the $\log(Q)$ versus $\log(V)$ regression. Four points were identified as potential outliers for a ΔP of _____ ksi. An examination of the testing programs information revealed no basis for rejecting the data, thus it was retained for the analysis.

7.6.3 Error-in-Variables Considerations

The potential effect of measurement errors in the regressor were discussed in the section on burst pressure relative to bobbin amplitude. It was noted that the variance, σ^2 , of a variable, say X , with measurement error, as estimated from the data, consists of two parts, the intrinsic variation of the variable, x , and the variation due to measurement error, η , i.e.,

(7.16)

where the various contributors to the variance are as described respectively. A Wald-Bartlett type of analysis was performed for each direction of regression. Considering $\log(Q)$ as the regressor resulted in a line indistinguishable from the standard regression line. Considering $\log(V)$ as the regressor resulted in a line with a slightly larger slope than the standard fit. This was to be expected since the previous use of the technique for the burst pressure correlation

indicated that measurement errors for the bobbin amplitude were not significant. Omitting the consideration of variable measurement errors results in a conservative prediction of leakage for all levels of bobbin amplitude. It is recognized that the use of the Wald-Bartlett technique has met with some controversy with some members of the EPRI Committee for Alternate Repair Limits for ODSCC, however, it is generally accepted as a viable technique for determining if errors in the variables are significantly affecting the regression line. Since no accepted quantitative values for the variance of the errors exists, a rigorous errors-in-variables analysis cannot be performed. The results obtained here imply that errors in the independent variable are not significantly biasing the analysis.

7.6.4 SLB Leak Rate Correlation for 7/8 Inch Diameter Tubing

The final regression curve fit to the data is shown on Figures 7-8 through 7-10 for ΔP_{SLB} values of _____ ksi respectively. The correlation lines are given by

$$(7.17)$$

The coefficients for the above equation are provided in the following table for three ΔP_{SLB} levels. In addition to the least squares regression line, the upper _____ one-sided, simultaneous confidence bound, the upper _____ prediction bound, and the arithmetic average of the regression line were determined. These are depicted on Figures 7-11 through 7-13 for the regression of $\log(Q)$ on $\log(V)$.

The expected, or arithmetic average (AA), leak rate, Q , corresponding to a voltage level, V ,

Regression Coefficients for SLB Leak Rate to Bobbin Amplitude Correlation			
	SLB @ ksi	SLB @ ksi	SLB @ ksi
a_0			
a_1			

from the above expressions was also determined. Since the regression was performed as $\log(Q)$ on $\log(V)$ the regression line represents the mean of $\log(Q)$ as a function of bobbin amplitude. This is not the mean of Q as a function of V . The residuals of $\log(Q)$ are expected to be normally distributed about the regression line. Thus, the median and mode of the $\log(Q)$ residuals are also estimated by the regression line. However, Q is then expected to be distributed about the regression line as a log-normal distribution. The regression line still estimates the median of Q , but the mode and mean are displaced. As a uniform example, the values, 0.1 and 10 have a numerical average of 5.05, while the average of their logarithms is 0 with an anti-logarithm of the average of 1. The corresponding adjustment to the normal

distribution to obtain the arithmetic average, i.e., mean, for a log-normal distribution results in

(7.18)

for the expected AA of Q for a given V , where σ^2 is the estimated variance of $\log(Q)$ about the regression line.

To complete the analysis for the leak rate, the expected leak rate as a function of $\log(V)$ was determined by multiplying the arithmetic average leak rate by the probability of leak. The results of this calculation are also depicted on Figure 7-12 for a steam line break differential pressure of psi..

Analysis of Residuals

Analysis of the regression residuals was performed per the descriptions given in Appendix D to this report. As previously noted, the correlation coefficients obtained from the analyses indicate that the log-log regressions at the various SLB ΔP 's are significant at a level greater than . Additional verification of the appropriateness of the regression was obtained by analyzing the regression residuals, i.e., the actual variable value minus the predicted variable value from the regression equation.

Figures 7-14 through 7-16 show the $\log(Q)$ residuals as a function of predicted $\log(Q)$ for the three SLB differential pressures of interest. For each, the arrangement of the data points is non-descript, indicating no apparent correlation between the residuals and the predicted values.

Cumulative normal probability plots were prepared for steam line break differential pressures of and psi, see Figures 7-17 and 7-18. An alternate approach was taken for ΔP_{SLB} of psi, Figure 7-19. Here the actual cumulative probability of the residuals was plotted against the expected cumulative probability of the residuals. For each of these cases a straight line is approximated, typical of the behavior of normally distributed residuals.

Given the results of the residuals scatter plots and the normal probability plots, it is considered that the regression curve and statistics can be used for the prediction of leak rate as a function of bobbin amplitude, and for the establishment of statistical inference bounds.

Table 7-1

**Non-Leaking 7/8 Inch Specimens with
Throughwall or Near Throughwall Cracks ⁽¹⁾**

Table 7-2

Dependence of SLB Leakage on Throughwall (TW) Crack Length

Table 7-3: Database for Probability of Leak for 7/8" Diameter Tubes

Figure 7-1: Bobbin Coil Voltage vs. Maximum Examination Depth
7/8" Pulled Tubes Data, Destructive Examination

Figure 7-2: Bobbin Coil Voltage vs. Maximum Examination Depth
3/4" Pulled Tubes Data, Destructive Examination

Figure 7-3

SLB LEAKAGE - VOLTAGE DISTRIBUTION
COMBINED DATA (7/8 INCH NORMALIZATION)

Figure 7-4

SLB LEAKAGE PROBABILITY
COMBINED DATA (7/8 INCH NORMALIZATION)

Figure 7-5

SLB LEAKAGE - VOLTAGE DISTRIBUTION
7/8 INCH TUBING DATA

Figure 7-6

SLB LEAKAGE PROBABILITY
7/8 INCH TUBING DATA

Figure 7-7: Probability of Leak vs. Bobbin Amplitude
7/8" Tubes, Model Boiler & Field Data

Figure 7-8: 2335 psi SLB Leak Rate vs. Bobbin Amplitude
7/8" x 0.050" SG Tubes, Model Boiler & Field Data

Figure 7-9: 2560 psi SLB Leak Rate vs. Bobbin Amplitude
7/8" x 0.050" SG Tubes, Model Boiler & Field Data

Figure 7-10: 2650 psi SLB Leak Rate vs. Bobbin Amplitude
7/8" x 0.050" SG Tubes, Model Boiler & Field Data

Figure 7-11: 2335 psi SLB Leak Rate vs. Bobbin Amplitude
7/8" x 0.050" SG Tubes, Model Boiler & Field Data

Figure 7-12: 2560 psi SLB Leak Rate vs. Bobbin Amplitude
7/8" x 0.050" SG Tubes, Model Boiler & Field Data

Figure 7-13: 2650 psi SLB Leak Rate vs. Bobbin Amplitude
7/8" x 0.050" SG Tubes, Model Boiler & Field Data

Figure 7-14: 2335 psi SLB Leak Rate vs. Bobbin Amplitude
7/8" x 0.050" SG Tubes, Model Boiler & Field Data

Figure 7-15: 2560 psi SLB Leak Rate vs. Bobbin Amplitude
7/8" x 0.050" SG Tubes, Model Boiler & Field Data

Figure 7-16: 2650 psi SLB Leak Rate vs. Bobbin Amplitude
7/8" x 0.050" SG Tubes, Model Boiler & Field Data

Figure 7-17: 2335 psi SLB Leak Rate vs. Bobbin Amplitude
7/8" x 0.050" SG Tubes, Model Boiler & Field Data

Figure 7-18: 2560 psi SLB Leak Rate vs. Bobbin Amplitude
7/8" x 0.050" SG Tubes, Model Boiler & Field Data

Figure 7-19: 2650 psi SLB Leak Rate vs. Bobbin Amplitude
7/8" x 0.050" SG Tubes, Model Boiler & Field Data

Appendix A

DESTRUCTIVE EXAMINATION RESULTS FOR 7/8" MODEL BOILER SPECIMENS

A.1 Objectives

The objective of this task is to characterize the size, shape, and morphology of the laboratory created corrosion in alloy 600 tube specimens which have been leak rate and burst tested. The crack morphology is also to be compared generally to the corrosion morphology observed in tubes pulled from operating power plant steam generators. A summary of the results is presented in this section.

A.2 Examination Methods

Examination methods include visual examinations, macrophotography, light microscopy and/or SEM (scanning electron microscopy) examinations, SEM fractography, and metallography. A total of 19 model boiler test specimens and one doped steam specimen were selected for destructive examinations. Most of these were leak and burst tested.

The specimens were initially examined visually and with a low power microscope. The burst opening and visible cracks around the circumference of the tube within the tube support plate intersection were visually examined and their location in relation to the burst crack noted. (When the crack networks were particularly complex, such as when circumferential components were strongly present, photographs of the crack networks were taken and included in this report for more complete documentation of the data.) The major burst crack was then opened for fractographic observations including crack surface morphology, crack length, and crack depth using SEM. One metallographic cross section of each tube specimen was selected containing the majority of secondary cracks within the tube support plate region. The location of the cracks within this metallographic cross section was noted, the cracks measured as to their depth and a crack was photographed to show the typical crack morphology. Note that the one metallographic section through each specimen will provide the secondary crack distribution at that location. Secondary cracks at other elevations would not be recorded unless the burst test happened to open the secondary cracks sufficiently for visual examination to record their location.

A.3 Results

Tube 509-2

The burst fracture in tube 509-2 was caused by four small, axial, through-wall cracks which formed the larger macrocrack at the burst opening. Ligament features were all intergranular. The macrocrack morphology was that of IGSCC. Only minor IGA was associated with the IGSCC. The D/W ratio was . . . (See paragraph 2.2 for definitions of these morphological

terms). The macrocrack was inch long on the OD and penetrated through-wall for a length of inch. Some secondary cracks adjacent to the macrocrack were quite deep. All cracks were axially orientated, originated on the OD and were confined to the crevice region. The crack distribution within the crevice region is shown in figure A-1 together with the description of the main burst crack. A metallographic cross section through the most populous crack region within the crevice region is depicted in figure A-2 together with a photomicrograph of one of the secondary cracks. No surface IGA was observed. From surface photographs, it is possible that local patches of cellular IGA/SCC exist within the crevice region.

Tube 509-3

Tube 509-3 burst from a single through-wall crack which was inch long and through-wall for inch. The morphology of the OD origin crack was IGSCC. Three other prominent cracks, were found that were not through-wall, but were relatively deep, up to through-wall. All cracks were confined to the lower region of the simulated SP crevice region. A metallographic cross section through some of the secondary cracks within the crevice region produced a crack distribution as shown in figure A-3. The morphology of one of these cracks is shown in a photomicrograph in the lower portion of this figure. A summary of the shape, size and morphology of the burst crack, together with a sketch of the overall crack distribution is shown in figure A-4. No surface IGA was observed and the IGSCC had a minor D/W ratio of

Tube 510-1

Corrosion in tube 510-1 occurred in the simulated support plate crevice region where many small, but deep, cracks caused the tube rupture during the burst test. The burst crack network of corrosion cracking is shown in figure A-5. The burst opening was very irregular. It was formed by at least axial microcracks which joined by circumferential, corroded ligaments to form the larger macrocrack. The macrocrack was inch long with a total through-wall length of inch. The morphology of the macrocrack was IGSCC. Examination of the macrocrack and other secondary cracks on the tube OD within the crevice region revealed a crack distribution as shown in figure A-6. A metallographic cross section through the crevice region containing most of the cracks produced a crack distribution as shown in figure A-7. A photomicrograph of one of the secondary cracks is also shown in this figure. No surface IGA was observed. The IGSCC had a moderate D/W ratio of (moderate amounts of IGA associated with the crack).

Tube 525-1

The burst crack was relatively short (inches long) but deep, through-wall. The macrocrack was composed of three microcracks which grew together by intergranular corrosion. The secondary cracks were all short and axially orientated. A summary of the shape, morphology and distribution of cracks found in Tube 525-1 is presented in figures A-8 and A-9. No surface IGA was observed and the IGSCC had a moderate D/W ratio of

Tube 528-1

A concentrated group of small axial, OD origin, cracks in the center of the simulated SP crevice region formed the location of the burst opening. Figure A-10 shows photographs of the burst opening which had an irregular crack pattern due to the complex network of microcracks. The intergranular macrocrack was inch long and through-wall for inch. It was formed from at least microcracks which joined together at ligament locations which had only intergranular features. Metallography showed that the burst crack morphology was that of IGSCC. A metallographic cross section through the center of the crevice region revealed a second cluster of secondary cracks approximately at the opposite side of the tube from the burst opening. The crack distribution in this section is shown in a sketch in figure A-11 together with a photomicrograph showing two of the secondary cracks. Their morphology is that of IGSCC. A summary of the burst crack and of the overall crack distribution is given in figure A-12. No surface IGA was observed and the IGSCC had a minor D/W ratio of

Tube 528-2

A grouping of many small, OD origin, axial cracks, interconnected by ligaments and by circumferential extensions, formed the curved major burst opening shown in figure A-13. Other small axial cracks with circumferential involvement were observed in other areas of the simulated tube support plate crevice region. Fractographic observations of the major burst opening revealed that the corrosion crack consisted of at least microcracks with intergranular ligaments. These ligaments often ran in the circumferential direction. The combined length of the microcracks that formed the macrocrack was inch. Through-wall cracking extended for inch. The morphology of the macrocrack was IGSCC with no to negligible IGA components, as shown in figure A-14. Circumferential, intergranular extension of the axial crack can be observed in this figure. Transverse metallography through the center of the crevice region revealed the crack distribution shown by a sketch in figure A-15. An example of the morphology of one of the secondary OD cracks is also shown in this figure; the morphology is again that of IGSCC with negligible IGA aspects. A summary of the major crack shape and corrosion morphology and the distribution of OD cracks observed within the crevice region of tube 528-2 is shown in figure A-16. No surface IGA was observed and the IGSCC had a moderate D/W ratio of

Tube 532-1

A large number of long and short, OD origin, axial cracks were observed in the simulated tube support plate crevice region of tube 532-1, many of which were through-wall. Figures A-17 and A-18 show photographs of the burst tube and convey the extensive cracking around the tube within the crevice region. A grouping of small axial cracks combined to form of the burst crack openings which were examined in some detail. The longer of the was inch long and was formed from microcracks interconnected with ledges having intergranular features. The length through-wall was inch. The crack morphology was IGSCC. Cracks seen on a metallographic cross section through the center of the crevice are

depicted in a sketch in figure A-19 together with two micrographs showing typical crack morphologies of secondary cracks. A summary of the major burst crack and its morphology together with a distribution of cracks seen in the crevice region is shown in figure A-20. No surface IGA was observed and the IGSCC had a moderate D/W ratio of

Tube 532-2

OD origin cracking within the simulated tube support plate crevice region of tube 532-2 can be seen in the post-burst test photographs of the tube in figures A-21 and A-22. Many of the axial cracks were through-wall. A group of many through-wall microcracks formed the weakest area in the tube where the main burst fracture occurred. Fractography of this macrocrack showed at least microcracks combined to form the main burst fracture. The total length of the macrocrack was inch and it was through-wall for inch. While most ligament features were intergranular, occasional areas had ductile features, indicating that the ligaments had not completely interconnected by intergranular corrosion. The corrosion crack morphology of the main burst crack was that of IGSCC. A metallographic cross section through the center of the crevice region revealed many cracks shown by a sketch in figure A-23. Typical crack morphologies are also shown in photomicrographs for two secondary cracks in this figure. A summary of the main burst crack description, morphology, and crack distribution are given in figure A-24. No surface IGA was observed and the IGSCC had a moderate D/W ratio of

Tube 533-3

The collars of this model boiler specimen were removed. Several small axial cracks were observed at the support intersections. One was located under the Teflon collar and a few were located under the top steel collar. The crack within the Teflon collar intersection was opened and examined by SEM. The macrocrack face exhibited intergranular features and some ductile tearing was observed on one of the three ligaments found. The macrocrack was inch long and was composed of microcracks. The OD origin crack penetrated the ID wall for a length of inch. A metallographic cross section through the center of the Teflon collar intersection revealed numerous small intergranular stress corrosion cracks. The location (on the tube) and depth of these cracks is shown in figure A-25, together with one micrograph. A metallographic cross section through some of the cracks within the steel collar intersection revealed the crack distribution as shown in figure A-26. The characterization of the through-wall crack found under the Teflon collar and the crack distribution around the tube within the Teflon support is shown in figure 7-27. No surface IGA was observed and the IGSCC had mostly minor D/W ratios (ratios varied from).

Tube 533-4

A network of axial and circumferential secondary cracks was observed near the burst crack. The burst crack was composed of at least microcracks which joined to form the macrocrack. Ledges separating these microcracks showed partially ductile features (shear dimples) while the crack faces were entirely intergranular. The OD origin major crack was

inch long and penetrated the ID wall for a length of inch. The secondary crack distribution found in the metallographic cross section is shown in figure A-28, and a summary of the cracks observed in the support plate region of the tube is presented in figure A-29. No surface IGA was observed and the IGSCC had a moderate D/W ratio of

Tube 535-1

The burst opening in tube 535-1 formed from a cluster of small axial OD origin cracks. Numerous secondary, but small, microcracks were observed around the circumference within the crevice region. Fractography of the burst crack showed that it was composed of microcracks which joined together by intergranular corrosion to form the macrocrack. The morphology of the macrocrack was IGSCC with negligible IGA aspects. The macrocrack was relatively short (inch in length) and penetrated through-wall for inch. A metallographic cross section through the center of the crevice showed numerous secondary cracks, some of which had negligible to minor IGA aspects. The distribution of cracks from the cross section is shown in figure A-30 along with a photomicrograph of a secondary crack. A summary of the of burst crack description and of the overall crack distribution is given in figure A-31. No surface IGA was observed and the IGSCC had a moderate D/W ratio of

Tube 536-1

Many small secondary axial cracks are clustered around the burst opening. Other larger secondary cracks were found at a location degrees from the burst opening. The main burst crack and the largest of the secondary cracks located at degrees were opened and examined by SEM. In both cases the OD origin cracking morphology was intergranular and typical of SCC. The major crack was inch long and through-wall. The macrocrack consisted of at least microcracks which joined, mostly by ductile fracture, to form the macrocrack. The largest secondary crack was inch long and through-wall. It was also formed by several microcracks. A metallographic cross section through the remaining piece of the tube at the support plate intersection showed intergranular OD origin stress corrosion cracks (figure A-32). The largest of these cracks was through-wall. A summary of crack observations on Tube 536-1 is shown in figure A-33. No surface IGA was observed and the IGSCC had a minor D/W ratio of

Tube 543-4

Visual examination was performed on the secondary cracks adjacent to the main burst opening. The short secondary cracks were orientated axially, inclined, and in some instances circumferentially. Fractography of the burst crack showed that the environmental cracks were intergranular and typical of stress corrosion cracking (SCC). The macrocrack was inches long and did not penetrate the ID wall although it was at many locations up to through-wall. The macrocrack was composed of at least microcracks, all of which had joined together by intergranular corrosion. A metallographic cross section through many of the secondary cracks observed on the tube OD within the simulated tube support plate intersection

revealed cracks with depths ranging from through-wall. A sketch of the location of these cracks relative to the burst fracture is shown in figure A-34. A typical crack morphology of a secondary crack is shown in this figure. A summary of the observed OD origin secondary cracks and morphology of the main crack are shown in figure A-35. No surface IGA was observed and the IGSCC had a minor D/W ratio of

Tube 555-3

The most degraded area in tube 555-3 was confined to one location within the crevice region, the location where the burst opening occurred. The crack distribution was complex in this region, with numerous parallel axial cracks with short circumferential branches. All cracks were of OD origin. Fractography showed the major macrocrack to be composed of microcracks which joined in an irregular pattern to form the burst crack. The connecting ledges showed a ductile fracture features, while the individual microcracks had intergranular features. The macrocrack was inch long with a through-wall length of inch. Metallography of a tube cross section through the region with the highest crack density showed a morphology of IGSCC with some IGA or SCC branch characteristics near the main fracture. A photograph of the burst opening and a photomicrograph of the fracture face at the burst opening is shown in figure A-36. Other crack details are summarized in figures A-37 and A-38. No surface IGA was observed and the IGSCC had a minor D/W ratio of

Tube 558-1

The major macrocrack originated from a cluster of smaller secondary cracks which joined in an irregular pattern to form the macrocrack. Visual examinations of the remaining tube support plate region indicated that no other secondary cracks existed. The opened fracture face of the burst crack revealed more clearly the irregular cracking pattern of this major crack caused by the joining of the widely separated microcracks. The macrocrack showed at least major ledges which separated the microcracks. The features of the OD origin macrocrack were intergranular and the ledges had mostly intergranular features. The crack was inch long and it penetrated the ID wall for approximately inch. A summary of the crack observations is shown in figure A-39. No metallography was done on this tube since no secondary cracks away from the burst opening were observed.

Tube 568-6

Tube 568-6 was not burst tested as it was a very short specimen. Destructive examination did not find any corrosion degradation. This specimen had been repaired during the corrosion testing by removing a leaking end cap and welding on a new fitting. It is possible that corrosion may have been present within the welded region since eddy current had previously detected an indication.

Tube 571-1

The burst crack appears to consist of a major axial crack whose length was [redacted] inch. No obvious separation of the macrocrack into different microcracks was found within the burst crack, alternatively there were hints of [redacted] microcracks which nucleated in almost identical planes. The OD origin crack penetrated the wall for a length of [redacted] inch. It was entirely intergranular and typical of stress corrosion cracking, based on examination of the fractographic details. No other secondary cracks were observed along the circumference of the tube. A metallographic cross section through the center of the support plate region found no secondary cracking. A summary of crack observations is shown in figure A-40. No surface IGA was observed and the IGSCC had a minor D/W ratio of [redacted].

Tube 576-2

Only [redacted] axial crack was observed after burst testing of tube 576-2. Fractography showed the crack to be [redacted] inch long and it was through-wall for [redacted] inch. The macrocrack appeared to be composed of a [redacted] microcrack and its morphology was that of IGSCC. A metallographic cross section through the center of the crevice region found no secondary cracks around the circumference. Crack details and crack morphology data are shown in figures A-41 and A-42. No surface IGA was observed and the IGSCC had a minor D/W ratio of [redacted].

Tube 576-4

Tube 576-4 also burst with a [redacted] crack. Fractography showed the crack to be [redacted] inch long and it was through-wall for [redacted] inch. The OD origin intergranular macrocrack was composed of [redacted] axial microcracks joined together by ligaments with intergranular features. Visual examination showed a few small axial cracks nearby the burst crack. The morphology of the burst crack was IGSCC with negligible IGA aspects. A metallographic section cut through the center of the crevice found only the burst crack. Crack details and crack morphology data are shown in figures A-43 and A-44. No surface IGA was observed and the IGSCC had a moderate D/W ratio of [redacted].

Tube SL-FH-11

Doped steam specimen SL-FH-11 developed a large number of OD origin cracks. The largest agglomeration of these cracks was opened for fractographic examinations and cross sectional cuts were made above (A) and below (B) the opened section of the macrocrack for metallographic examinations. The opened section of the tube showed an intergranular macrocrack, [redacted] inch long. The ligaments separating the [redacted] microcracks of the macrocrack had only intergranular features. The crack penetrated the ID wall for a length of [redacted] inch. The cross sectional cuts made through planes A and B produced the crack distributions and typical crack morphologies depicted in figures A-45 and A-46. A summary of the crack observations

made at this location is shown in figure A-47. No surface IGA was observed and the IGSCC had a moderate D/W ratio of

A longer but more shallow crack network was found on the opposite side of the tube from the crack just described. The crack network was opened and examined fractographically. The results are shown in figure A-48. The macrocrack was inch long and was composed of at least microcracks. It penetrated the ID wall only locally for a length of inch. The crack morphology was intergranular with some ductile features at ligament locations.

A.4 Comparison with Pulled Tube Crack Morphology

Table A-1 compares the corrosion morphology on pulled tubes with that found on tubing from laboratory tests. Most of the support plate cracking on pulled steam generator tubes was OD origin, intergranular stress corrosion cracking that was axially orientated. Large macrocracks were frequently present and were composed of numerous short microcracks (typically inches long) separated by ledges or ligaments. The ledges could have either intergranular or dimple rupture features depending on whether or not the microcracks had grown together during plant operation. Most cracks had minimal to moderate IGA features (minor to moderate D/W ratios) in addition to the overall stress corrosion features. Even when the IGA was present in association with the cracks in significant amounts, it did not dominate over the overall SCC morphology. The numbers of cracks distributed around the circumference at a given elevation within the crevice region varied from a few cracks to typically less than . In a few cases, the number of cracks was significantly larger than this, in one case possibly approaching . For this situation, patches of IGA formed where the cracks were particularly close and the individual cracks had some IGA characteristics. Even for this situation, the axial SCC was still the dominant corrosion morphology as the IGA was typically the depth of the IGSCC. In addition, cellular IGA/SCC was occasionally observed confined to small areas within the crevice region. Finally, IGA, separate and independent of SCC, has been observed. It is usually present as small isolated patches of IGA. In the few cases where more uniform IGA has been observed, it is typically shallow and intermittently distributed within support plate crevice regions.

The model boiler corrosion observed in this investigation was similar to that observed within typical pulled tube support plate crevice locations. Most corrosion was axially orientated IGSCC with negligible to moderate IGA aspects (minor to moderate D/W ratios) in association with the cracking. Some of the model boiler specimens had cracking with almost pure IGSCC, i.e., with no obvious IGA aspects (D/W ratios of or higher), more similar to PWSCC than to the typical OD IGSCC observed within support plate crevice corrosion on pulled tubes. IGA independent of the cracking was not observed in the model boiler specimens. The numbers of cracks at a given elevation was typically less than , similar to that observed in many of the pulled tubes. However, only one model boiler specimen had a moderate crack density and none had high crack densities as have been occasionally observed in plants. A number of the model boiler specimens from the second set of tests conducted in 1991, however, did have very complex crack networks that frequently had circumferential cracking in association with the

predominant axial cracking. Some of the complex crack networks may have had cellular IGA/SCC components similar to that occasionally observed in pulled tubes.

A.5 Conclusions from Specimen Destructive Examinations

It is concluded that the laboratory generated corrosion cracks have the same basic features as support plate crevice corrosion from pulled tubes. The laboratory created specimens frequently had somewhat lower crack densities, but individual cracks usually had similar IGA aspects (minor to moderate D/W ratios). IGA independent of IGSCC was not observed in the model boiler specimens as was sometimes observed in pulled tubes. The observed differences in corrosion morphology between the model boiler specimens and the pulled tubes is not believed to be significant.

Figure A-1. Summary of Burst Crack Observations and Overall Crack Distribution on Tube 509-2

Figure A-2. Secondary Crack Distribution in a Metallographic Cross Section in TSP Crevice Region and a Photomicrograph of a Crack in Tube 509-2. The burst crack and a secondary crack from the burst opening were observed. The crack morphology is that of IGSCC. Mag. 100X

Figure A-3. Secondary Crack Distribution in a Metallographic Cross Section Through the Center of the TSP Crevice Region and a Photomicrograph of a Crack in Tube 509-3. Only the burst crack and other cracks were present. The crack morphology is that of IGSCC. Mag. 100X

Figure A-4. Summary of Burst Crack Observations and Overall Crack Distribution on Tube 509-3

Figure A-5. Photographs of Burst Opening in Tube 510-1

Figure A-6. Summary of Burst Crack Observations and Overall Crack Distribution on Tube 510-1

Figure A-7. Secondary Crack Distribution in a Metallographic Cross Section in TSP Crevice Region and a Photomicrograph of a Crack in Tube 510-1. The burst crack and a number of secondary cracks on the opposite side from the burst opening were observed. The crack morphology is that of IGSCC. Mag. 100X

Figure A-8. Secondary Crack Distribution in a Metallographic Cross Section in TSP Crevice Region and a Photomicrograph of a Crack in Tube 525-1

Figure A-9. Summary of Crack Distribution and Morphology on Tube 525-1

Figure A-10. Photographs of Burst Opening in Tube 528-1

Figure A-11. Secondary Crack Distribution in a Metallographic Cross Section in TSP Crevice Region and a Photomicrograph of Cracks in Tube 528-1. The burst crack network and a cluster of secondary cracks at the opposite side of the burst opening were observed. The crack morphology is that of IGSCC. Mag. 100X

Figure A-12. Summary of Burst Crack Observations and Overall Crack Distribution on Tube 528-1

Figure A-13. Photographs of Burst Opening in Tube 528-2

Figure A-14. Crack Morphology of the Major Burst Opening (Transverse Section) in Tube 528-2 Showing IGSCC with Circumferential Extension. Mag. 100X

Figure A-15. Secondary Crack Distribution in a Metallographic Cross Section Through the Center of the TSP Crevice Region and a Photomicrograph of a Crack in Tube 528-2. The burst crack and several other cracks were present. The crack morphology is that of IGSCC with negligible IGA aspects. Mag. 100X

Figure A-16. Summary of Overall Crack Distribution and Morphology on Tube 528-2

Figure A-17. Photographs of the Largest Burst Opening and of the Nearby Secondary Cracks in Tube 532-1

Figure A-18. Photographs of Additional Secondary Cracks and of a Second Major Burst Crack in the Crevice Region of Tube 532-1

Figure A-19. Crack Distribution in a Metallographic Cross Section Through the Center of the TSP Crevice Region and two Photomicrographs of Tube 532-1. Mag. 100X

Figure A-20. Summary of Overall Crack Distribution and Morphology on Tube 532-1

Figure A-21. Photographs of the Major Burst Opening and of the Secondary Cracks in Tube 532-2

Figure A-22. Additional Photographs of Secondary Cracks in Tube 532-2

Figure A-23. Crack Distribution in a Metallographic Cross Section Through the Center of the TSP Crevice Region and two Photomicrographs of Secondary Cracks in Tube 532-2. Mag. 100X

Figure A-24. Summary of the Burst Crack and Overall Crack Distribution in the Crevice Region of Tube 332-2

Figure A-25. Secondary Crack Distribution and a Photomicrograph of Cracks in a Cross Section of Tube 533-3 within the Teflon Collar

Figure A-26. Crack Distribution and a Photomicrograph of one of These Cracks in a Cross Section of Tube 533-3 within the Steel Collar

Figure A-27. Summary of Crack Distribution and Morphology on Tube 533-3 at the Teflon Intersection

Figure A-28. Secondary Crack Distribution and a Photomicrograph of one of These Cracks in a Metallographic Cross Section of Tube 533-4

Figure A-29. Summary of Crack Distribution and Morphology on Tube 533-4

Figure A-10. Crack Distribution in a Metallographic Cross Section Through the Center of the Crevice Region and Photomicrograph of a Crack in Tube 535-1. Mag. 100X

Figure A-31. Summary of the Burst Crack and Overall Crack Distribution in the Crevice Region of Tube 535-1

Figure A-32. Secondary Crack Distribution and a Photomicrograph of one of These Cracks in a Metallographic Cross Section of Tube 536-1

Figure A-33. Summary of Crack Distribution and Morphology on Tube 536-1

Figure A-34. Sketch of a Metallographic Cross Section Through Secondary Support Plate Crevice Cracks and a Typical Crack Micrograph in Tube 543-4

Figure A-35. Summary of Crack Distribution and Morphology on Tube 543-4




Figure A-36. Photograph of the Burst Opening and a Photomicrograph of the Burst Fracture in Tube 555-3. Mag. 100X

Figure A-37. Sketch of the Metallographic Cross Section and a Photomicrograph of Tube 555-3. Mag. 100X

Figure A-38. Summary of the Burst Crack and Overall Crack Distribution in the Crevice Region of Tube 555-3

Figure A-39. Summary of Crack Distribution and Morphology on Tube 558-1

Figure A-40. Summary of Crack Distribution and Morphology on Tube 571-1

Figure A-41. Sketch of a Metallographic Cross Section Through the Center of the Crevice Region and a Photomicrograph of the Burst Crack in Tube 576-2. Mag. 100X

Figure A-42. Summary of Burst Crack Observations and the Overall Crack Distribution in Tube 576-2

Figure A-43. Sketch of a Metallographic Cross Section Through the Center of the Crevice Region and a Photomicrograph of the Burst Crack in Tube 576-4. Mag. 100X

Figure A-44. Summary of Burst Crack Observations and the Overall Crack Distribution in Tube 576-4

Figure A-45. Crack Distribution and a Micrograph of One of These Cracks in a Cross Section of Tube SL-FH-11 in Plane A

Figure A-46. Crack Distribution and a Micrograph of One of These Cracks in a Cross Section of Tube SL-FH-11 in Plane B

Figure A-47. Summary of Crack Distribution and Morphology on Tube SL-FH-11

Figure A-48. Summary of Crack Distribution and Morphology Observed on a Second Crack Opened in the Laboratory on Tube SL-FH-11

Appendix B

Leak Rate Adjustment For 7/8" Tubes

B.1 Objectives

This appendix summarizes adjustment procedure for leak rate test data for 7/8" outside diameter tubes with cracks. The tests were conducted under typical pressure differentials of normal power operation (NOP) and steam line break (SLB). However, the test conditions may not be identical to specific plant conditions. For instance, measurements at SLB conditions were obtained at a psi pressure differential but with a psia secondary side pressure rather than a prototypic psia pressure to improve the maintenance of constant test conditions in the measurement facility.

Adjustment procedure has been developed to scale the test conditions to specific plant conditions. The objectives of this appendix are as follows.

1. Adjust the French room temperature measurements of leak rate to operating temperature, and adjust to reference pressure differential from measured pressure differential.
2. Adjust Westinghouse measurements at operating temperature from high primary pressure to realistic primary pressure during steam line break.
3. Adjust leak rates at temperature between measured and reference pressure differentials.

B.2 Leak Rate Adjustment Procedure

Paul Hernalsteen of Laborelec in Belgium has developed adjustment procedures to scale the Belgian data to operating temperature and pressures different from the measured ones. First, we define the leak rate as follows.

(1)

where

L = volumetric leak rate

K = discharge coefficient

A = leakage flow area; a function of Δp and temperature T

ρ = water density; a function of temperature T

T = water temperature

Δp = pressure differential; $p_1 - p_2$ if no flashing or $p_1 - p_{1f}$ if flashing at p_{1f}

p_1 = upstream pressure, or primary side pressure

p_2 = downstream pressure, or secondary side pressure

p_{1f} = saturation pressure corresponding to upstream temperature T_1

The pressure differential is the difference between upstream and downstream pressure of the cracked passage of the tube. During steam line break, the leak flow may flash on the secondary side. So the effective downstream back pressure is equal to the saturation pressure p_{1f} if it flashes at the saturation point of the upstream temperature T_1 .

B.2.1 Adjustment under the Same Temperature

Let us consider the measurement conditions of leak rate at a reference temperature T_o . Now we can write

(2)

(3)

where the subscript o indicates the condition at the reference temperature T_o at which leak rate test is made. The reference temperature T_o may be at room temperature T_a (say, 70°F) or operating temperature about 616°F. The subscript m refers to measurement. In addition,

Δp_o = desired pressure differential at the reference temperature

Δp_{mo} = listed measurement pressure differential at the reference temperature

Both Eqs (2) and (3) describe the leak rate at the reference temperature but at different pressure differentials. We reserve Eq (2) for the test measurements. Eq (3) is for desired conditions, to which Eq (2) is to be adjusted. We will adjust leak rate from the measured pressure differential Δp_{mo} to a desired pressure differential Δp_o under the same temperature T_o . To do so, we write the following.

(4)

where the coefficient δ is a function of pressure differential as follows.

This coefficient δ involves two parameters. The first one is the area of crack flow opening. The second one is the pressure differential. We will rearrange the above expression as follows.

(5)

where we have used the following definition.

$$\Delta p^* = p_1 - p_2$$

The superscript * emphasizes the total difference of the upstream and downstream pressures, irregardless of whether water flashing taking place or not. When the Δp is used without the superscript * it can be $p_1 - p_2$ for non-flashing situation or $p_1 - p_{1f}$ for flashing situation. Explicit function of Eq (5)

will be given later. Eqs (4) and (5) adjust the laboratory test data to any Δp_o to be analyzed at the same temperature.

B.2.2 Adjustment under Different Temperature

Steam generator tube leak occurs in general at the operating temperature T of about 616°F. The Belgian data were measured at the room temperature. One has to scale the laboratory, room temperature data to the operating temperature. For this goal, we write the following equality

(6)

Using Eq (4), Eq (6) becomes

(7)

Using Eq (1), Eq (7) appears as follows.

(8)

The above expression describes the procedure to adjust a measured leak rate at Δp_{mo} and T_o to an equivalent leak rate at Δp^*_o ($= \Delta p^*$) and T .

The leak rate $L(\Delta p, T)$ is the volumetric rate at operating temperature T . But, leak rate detected in actual plant monitoring is collected at room temperature T_a . Laboratory test of leak rate under the operating temperature is generally collected at room temperature, too. An equivalent room temperature, volumetric leak rate, say $L(\Delta p, T)_{T_a}$ can be obtained from

(9)

Using Eqs (8) and (9), we get

(10)

We can write the above equation as follows.

(11)

where

(12)

(13)

(14)

The α factor involves a ratio of flow area of the crack opening as a function of Δp^*_{mo} and Δp^*_o under the same upstream temperature T_o . The α factor captures a mechanical effect of total pressure differential on crack opening area. The β factor adjusts temperature effect on the leak rate through flow area change and upstream water density variation under the same total pressure differential (i.e., $\Delta p^*_o = \Delta p^*$). The γ factor takes care of hydraulic effect of pressure differential on leakage flow rate.

B.2.3 The Mechanical Factor α

According to report by Hernalsteen of Laborelec, significant tearing of crack length took place during tube pulling. Measured leak rates in Table B-1 represent the behavior of significant tearing of crack length of 3/4" tubing. For each of the eleven leaking tubes, the leak rates have been plotted as a function of pressure differential on a semi-logarithmic paper. There are usually 4 data points per test tube and they reasonably align along a straight line. According to these straight line fitting of leak rate, Hernalsteen developed the following correlation for scaling measured leak rate from one pressure differential to another one at same room temperature.

(15)

where the pressure differentials are in psi, and b is a correlation constant. This correlation of the mechanical adjustment factor α fits the Belgian pulled tubes data of Table B-1. Behavior of the pressure adjustment factor may vary from one pulled tube to another. For the Plant E-4 data, the constant b in Eq (15) principally varied from with one indication at about . The larger constants tended to occur when there was increased evidence of damage from tube pulling effects which would likely lead to higher than expected leak rates at low pressure differentials such as normal operating conditions.

Table 1
Results of Leak Rate Tests under Room Temperature
and Typical Pressure Differentials during Steam Line Break

Leak rate at higher pressure differentials such as SLB conditions would be less influenced by ligament tearing in tube pulling operations as some ligaments would likely tear away at the higher pressure differential. For this reason, Laborelec has recommended the constant of $\Delta P = 100$ psi for all Plant E-4 tube intersections. Thus, it follows that

(16)

Equation (15) is equivalent to the following expression.

or

(17)

(18)

(19)

The correlation constant b or b^* can be determined from straight line fitting of test data. Based on Belgian data base, the constant $b = 0.0001$ is recommended by Hernalsteen. Thus, it follows that

(20)

is appropriate for the Belgian Data. The slopes of leak rate vs. pressure differential for the Belgian data were steeper than generally expected which is typical of tearing ligaments as the pressure differential is increased.

B.2.4 The Temperature Factor β

The flow opening area of the crack is approximately (confirmed by CRACKFLO analyses) inversely

proportional to the product of flow stress σ_f and Young's modulus E of the tube metal. Both flow stress and Young's modulus are functions of temperature. Therefore, it follows that

(21)

where ρ is the water density corresponding to upstream temperature $T_I = T$ and pressure p_I . The ρ_o refers to a $T_I = T_o$, and ρ_a to a $T_I = T_a$.

B.2.5 The Hydraulic Factor γ

The γ factor describes the effect of pressure differential on leakage flow rate. When there are no water flashing at T_o and T , $\Delta p = \Delta p^*_o$ and $\Delta p_{mo} = \Delta p^*_{mo}$, so $\gamma = 1$. When there are water flashing we have to use effective pressure differentials for Δp and Δp_{mo} . We can now write the γ factor as follows.

(22)

where C_p is a parameter to correlate the effective pressure differential through flashing pressure. For an isentropic process, the flashing takes place at the saturation pressure corresponding to the upstream water temperature T_I (e.g., T_I, T_{oI}). So $C_p = 1$ is for an isentropic process. If a real process deviates significantly from an isentropic one, and the parameter C_p will be less than unity.

B.3 The Mechanical Factor α

B.3.1 Belgian Factor α and Leak Rate Adjustment for Plant E-4 Data

Table 1 presents measured leak rates for the pulled tubes from Plant E-4 steam generators. The leak rate tests were done at room temperature (70°F). There are eleven sample pulled tubes being tested. These data have been used to establish Eq (15) for the mechanical adjustment factor α . The CRACKFLO has been developed based on Westinghouse fatigue crack and pulled tube data. The CRACKFLO pressure adjustment factor is different from the Belgian. The difference is believed due to minimal ligament tearing used in the CRACKFLO model compared to significant tearing in the Belgian pulled tubes. Next subsection will discuss the mechanical adjustment factor for minimal ligament tearing.

B.3.2 General Mechanical Factor α and Leak Rate Adjustment for Minimal Ligament Tearing

We will verify the applicability of Eq (18) or (15) with the CRACKFLO code. Table 2 presents the CRACKFLO code results of leak rate at different crack lengths under a variety of pressure differentials during power operation. It also includes comparison of the CRACKFLO adjustment factor and the α factor by Eq (15) with $b =$ and Eq (18) with $b^* =$. Similar to Table 2, Table 3 presents the comparison for a variety of pressure differentials under steam line break.

The Belgian α adjustment factor for Plant E decreases faster than the CRACKFLO and exponential adjustment factors having $b^* = b$ for decreases in Δp from the reference point. Use of the exponential adjustment factor is then conservative in estimating the leak rate when the adjustment is toward a lower Δp . Adjustment to Westinghouse measurements in this report are to lower pressure differentials such that the use of the exponential form of Eq (18) with $b^* =$ leads to higher adjusted leak rates than if Eq (15) with $b =$ were applied.

As shown in Tables 2 and 3, Eq (18) with $b^* =$ yields good agreement with crack opening models such as CRACKFLO which do not and cannot account for tearing of ligaments within macrocrack. Smaller values of b^* , such as the Belgian , can be expected when ligament tearing occurs and larger values than about when ligaments do not tear and retard crack opening compared to a uniform crack. The use of $b^* =$ for Eq (18) introduces an arbitrary conservatism. This conservatism yields higher leak rates when adjusting from higher to lower pressure differentials. It can add arbitrary scatter to the adjusted data set.

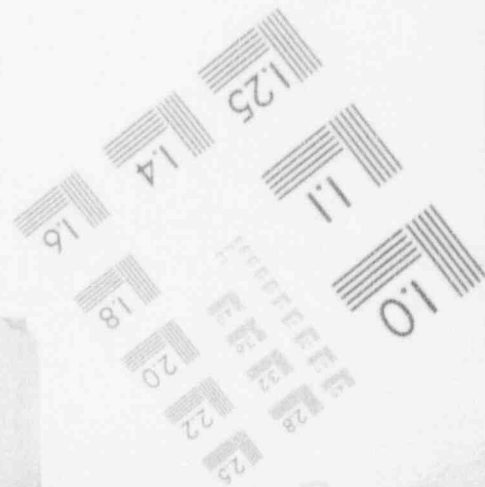
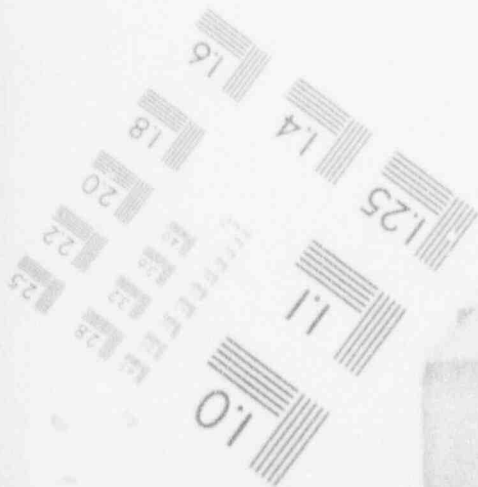
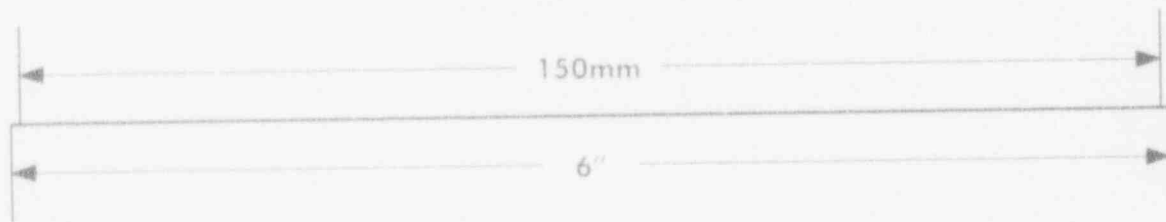
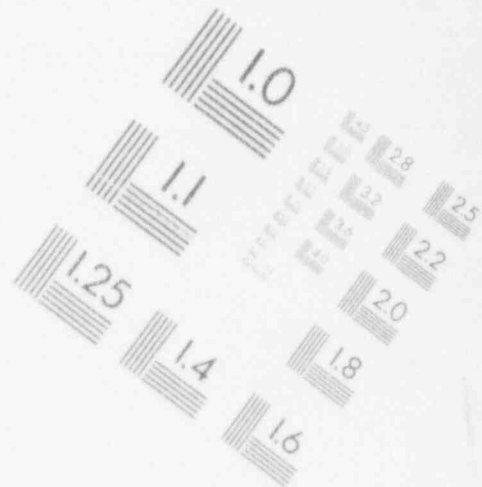
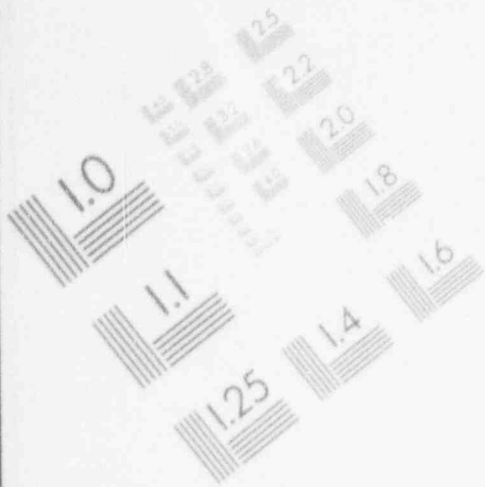
To assist interpretation of the adjustment procedure, only Eq (18) will be applied where b^* is obtained for a given data set (Belgian data) or for an individual specimen. Determination of b^* by fitting Eq (18) on an individual specimen basis to the measured data is the preferred method. Equation (18) is then applied to interpolate or extrapolate the measurements to the desired pressure differential. Equation (18) with $b^* =$ will be used only for specimens having a single pressure differential with measured leakage. This approach is based on good agreement with the CRACKFLO analytical crack opening model with $b^* =$ as described above.

Table 2
Comparison of the Pressure Adjustment Factor α between
the CRACKFLO Prediction and Proposed Correlation at Temperature
--Power Operating Pressure Differentials--

Table 3
Comparison of the Pressure Adjustment Factor α between
the CRACKFLO Prediction and Proposed Correlation at Temperature
--Steam Line Break Pressure Differentials--

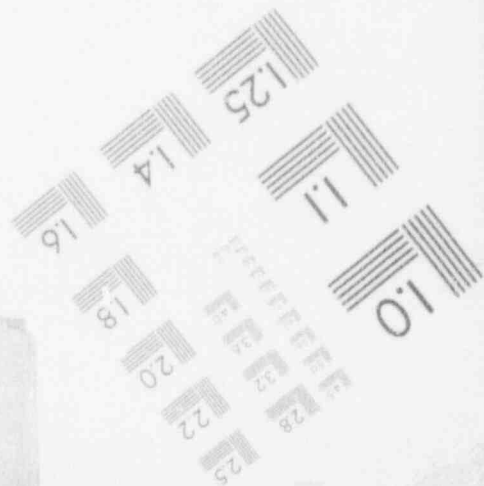
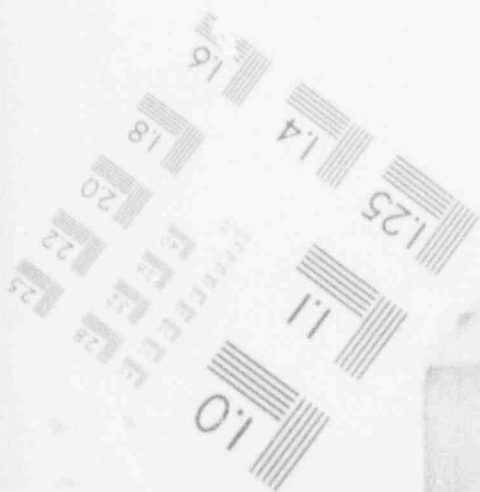
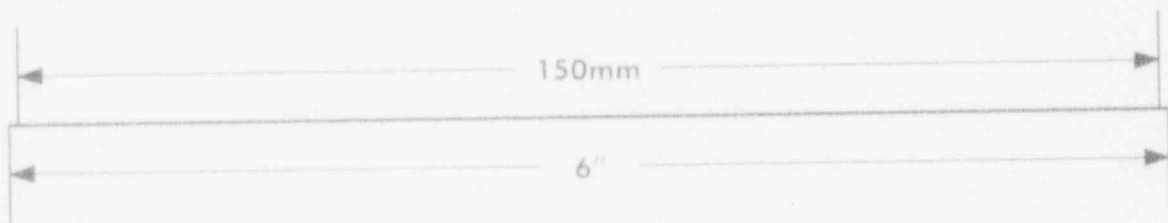
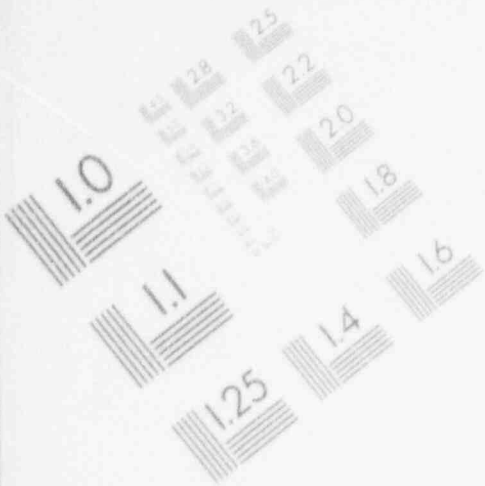
1

IMAGE EVALUATION TEST TARGET (MT-3)



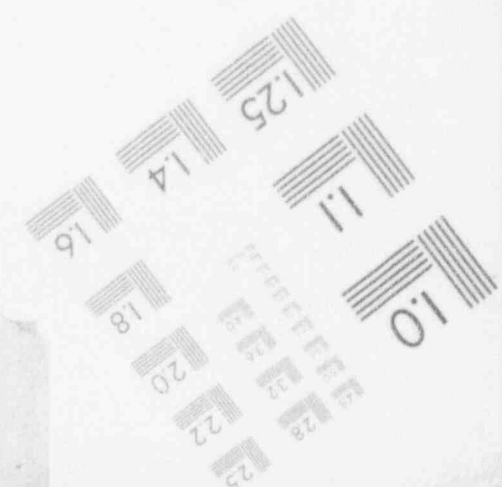
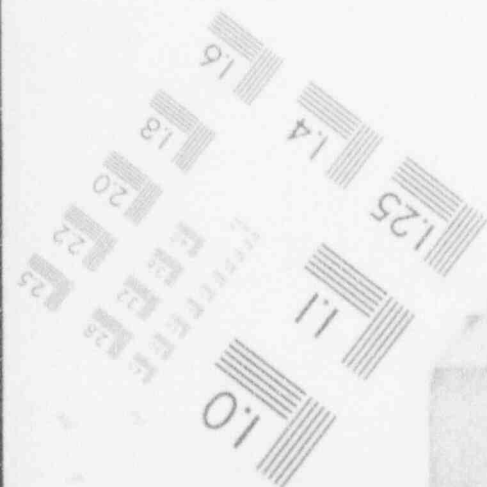
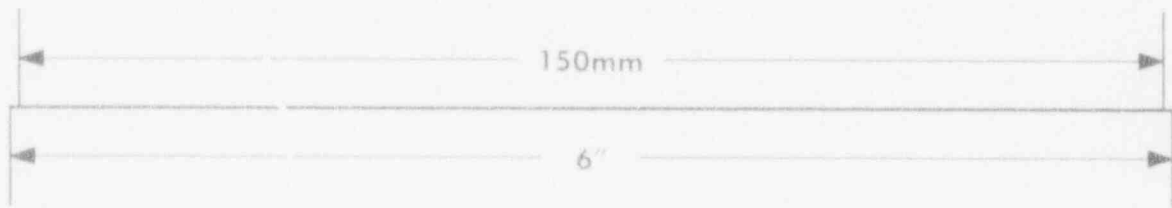
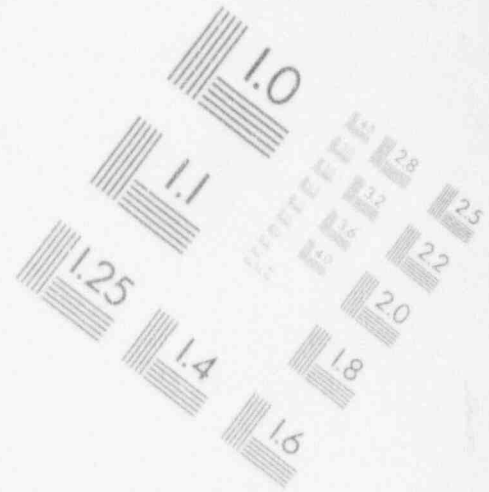
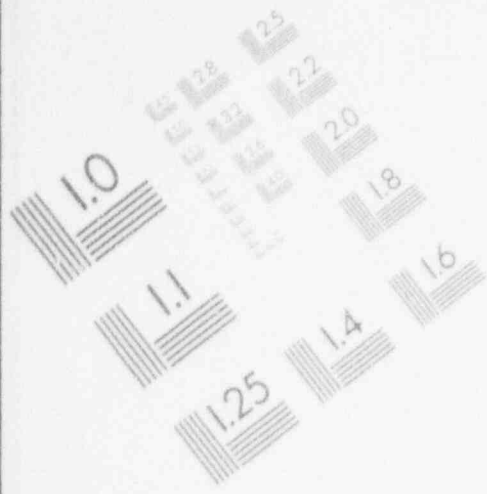
1

IMAGE EVALUATION TEST TARGET (MT-3)



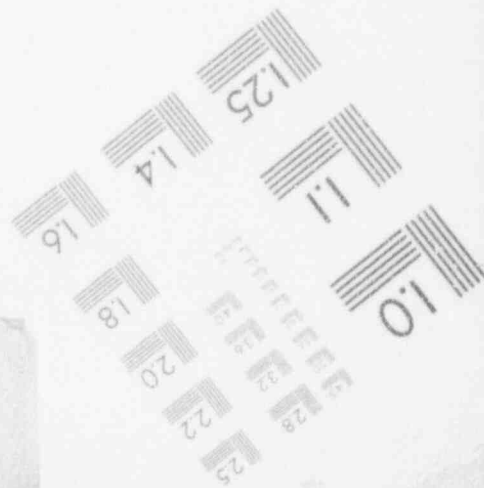
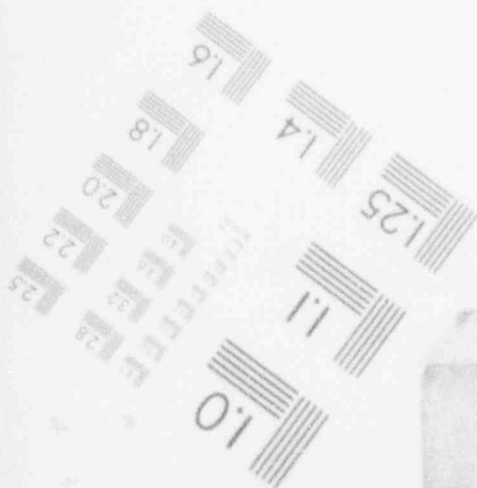
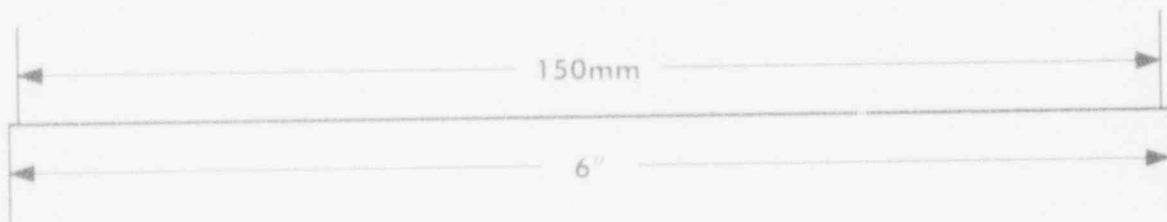
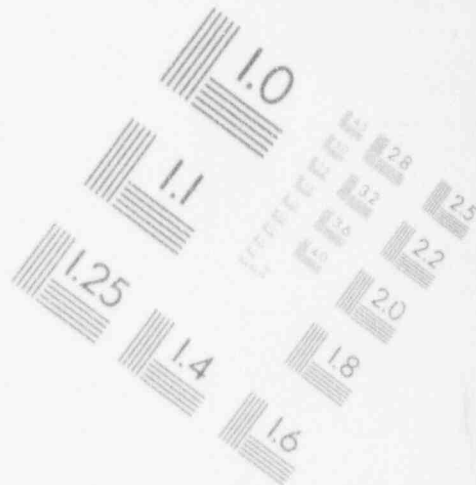
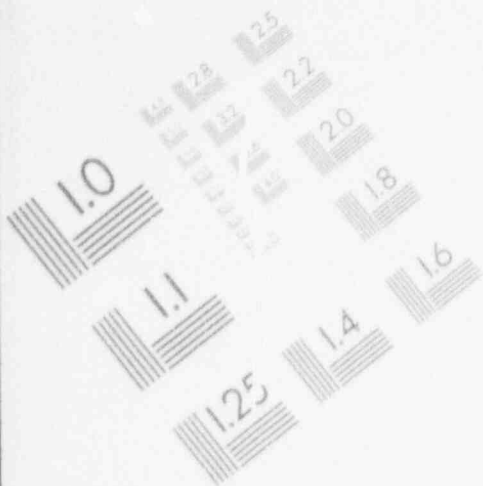
1

IMAGE EVALUATION TEST TARGET (MT-3)



1

IMAGE EVALUATION TEST TARGET (MT-3)



B.4 Temperature and Flashing Adjustment Factors

Temperature adjustment factor β is defined by Eq (21) Flashing adjustment factor γ is defined by Eq (22).

B.4.1 Temperature Factor β Only and Leak Rate Adjustment (i.e., without Flashing)

For water without flashing at T_o and T and $\Delta p = \Delta p_o = \Delta p_{mo}$, it follows that

We will compare this β factor with the CRACKFLO calculated adjustment factor under non-flashing conditions. Table 4 presents the comparison for the case without water flashing. Note that the reference temperature T_o is equal to the room temperature T_a . Similar results were obtained for crack lengths of _____ inch. These results indicate that the approximation of Eq (21) to Eq (13) yields good agreement with the more detailed crack area models in CRACKFLO for leak rate ratios between different temperatures.

Table 4
Comparison of the Temperature Adjustment Factor β between
the CRACKFLO prediction and Proposed Expression for the Case without Water Flashing

B.4.2 Adjustment Factors β and γ from Room to Operating Temperature under SLB Conditions

For water flashing at T and non-flashing at T_o and $\Delta p_o = \Delta p_{mo}$, it follows that

where β is given in Eq (21) and γ by the second expression of Eq (22). Note that the reference temperature T_o is equal to the room temperature T_a . Table 5 presents the comparison of leak rate adjustment between the CRACKFLO code and the proposed expressions with a pressure coefficient $C_p = 1.0$.

For $C_p = 1.0$, the proposed expressions of β and γ factors yield an adjustment lower than the CRACKFLO calculated factor. The deviation comes from the flashing point. A $C_p = 1.0$ implies that flashing takes place at the saturation pressure corresponding to upstream temperature T_1 . For $T_1 = 616^\circ\text{F}$, the saturation pressure $p_{1f} = 1736$ psia. However, because of heat transfer and friction along the leakage passage, the water flashing will occur at lower pressure, or a saturation pressure corresponding to a temperature lower than the upstream temperature T_1 . In fact, the CRACKFLO code predicts a flow choking at a pressure less than p_{1f} .

Table 5
Comparison of the Temperature and Flashing Adjustment Factors between
the CRACKFLO prediction and Proposed Expression for the Case with Water Flashing

To bring the proposed equation to yield a result equal to the CRACKFLO calculation, we obtain a C_p for each case. Table 6 presents the results for C_p . The longer the crack length the larger the pressure coefficient for a given pressure differential. A longer crack length means a larger crack opening, and thus less friction and smaller heat transfer effect. It approaches the ideal case: an isentropic (i.e., frictionless and adiabatic) process; a situation with less leak rate. We can use $C_p =$ for $\Delta p =$ psia, and $C_p =$ for $\Delta p =$ psia.

B.4.3 Adjustment Factors α and γ for Primary Δp Changes at Temperatures with Flashing

Westinghouse model boiler testing of leak rate of pulled tubes are conducted at a primary pressure higher than the typical pressure during steam line break. The tests were conducted at the operating temperature of 616°F . We will adjust the leak rate to the typical primary pressure. The relevant adjustment factors are the mechanical adjustment factor α and the flow flashing adjustment factor γ . Now it follows that

where the α factor is defined by Eqs (18), and the γ factor by the first expression of Eq (22) or (23). Note that $T_o = T = 616^\circ\text{F}$. We would like to convert the leak rate to the equivalent volumetric rate at the room temperature ($T_a = 70^\circ\text{F}$). To do so, we use the following expression.

Table 6
Pressure Coefficient C_p

As an illustration, Table 7 presents some results of the adjustment factors for scaling from one flashing conditions to another flashing ones. We have used Eq (18) with the constant parameter b^* being to calculate the α factor. Table 7 also lists the comparison between the CRACKFLO code prediction and the proposed expressions with appropriate choice of the pressure coefficient C_p . There are good agreements. These lead to confidence in using the proposed expressions of the adjustment factors α and γ .

Table 7
Comparison of the Mechanical and Flashing Adjustment Factors α and γ between the CRACKFLO Prediction and Proposed Correlations at Operating Temperature

Crack	Pressure, psia	Temp	Leak Rate @	Adjustment Factors α and γ
-------	----------------	------	-------------	--

The C_p factor was included in the adjustment factor to improve agreement with the CRACKFLO code and is an empirical factor. The CRACKFLO code is a more rigorous solution to the momentum equations than Eq (1) and is felt to be more accurate solution. The use of C_p is slightly more conservative than assuming $C_p = 1$ as the use of C_p reduces the correction for flashing (increases γ closer to 1.0) and thus leads to slightly higher leak rates. The momentum equation can predict the effect for which the CRACKFLO solution was preferred over Eq (1), which results in the C_p factor being dependent on the pressure differential. C_p is a hydraulic correction which should not be dependent on the pressure differential and not a leak rate variation with the crack opening leakage area.

The inclusion of C_p is not critical to the adjustment model since the effect is small and inclusion reduces the generality of the adjustment model. For these reasons, it is fine to drop C_p from the model. Thus, Eq (22) becomes as follows.

(23)

It can be shown that the above expression are applicable to both isentropic and non-isentropic flashing process. The effect of the non-isentropic flashing appears in the discharge coefficient K in Eq (1), and it

is not necessary to introduce an empirical factor C_p to account for the non-isentropic effect to the saturation pressure p_f .

5.0 Leak Rate Adjustment to Belgian Plant E-4 Data

Table 8 presents leak rates measured for Plant J-1 cracked tubes for both normal operating and steam line break conditions. Both conditions simulate the typical pressure differentials across the tube, but tests were conducted at room temperature. We would like to scale these room temperature data to hot temperature of 616°F. First, we scale the normal operating data.

Table 8
Results of Leak Rate Tests for Plant J-1 Tubes under Room Temperature
and Typical NOP and SLB Pressure Differentials

B.5.1 Adjustment for Normal Operating Data

All of normal operating conditions involve no flashing of water. So the adjustment factors are as follows.

where the factor α is defined by Eq (18) and the factor β by Eq (21). Individual correlation constant b^* is obtained for each specimen. The Δp_{mo} is given in Table 1, for example, tube R8C74 was tested at _____ psi, and $T_a = T_o =$ _____. We will scale to $\Delta p_o =$ _____ psi and $T =$ _____. When there is no water flashing $\Delta p = \Delta p_o$, so $\gamma = 1$. The properties of flow stress, Youngs modulus and water density can be found in Table 4. Table 8 presents results of leak rate at the target conditions.

B.5.2 Adjustment for Steam Line Break Data

Now we are ready to adjust the steam line break (SLB) data. Table 1 lists the measured leak rate and pressure differentials Δp_{mo} . We are going to scale them to $T =$ _____ and $\Delta p_o =$ _____ psi, _____ psi and _____ psi, respectively. Now it follows that

where the α and β factors are defined by Eqs (18) and (21), respectively, and the γ factor by the second expression of Eq (23). Individual correlation constant b^* is obtained for each specimen. Table 9

shows the adjusted leak rate at pressure differentials of

Table 9
Results of Leak Rate Tests and Their Adjustments at and Normal Operating and
Steam Line Break Pressure Differentials (7/8" Tubing for Plant J-1)

B.6 Adjustment to Leak Rate Data Base for Alternate Δp

Table 10 lists the model boiler tests and plant data. These tests were conducted at the operating temperature of about , and at the primary pressures higher than the typical pressure during steam line break. The relevant adjustment factors are the mechanical factor α and flow flashing factor γ . The leak rates were collected and cooled from $T_o =$ to room temperature $T_a =$. Thus the β factor is not required in the leak rate adjustment because it was adjusted already by test procedure.

B.6.1 The Correlation Constant b^* for the α Factor

Tubes used for these tests had minimal ligament tearing at cracks. As discussed in Sect. 3.2, the α factor is defined by Eq (18), which involves a correlation constant b^* . Rather than using $b^* =$ derived from the Belgian tubes with significant ligament tearing, it is to be estimate on a tube-by-tube basis using test data shown in Table 10.

We define the following variables for deriving expression for estimating the correlation constant b^* .

where

- R = Ratio of volumetric leak rates
- L_{SLB} = Volumetric leak rate under SLB conditions
- L_{NOP} = Volumetric leak rate under NOP conditions

This ratio R is equal to the product of α and γ factors. We write the α factor as follows.

where

- Δp_{SLB} = pressure differential under SLB condition
- Δp_{NOP} = pressure differential under NOP condition

Since there is no water flashing under the NOP condition the γ factor appears as follows.

where

p_{SLB} = upstream pressure during SLB

p_f = upstream saturation pressure corresponding to upstream temperature T_o

Equating R to $\alpha\gamma$ and solving for b leads to the following equation.

(24)

Some tests yielded no leak flow under the NOP conditions. Thus the ratio R becomes infinite, and the correlation constant b^* approaches zero. A zero constant b^* results in a zero adjusted SLB leak rate when scaling from the measured SLB leak rate at \quad psi to lower pressure differentials. A meaningful lower bound of the ratio R will lead to a conservative adjustment, and such a ratio is selected to be based on the cases where the NOP leak rate being not zero. Therefore, $R = \quad$ is used for the tests which have zero NOP leak rate. Note that the Belgian constant $b^* = \quad$ corresponds to a $R = \quad$. The other choice is to take the average over all data, which is $R = \quad$ and $b^* = \quad$. In addition, we set $R = \quad$ if the measured data yields a value less than unity. Use of $R = \quad$ results in an adjusted leak rate being less than $R = \quad$ when adjusted from higher measured pressure differential to lower differentials. For conservatism, we set $R = \quad$ for the case with zero NOP leak rate.

B.6.2 Results of the Leak Rate Adjustment

Leak rate adjustment for these data was made using both mechanical and hydraulic factors as described above. Table 11 presents the adjusted leak rate for the normal operating (NOP) and SLB conditions. Four sample tubes results in adjusted leak rates for both \quad psi and \quad psi differentials under SLB being less than the adjusted leak rate under NOP. For conservatism, we retain the measured SLB leak rate as the final value for those four tubes.

Table 10
Results of Leak Rate Tests at and Normal Operating and
Steam Line Break Pressure Differentials

Table 11
Results of Leak Rate Tests and Their Adjustments at and Normal Operating and
Steam Line Break Pressure Differentials

Appendix C

Crack Morphologies for ARC Applications

C.1 Introduction

With the development of alternate repair criteria (ARC), pulled tube destructive examinations have placed greater emphasis on characterizing crack morphology relative to structural integrity and NDE results. Prior to ARC development, pulled tube exams emphasized maximum depth relative to NDE depth and broad definitions of crack morphology. The more recent tube exams identified patches of cellular corrosion, as described in Section C.3, in addition to the prior stress corrosion cracking (SCC) and intergranular attack (IGA) morphologies. Cellular corrosion is not a new morphology but rather a newly named and characterized feature of morphologies that have been present in prior tube examinations and frequently labeled circumferential branch cracking. Significant IGA has generally not been found. IGA is sometimes found as IGA fingers or adjacent to the faces of an SCC crack rather than having significant volumetric involvement. Consequently, IGA is not a significant structural concern for ARC applications. The more common morphologies are SCC and SCC with cellular patches. This Appendix describes the various types of cellular corrosion (CC) found in the more recent tube examinations. The most common occurrence of CC is as small patches in a group of axial cracks. In some cases, CC is found as bands of indications around the tube circumference.

In addition, this section addresses the cause for indications extending outside the TSP, the influence of ligaments within the major macrocrack and crack morphology on bobbin voltage response and the influence of morphology on RPC responses to identify typical acceptable RPC responses for ARC applications.

The objectives of this section are:

- 1) Identify indications extending outside of TSP and assess source as initiation outside TSP or growth from inside TSP.
- 2) Characterize crack morphologies with emphasis on cellular corrosion as found by destructive exam of pulled tubes.
- 3) Identify typical NDE bobbin coil, RPC and UT responses to SCC + CC.
- 4) Demonstrate that tube burst capability for axial SCC + CC is dominated by the most limiting axial crack with negligible influence of the multiple axial and cellular cracks. This demonstration is performed by comparing the measured burst pressure with the calculated burst pressure for a single crack model having the corrosion length and depth found by fractography of the burst crack face.
- 5) Demonstrate that the axial SCC + CC indications fall within the burst and leakage correlations used to support IPC/ARC applications.

- 6) Qualitatively assess the effects of ligaments remaining within limiting burst crack and crack morphology on bobbin voltage response.
- 7) Identify the types of RPC responses for volumetric indications that can be considered to be acceptable for IPC/ARC applications.

C.2 Axial Indications Extending Outside the TSP

Seven indications with ODSCC at non-dented TSPs have been reported to have indications extending outside the TSPs. These indications are summarized in Table C-1. The indications extend outside the TSP up to about inch, are shallow (maximum depth of) and are intermittent indications. None of the extent outside the TSP was detected by NDE including field UT for Plant A-1 tube R19C41.

As found generally for ODSCC at TSPs, the indications outside the TSPs are initiated as multiple initiation sites which have grown together to varying extent. Figure C-1 shows a schematic of the crack distribution for R19C41. The multiple indications outside the TSP are very short with a maximum depth of . They are seen in the burst crack fractography more within crack tip tearing than as a contributor to the major macrocrack. Similar multiple initiation sites outside the TSP were found for Plant A-1 tube R20C26.

An additional example of the intermittent indications outside the TSP is shown in the sketch of Figure C-2 for the burst crack of tube R16C31 from Plant E-4. The intermittent indications above the TSP vary from depth.

Figure C-3 shows a map of the tube degradation for Plant J-1 Tube R5C28, TSP2. This sketch shows degraded areas of the tube. Sections cut at the edges of the TSP were examined for maximum depth as shown in the tabulations given in Figure C-3. The corrosion at the edges of the plate had maximum depths of . Photographs of the tube OD show cellular patches of degradation as well as axial indications. For reporting of morphology by the French, cellular is classified as IGA.

The intermittent and multiple indications outside the TSP suggest the same initiation mechanism outside as inside the TSP. This would indicate sludge deposits on the top of the TSP or bridging of sludge between the tube and TSP. This mechanism cannot readily be confirmed by eddy current analyses for sludge deposits due to limited detectability given deposit thicknesses present also on the free span tubing. Eddy current data review for the Plants L and J-1 indications of Table C-1 could not confirm sludge deposits.

Overall, the pulled tube exams show that indications outside the TSP are intermittent and resulting from additional initiation sites. There is no evidence that crack growth from indications within the TSP leads to crack extension outside the TSP.

Plant L Examples

Destructive examination results have been obtained for 8 tubes (23 intersections) removed from Plant L in 1991. The burst cracks are characterized as a macrocrack comprised of short microcracks with both uncorroded and corroded ligaments between microcracks. This is typical of ODS-SCC with initiation as individual microcracks which grow to link up with other microcracks to form macrocracks. In a burst test, the weakest macrocrack or nearly axially aligned microcracks result in the tube rupture.

About half of the indications have morphologies comprised of SCC with small patches of cellular corrosion. These descriptions are based on visual observations of the OD surface of the tube following the burst test which tend to open the crack faces. The cellular patch at the 1st TSP intersection of R16C74 was examined in detail by flattening the tube section and progressively polishing the tube surface radially to characterize the cellular structure as a function of depth. Flattening the tube tends to open circumferentially oriented cracks while axial cracks tend to close. Figure C-6 shows the results of radial grinds to depths of _____ mils. The cellular structure consists of SCC (sometimes IGA features) at the edges of each cell with no tube degradation within the cell. In general, the axially oriented cracks tend to be more continuous or longer with the included or oblique cracks tending toward short cracks between axial indications. In many occurrences, the full cellular structure is not formed but is approached as a matrix of axial cracks with oblique cracks intersecting the axial indications.

From Figure C-6, it is seen that the inclined cracks essentially disappear between the grinds at _____. This feature of cellular patterns changing to only axial indications at depths of _____ has been found for all cellular patterns examined by radial metallography. For R16C74, a radial grind at _____ found no remaining axial indications. The maximum crack depth found at this indication was _____.

The presence of cellular patches cannot be identified by bobbin coil inspection which indicates the presence of a flaw. Also, an RPC inspection cannot uniquely identify cellular patches and can only infer the possible presence of cellular corrosion. Cellular patches near a detectable axial crack tend to show on an RPC trace as circumferential broadening of the axial indication. Closely spaced (_____ apart or less) axial indications cannot be individually resolved by RPC and can approach the appearance of a volumetric indication. Similarly, a cellular patch within a group of axial indications could appear to be a volumetric indication on an RPC trace.

Application of a modest axial force on an indication with a SCC + CC morphology can be expected to slightly open the oblique crack faces (not tearing or fatigue that increases crack size) which increases the voltage amplitude response and also increase the volumetric or circumferential appearance of the RPC response. This trend can be observed on some of the pulled tubes by comparing the pre-pull and post-pull RPC traces. Figures C-7 to C-9 show examples of this affect for R16C74-TSP 1, R30C64-TSP1 and R12C8-TSP 2. The tube pull forces can open crack faces or damage small ligaments between microcracks and can result in increased volumetric and/or axial response. Some of the post-pull responses, such as that for R30C64 and R12C8 show significant circumferential responses. These post-pull RPC responses are similar to that found for a few indications in the 1992 inspection as described below. Thus, it can be expected that these responses are indicative of axial SCC + CC or closely spaced axial SCC morphologies. Circumferential cracks (as distinct from cellular) have not been found at non-dented TSP intersections in S/Gs. This further supports the interpretation of volumetric, circumferential oriented RPC indications as axial SCC + CC morphologies.

RPC responses to cellular corrosion can be influenced by sleeving efforts above or below the TSP intersection of interest as found in the 1992 Plant L inspection. In this case, tubes sleeved at TSPs in 1991 were inspected in 1992 by RPC at non-sleeved intersections and, in some cases, found to have strong volumetric and circumferential RPC responses. Figures C-10 and C-11 show examples of circumferential involvement for tubes R32C75 and R19C66. These indications were further evaluated by UT as the circumferential involvement was greater than previously found in Plant L inspections. The RPC responses can vary with axial translation speed. The RPC response of Figure C-12 from an RPC probe coupled with the UT probe and applied with smaller pitch shows a more dominant axial indication for R32C75 than found in Figure C-10. Figure C-13 shows the UT inspection results for R32C75. The circumferential aim transducer shows a number of closely spaced axial indications. The axial aim transducer shows a patch of intermittent circumferential indications which overlaps the upper end of the axial indications. The circumferential response is attributed to a patch of cellular corrosion which is expected to have opened crack faces as a result of the sleeving operations at an adjacent TSP intersection. The sleeving operations involved explosively expansion welding followed by heat treatment. These operations result in peak and residual axial stresses which are expected to have increased the NDE visibility of the cellular patch by opening of the crack faces.

Plant A-2 Example

Figure C-14 shows a sketch of the morphology of tube R38C46 from Plant A-2. The indication of the burst opening was described as spider-shaped and would currently be classified as a variation of cellular corrosion. The volt indication had a high burst pressure of psi.

Plant P-1 Example

Figure C-15 shows a post-burst photograph of R11C60 from Plant P-1. Bulging of the tube as a result of the high burst pressure of psi has opened the SCC + CC structure on the tube OD as seen particularly in the photos. Figure C-16 shows the RPC data for this indication. Both axial and volumetric responses are seen in the RPC data for this indication. This indication was also UT inspected in the field with the results shown in Figure C-17. The upper figure shows the circumferential aim transducer results for a large number of axial indications which is consistent with the indications shown in Figure C-15. The lower part of Figure C-17 shows the axial aim results of the UT inspection. The more dense intermittent circumferential indications at the bottom of the figure have been traced to changes in deposit thickness at the bottom edge of the TSP. Evaluation of the intermittent circumferential indications within the TSP show that these responses include both flaw and deposit indications. The intermittent flaw indications are attributable to the cellular corrosion found at this TSP intersection.

Plant D-1 Examples

Additional variations on the axial + SCC morphology are shown in Figure C-18 for a TSP indication and an indication found just below the top of the tubesheet. These indications from Plant D-1 include the cellular pattern seen in R11C60 at the top of the tubesheet. The RPC response indicated a circumferential indication and axial indications. All indications opened axially at high burst pressures including the cellular pattern. The laboratory UT inspection for these indications show multiple short axial and intermittent circumferential indications typical of cellular corrosion.

Plant G-2 Examples

All the above pulled tube results indicate that the axial SCC and/or cellular morphologies burst axially even with cellular patterns. This result is also demonstrated for indications from Plant G-2 with extensive circumferential bands of cellular corrosion at the edges of the TSPs. of the indications show axial bursts centered at the band of CC at the upper edge of the TSP while the other indications, with more significant indications within the TSP, burst axially centered within the TSP. Figure C-19 shows the OD crack patterns for R7C25-TSP 1 and R11C43-TSP 2 as examples of these indications and burst locations.

The bobbin coil responses for these indications have significant voltages even for the circumferential CC bands. Figure C-20 shows the RPC responses for the destructive exam results of Figure C-19. Both indications show strong circumferential indications with axial extent of about 1/8 inch at the edges of the TSPs with smaller axial responses within the TSPs. The axial indications are marginally visible for R11C43. The burst for R7C25 was centered within the TSP at the cellular indications while R11C43, which has no significant indications within the TSP, had the burst centered at the upper edge of the TSP at about 1/8 inch. The cellular pattern was found by radial polishing to change to axial cracking at depths of 1/8 inch on R7C25 and R11C43. This trend for cellular changing to axial has been found in all radial polishing performed to date for cellular corrosion.

Summary

The above NDE and destructive examination results indicate that axial SCC + local CC is a common morphology and associated with axial or volumetric RPC indications. Circumferential bands of principally CC are found for indications showing strong circumferential RPC responses. No occurrences of true circumferential cracks (PWSCC, ODSCC or fatigue) have been found at non-dented TSP locations. The pulled tube results show that the circumferential and/or volumetric RPC responses for non-dented TSP intersections are associated with bands or patches of cellular corrosion. Volumetric RPC responses also result from closely spaced axial indications. In all cases, including circumferential CC bands, the tubes burst in the axial direction.

The cellular patterns show significant bobbin voltage responses even when limited to circumferential bands of 1/8 inch height and depths of 1/8 inch. This is in contrast to circumferential cracks which would not likely be detectable by bobbin inspection at these depths. Bobbin, RPC and UT inspections, as a combined inspection, can identify significant cellular patches or bands. This characterization includes significant bobbin voltages (100 mV), RPC volumetric or circumferential bands with modest RPC voltages (typically the order of 10 mV the bobbin voltage or less) and UT intermittent circumferential indications. However, since circumferential cracks have not been found or would not be expected at non-dented TSP locations, the presence of significant bobbin voltages and volumetric RPC responses are indications of axial SCC + CC, CC or closely spaced axial SCC. These types of indications fall within the burst correlations supporting IRC/ARC as shown in Section C.4 below. Thus IRC and ARC can be applied for these indications at non-dented TSP locations.

The crack length, depth and burst pressure data are used in Section C.4 to compare measured with calculated burst pressures.

It is shown that the measured burst pressures are essentially equal to or greater than that calculated for a single crack model which ignores the cellular and multiple crack morphologies found on some of the indications. This result shows that the burst pressure capability is limited by the most dominant axial macrocrack and is negligibly influenced by the cellular morphology.

C.4 Influence of Crack Morphology on Tube Burst Capability

Crack morphology can influence tube burst capability by conceptually reducing burst pressure for the limiting macrocrack as a consequence of other axial and cellular degradation on the tube circumference. This section assesses the influence of morphology on burst pressure by comparing the burst pressure predicted for the burst crack length and depth profile found by destructive examination with the measured burst pressure. If multiple and/or cellular indications significantly reduce burst pressure, the measured burst pressure would be expected to be lower than predicted for only the burst macrocrack dimensions. This comparison can be meaningfully performed as burst capability can be adequately predicted given the length and depth profile for a flaw.

Morphology variations can influence the bobbin voltage response and thus influence the burst/voltage and leakage/voltage correlations for ARC applications. Morphology influences can be uncorroded ligaments within the limiting macrocrack leading to reduced voltage amplitudes and multiple or cellular indications leading to increased amplitudes compared to that associated with the limiting macrocrack. The influence of morphology on voltage response is addressed in Section C.5.

For most of the tubes pulled in support of ARC for ODS/CC at TSPs, crack length and depth profiles or average depths are available for the burst macrocrack from destructive examination. These data are used to calculate the burst capability assuming the burst macrocrack was the only tube degradation.

An evaluation was performed to compare actual burst behavior with predicted burst behavior assuming a single dominant crack. Burst pressure from pulled tubes, from plants with 3/4" nominal outside diameter (OD) and plants with 7/8" nominal OD tubes, were compared to a partial through-wall burst pressure model using a linear approximation for ligament strength. This model has been previously referred to in Westinghouse documents as the Begley-Houtman (BH) model. The BH model simply assumes that the burst pressure, P_B , for a tube with a partial through-wall crack can be determined as a linear interpolation between the burst pressure without the crack, P_0 , and the burst pressure assuming the crack to be through-wall, P_{TW} . The linear interpolating parameter being the depth, d , to thickness, t , ratio for the crack, i.e.,

(1)

Since the model assumes a rectangular or "bathtub" shaped crack, an equivalent, or average, depth for the modeled crack is calculated based on matching the area of the real crack.

The basis for the model is the correlation of burst pressure to crack length for through-wall axial cracks for tests performed without reinforcing of the bladder used to prevent leakage prior to reaching the burst pressure. In general, this model has been found to underestimate the burst pressure for tubes with through-wall cracks. However, owing to the reduced strength of the ligament for deep cracks, the use of a lower bound P_{TW} correlates better for such configurations. For a database of seventy-one (71) specimens ranging from undegraded tubes to tubes with axial crack lengths in excess of , the following equation form was found to correlate to the data with an index of determination of .

(2)

where a , b , c , and d are empirically determined coefficients, σ_f is the flow stress of the material, and λ is the non-dimensionalized (also referred to as normalized) crack length given by

(3)

where R_m is the mean radius of the tube, t is the tube thickness, and a is total crack length.

Figure C-21 shows the comparisons between predicted and measured burst pressures. The agreement between the predicted burst pressures assuming a single limiting crack and the measurements is seen to be quite good. As expected, the measured burst pressures tend to be significantly higher than predicted for shorter cracks. However, for longer cracks, i.e., lower burst pressures the model agrees relatively well with the data. In most of the cases the measured burst pressure is higher than the predicted value. Differences are not attributable to an particular crack morphology. Of a database of 64 tube specimens comparisons were possible for 57. On average, the measured burst pressure exceeded the calculated burst pressure by with a standard deviation of . The maximum value of the ratio of the measured burst pressure to the calculated burst pressure is , and the minimum value of the ratio is .

Thus, for the worst case, i.e., non-conservative, the burst pressure was under predicted by only . For all but one case the measured values are greater than a prediction based on of the calculated value.

Figure C-21 shows the comparisons between calculated and measured burst pressures. The agreement between predictions assuming a single limiting crack and the measurements is seen to be quite good. Differences are not attributable to any particular crack morphology. The agreement holds also for the Plant G-2 circumferential cellular bands and the top of tubesheet (TST) indications from Plant D-2. Available data for both 7/8 and 3/4 inch diameter tubing is included in Figure C-21.

The results show that the burst capability is determined by the most limiting single macrocrack and is essentially independent of the more detailed crack morphology such as cellular patches or multiple axial indications. ARC can be applied to all morphologies found at TSP intersections (3/4 inch thick plates). No morphologies have been found at TSPs that would have to be excluded from ARC applications.

C.5 Influence of Morphology and Ligaments on Bobbin Voltage Response

Details of crack morphology, while not significantly influencing burst capability based on limiting macrocrack length and depth profiles, can have significant influence on the bobbin voltage response for the indication. Multiple axial cracks of comparable length and depth and cellular corrosion significantly increase the bobbin voltage compared to the voltage response for the limiting macrocrack as an isolated crack. The presence of large or many uncorroded ligaments within the limiting macrocrack can significantly reduce the bobbin voltage compared to that for the limiting macrocrack without ligaments. These two influencing factors of morphology on voltage response contribute substantially to the spread of correlations on burst pressure or leak rate versus voltage. This section discusses these influencing factors on bobbin voltage.

Uncorroded ligaments between multiply-initiated microcracks remain in the limiting macrocrack in the earlier stages of crack development. Uncorroded ligaments are more prevalent in low voltage (volts) pulled tubes than in the model boiler specimens prepared by accelerated corrosion even at comparable voltage amplitudes. As the cracks develop to throughwall corrosion, most or all of the ligaments have frequently corroded. Voltage increases as a measure of crack growth can result from loss of ligaments with and without significant changes in crack length and depth. On occasion, a single, large ligament can remain between two deep macrocracks. This morphology typically results in a low voltage outlier on the burst correlation and possibly the leakage correlation. An example of a large ligament is Model Boiler specimen 601-6 (3/4 inch diameter tubing). This indication had a , axially aligned cracks. The ligament is of sufficient size to cause a reduction in the RPC amplitude at the center of the overall indication as shown in Figure C-22.

This specimen had the lowest burst pressure of all tested indications at psi with a relatively low bobbin voltage of volts. It is expected that the ligament substantially reduced the voltage compared to that for the total crack length (throughwall) but did not add significantly to the burst capability for the indication. The ligament likely did not tear at the SLB pressure differential of psi as the measured leak rate is not an outlier on the leak rate correlation.

Qualitatively, the presence of uncorroded ligaments extending through the crack face can be used to help explain low burst pressure outliers. Table C-2 shows pulled tube results for measured number and total width of ductile ligaments. Also noted are indications low or high relative to prediction interval bands on the burst pressure vs voltage correlation. Low voltages and burst pressures (Plant L) tend to be associated with deep indications (depth) with large ligament areas. The Plant D-1 results indicate that shallow indications with few ligaments tend toward high outliers. The Plant D-1 results are unusual in having shallow indications with few ligaments. The influence of uncorroded ligaments on voltage of deep indications is increased when the ligaments remain near the deeper region of the crack. This is shown in Figure C-23 for the low outliers on tubes R29C70 and R8C69. Figure C-24 shows the ligament locations for R30C64. At the first TSP with a relatively low voltage (volt), the ligaments are located throughout the crack while the higher voltage second and third TSPs have fewer and smaller ligaments at the deeper areas of the crack. The third TSP of R30C64 is typical of higher voltage, shallow indications such as Plant D-1 which has few ligaments and longer cracks. While the outliers appear as low or high burst pressures on the burst/voltage correlation, it is predominantly the morphology influence on voltage shifts toward low or high voltage that leads to the outlier tendency.

Bobbin voltage is sensitive to thin ID ligaments since voltage tends to increase exponentially with average depths particularly at approximately or greater depths. An example is Model Boiler Specimen 601-1 (3/4" diameter tubing) as shown in Figure C-25. Although this indication has a maximum length of only inch, the bobbin voltage is volts. This is a typical "bath tub" flaw with a throughwall indication and no remaining ligaments within the crack face except at one edge of the crack. In contrast, Model Boiler specimen 600-3 (3/4" diameter) has the same voltage but a longer and deeper indication (throughwall) with a much lower burst pressure (psi) than 601-1. Specimen 600-3 is unusual in having remaining uncorroded ligaments with significant throughwall penetration.

In summary, the presence of uncorroded ligaments between microcracks has a strong influence on bobbin voltage and, in the lower voltage range of volts, is the principal contributor to outlier behavior in the burst/voltage correlation. A single large ligament such as specimen 601-6 can lead to low outliers at higher voltages. The presence of uncorroded ligaments tends to have less influence on leakage correlation outlier behavior as the leakage would continue to be low if the ligaments do not tear at the tested pressure differentials.

In addition to ligament effects, the presence of multiple deep indications and to some extent cellular patches tends to lead to substantial spread in the burst and leakage correlations. The multiple indications lead to high voltages compared to that associated with the limiting macrocrack. This leads to horizontal spread in the correlations. The effect is particularly pronounced on the leakage vs voltage correlation which tends to have a steep voltage dependence on the voltage of the limiting or longest throughwall crack. High voltages for multiple indications with modest throughwall lengths lead to low outliers on the leakage correlations and high outliers on the burst correlation. The multiple indication effect on voltage tends to be more influential above _____ volts while the ligament influence is most pronounced at _____ volts.

High leakage outliers on the leak rate vs voltage correlation (576-4 for 7/8" diameter and 600-3 for 3/4" diameter tubing) have a dominant single crack which may include _____ or not include _____ uncorroded ligaments in the crack face. The high leakage outlier behavior is apparently due to smoother or less tortuous crack faces leading to reduced friction and is less apparent by crack morphology than burst outlier behavior. The indications tend to have nearly the same bobbin and RPC voltages (_____) whereas most other indications tend toward RPC voltages less than bobbin voltages.

Figure C-26 shows a typical burst pressure correlation for 7/8 inch diameter tubing. The high burst pressure outliers from Plants D and G were not included in the regression fit. Plant D-1 data has shallow indications with few ligaments and cellular patches contributing to high voltages causing the outlier behavior. As described in Section C.3, Plant G-2 has circumferential bands of cellular corrosion and, as such, does not meet current guidelines on axial indications within the TSPs for application of ARC limits. However, it can be seen that the Plant G-2 morphology leads to high voltages and burst pressures such that ARC repair limits would be conservative for this cellular morphology. As discussed above, the low outliers tend to result from large ligament areas while the high outliers result from few ligaments and/or increased cellular involvement. Overall, the cellular morphology has either no influence (small patches) on the correlation or tends to contribute to the high outliers (Plants D and G).

C.6 Acceptable RPC Responses for ARC Applications

As shown in the prior sections, burst capability is dominated by the length and depth profile of the limiting macrocrack with negligible influence of the remaining morphology outside the limiting macrocrack. Low burst pressure outliers on the burst/voltage correlation tend to be dominantly single cracks with many or large uncorroded ligaments within the crack face. High leakage outliers tend to be single cracks with or without a few remaining small ligaments. Thus the outliers appear by RPC inspection to be single axial indications. Multiple cracks and cellular patches add to a volumetric RPC response but do not lead to non-conservative burst or leakage outlier behavior.

As shown in Sections C.3 to C.5, all indications found at non-dented TSP intersections to have volumetric and circumferential involvement fall within the expected burst capability for the limiting macrocrack and within the burst and leak rate correlations. Alternatively stated, no morphology variations resulting in volumetric/circumferential RPC responses have been found to result in non-conservative burst or leakage behavior. All indications found with any morphology are included in the ARC correlations or result in conservative high burst or low leakage outliers.

Consequently, the extensive database from 7/8" and 3/4" tubing, with varying morphologies among the pulled tubes and model boiler specimens, minimizes the need for RPC inspection to support ODSCC as the dominant degradation mechanism. RPC sampling of bobbin indications is adequate to examine the data for alternate mechanisms to ODSCC which have not been found to date.

Various volumetric RPC responses with circumferential involvement fall within the ARC database. These include the volumetric response shown in Figure C-1 and the short axial lengths shown in Figures C-4 to C-6. Thus significant limitations on RPC response features are not needed for application of ARC repair limits. The available database support at least volumetric response and indications as short as inch in length (without RPC lead-in and lead-out adjustments). Thus RPC volumetric responses in extent and inch in length (azimuthal) are acceptable responses for ARC applications. RPC responses outside this range are also likely to be acceptable although examples have not been identified to date.

C.7 Conclusions

The conclusions from the crack morphology assessment of this appendix are:

- All crack morphologies found in pulled tubes and model boiler specimens for indications at non-dented TSP intersections are acceptable for ARC applications. None of the data suggests any need to limit morphology variations for ARC.
- The need for RPC inspection to support ODSCC as the dominant mechanism is minimal since all morphologies found in the extensive database are acceptable. Combinations of multiple axial and cellular patch indications lead to a wide range of RPC responses such that an unacceptable RPC response is difficult to define.
- Based on indications found to date, RPC responses up to azimuthal extent and greater than inch axially (without resolution corrections) if azimuthally are acceptable for ARC applications.

- Comparisons of measured and predicted burst pressures show that burst capability is dominated by the length and depth profile of the limiting macrocrack and is insignificantly influenced by multiple indications and cellular patches.
- Although burst capability is approximately independent of morphology, bobbin voltages are significantly influenced by detailed morphology. Spread in the burst and leakage versus voltage correlations results from morphology influence on voltage. In the lower voltage range (volts), voltage response is reduced by uncorroded ligaments between microcracks forming the limiting microcrack. In the higher voltage range and to some extent in the few volt range, multiple indications lead to significant voltage increases above that associated with the limiting macrocrack. The ligament effect is more influential on the burst than the leakage correlation as the ligaments have little influence on burst pressure but tend to reduce leakage as well as voltage. The multiple indication effect on voltage is more influential on the leakage correlation uncertainty as leakage has a steep slope with voltages spread horizontally by the effect.
- A few occurrences of crack indications extending outside the TSP have been found by destructive examination although too small to be detected by NDE. The morphology is that of multiple initiation sites outside the TSP suggesting the influence of sludge deposits on the TSP as a concentrating medium for corrosive species. There is no indication of growth of cracks from inside to outside the TSP.

Table C-1

Pulled Tubes with Indications Outside TSP

Plant L Pulled Tubes

- R8C69, TSP-1
 - 0.11 inch above TSP
 - 0% @ 0.11 inch to ~50% at TSP
- R12C70, TSP-1
 - 0.025 inch above TSP
 - Avg. depth 8% above TSP

Plant A-1 Pulled Tubes

- R19C41, TSP-1
 - 0.25 inch above TSP
 - Max. depth ~11% above TSP
- R20C26 TSP-1
 - 0.27 inch above TSP
 - Max. depth of intermittent indications ~10%

Plant E-4 Pulled Tubes

- R16C41, TSP
 - 0.16 inch above TSP
 - Max. depth of intermittent indications ~27%

Plant J-1 Pulled Tubes

- R5C28, TSP-2
 - 0.11 inch above TSP, Max. depth ~23%
- R22C26, TSP-1
 - 0.19 inch above TSP, depth not reported

Table C-2
Pulled Tubes with Measured Ligament Widths

Figure C-1(a) Sketch of the crack distribution found at the first tube support plate crevice region of Tube R19-C41. Included is the location of the burst test fracture face opening. All deep OD origin intergranular corrosion was confined to the crevice region, including that found on the burst fracture face. Some minor intergranular corrosion was observed up to $\frac{1}{8}$ inch above the crevice top.

Figure C-1(b) Field RPC probe eddy current inspection data for the first support plate region of Tube R19-C41. Multiple axial indications are observed. The maximum signal strength is 0.15 volt, as corrected for alternate plugging criteria.

Figure C-2 Sketch of Burst Crack for Plant E-4 Tube
R16C31, TSP 3

Figure C-3

Schematic of Corrosion Zones after Burst Test for
Plant J-1, Tube L05C28

Figure C-4 Radial Metallography of the Support Plate #1
Region of Tube R19C41 Showing Intergranular
Cellular Corrosion (ICC)

Figure C-5 UT Indications for Plant A-1 Tube R19C41

Figure C-6

R16C74, TSP-1: Cellular Corrosion as a Function
of Depth

Figure C-7 Pre- and Post-Pull RPC Responses for Plant L
Tube R16C74

Figure C-8

Pre- and Post-Pull RPC Responses for Plant L
Tube R30C64

Figure C-9

Pre- and Post-Pull RPC Responses for Plant L
Tube R12C8

Figure C-10 RPC Pancake, Axial and Circumferential Coil
Inspection Results for Plant L Tube R32C75

Figure C-11 RPC Pancake, Axial and Circumferential Coil
Inspection Results for Plant L Tube R19C66

Figure C-12 R32C75 Response for RPC Probe Coupled with
UT Probe

Figure C-13 R32C75 UT Inspection Results

Figure C-14 Description of OD Origin Corrosion at the First
Tube Support Plate Crevice Region of Tube R38C46

Figure C-15 Plant P-1 Tube R16C60 TSP#1 After Burst (5X)

Figure C-16 RPC Data for R16C60, TSP-1 from Plant P-1

Figure C-17 UT Inspection Results for R16C60, TSP-1 from
Plant P-1

Figure C-18 Plant D-1 Pulled Tube Morphologies at TSP
Intersection (top figure) and Top of Tubesheet
(bottom) Note: Openings are from Burst Testing

Figure C-19 Cellular Corrosion Patterns Found at Plant G-2

Figure C-20 RPC Inspection Results for R7C25 TSP-1 and
R11C43 TSP-2

Figure C-21: Measured Versus Calculated Burst Pressures

Figure C-22 RPC Response for Model Boiler Specimen 601-6

Figure C-23 Location of Ligaments in Plant L Tube R8C69
and R29C70

Figure C-24 Location of Ligaments in Plant L tube R30C64

Figure C-25 Model Boiler Specimen 601-1 with a "Bathtub" Flaw

Figure C-26: Burst Pressure vs. Bobbin Amplitude
7/8" x 0.050" Alloy 600 SG Tubes, Model Boiler & Field Data

Appendix D

Regression Analysis

D.1 Introduction

The analysis of the relationship between two variables is generally termed either *regression* analysis or *correlation* analysis. In addition, one may also find the term *confluence* analysis in the literature ^[1,2,3,4,5,6,7]. For each, the objective is to establish a mathematical model describing a predictive relationship between the variables. The use of the term regression is frequently interpreted to imply that some sort of causal relationship exists while correlation has been reserved for non-causal relationships. Other differentiations between the two terms involve the nature of the variables, i.e., whether or not one or both is stochastic. In addition, the term regression is also frequently used to mean the process by which the parameters of a relationship are determined.

For the purposes of the evaluations reported herein the name *regression analysis* is used in the broad sense of covering the aspects of the fitting of a curve, i.e., equation, referred to as the regression curve or line, to observed data points, where concern is with the slope and position of the curve that best fits the data, and to the analysis of how well the data points can be represented by the curve, i.e., the correlation analysis. The correlation analysis has two aspects, one is a measure of the degree of covariability between two variables, and the second is as a measure of the closeness of fit of a regression line to the distribution of the observations. The statistical analysis is performed for the purpose of establishing a stochastic dependence, and does not, nor does it have to, demonstrate the existence of a causal dependence.

For the analyses dealing with the APC it is desired that models be developed relating the burst strength and leak rate of degraded tubes to the morphology of the degradation. Unfortunately, the degradation morphology is only known exactly for tubes which have been destructively examined. However, a third variable, based on the non-destructive examination of the tubes, is available which is also directly related to the morphology of the degradation. Each degradation state is taken to correspond to a set of quantifiable characteristics or variables, such as the burst strength (measured by a burst pressure test), the leak rate (measured as a function of differential pressure), and a non-destructive examination (NDE) response, e.g., eddy current bobbin coil) signal amplitude in either an absolute or differential mode. Since the field examination of the tubes is based on the NDE response it is appropriate to examine the relationships between the first two variables and the third.

The experimental and field data for outside diameter stress corrosion cracking (ODSCC) at tube support plates (TSP's) consists of bobbin coil voltages and measured tube burst pressure, and leak rates at differential pressures corresponding to normal operating conditions and steam line break (SLB) conditions. As noted, these data are correlated, but not causally related.

For example, high burst pressures correlate with low voltages but high burst pressure does not cause low voltage. Similarly, low leak rates are correlated with low voltage, but low leak rates do not cause low voltage.

The degradation process determines the magnitude of the evolution of each variable, however, the degradation process is complex and the morphology and time history will vary even under conditions which would normally be termed identical. Thus, it is expected that the correlation between any pair of the three variables may have significant scatter. This is expected even if each of the variables is measured with perfect accuracy and contains no measurement error.

In order to predict burst pressures and leak rates under postulated conditions for degraded tubing, confirmed by field inspection by eddy current test, it is necessary to develop regression lines which relate average burst pressure to measured voltage and average leak rate to measured voltage. The "conventional" regression lines are usually determined by considering the variable which is to be predicted in the future, e.g., burst pressure, as the regressed variable, and the variable which will be measured in the future, i.e., voltage, as the regressor variable. While regression lines can also be established to predict voltages from measured burst pressures or leak rates, there is no particular reason to do so as these "inverse" correlations do not usually provide useful information beyond that which is obtained by the conventional regression lines.

It is to be noted that the causative factor relative to the magnitude of each variable is the crack morphology, and that none of the three characteristic variables can be considered to be the cause of the other. This means that for any pair, either may be treated as the predictor and the remaining variable treated as the response. Once a correlating relationship has been established, either variable may be used to predict an expected value for the other. For example, a correlating relationship may be mathematically determined using burst pressure as the response and bobbin amplitude as the predictor. Once the relationship is known, a mean bobbin amplitude associated with a given burst pressure or leak rate can be calculated.

Confidence limits for predicted burst pressure or for predicted leak rate can then be established about the regression line using standard statistical methods. The confidence limits which are determined directly from the regressions of burst pressure or leak rate on voltage will be narrower, for a fixed probability level, than the corresponding limits which could be deduced from the inverse regression lines. These correlations can then be used to determine high confidence values for the structural limit or leak rate, corresponding to the postulated SLB differential pressure.

D.2 The Linear Regression Model

The general, linear (meaning linear in the coefficients), first order regression analysis model relating two variables is given by

(D.1)

where y_i is taken here as the response or predicted variable, and x_i as the predictor, or regressor.

The ϵ , or error, term accounts for deviations from a perfect prediction. In order to establish confidence and prediction limits on y_i , the error is assumed to be normally distributed with a mean value of zero and a variance that is uniform over the range of interest. An analysis is then performed to determine the best values of a_0 and a_1 to use in equation (D.1). Three methods are commonly used for the analysis, maximum likelihood estimation, least squares (LS), and weighted least squares (WLS). For maximum likelihood analysis the values of a_0 and a_1 are found that maximize the probability of obtaining the observed responses. The use of maximum likelihood analysis is formally correct, however, if the errors are normally distributed, the maximum likelihood estimators (MLE) will be identical the estimators obtained using least squares. If both variables are stochastic and the errors are normally distributed then the application of least squares still leads to the maximum likelihood estimators of a_0 and a_1 .

The LS method is based on minimizing the sum of the squares of the errors, also referred to as residuals, between the observed and predicted values, thus, the best values of a_0 and a_1 are those that make

(D.2)

a minimum, where the caret indicates the predicted value,

(D.3)

Expression (D.2) is differentiated with respect to a_0 and a_1 and the resulting expressions set equal to zero and solved for the coefficients. For WLS the same expression for the errors is established by considering the error term, ϵ , to be weighted non-uniformly, i.e., the error distribution is

(D.4)

and the expression to be minimized becomes

(D.5)

where the Σ_i and hence the w_i are known. In situations where the variance of the response is not uniform it is possible to find appropriate weights such that the resulting estimators are MLE's.

For the unweighted LS analysis the slope of the regression or correlation line is found to be

(D.6)

where the summation limits are understood. The intercept is then found as

(D.7)

if y has been regressed on x . If x is regressed on y the slope will be

(D.8)

relative to the ordinate, or y , axis. If this is reckoned to the x axis, i.e., the abscissa of the original coordinates, the slope is

(D.9)

If the data used for the analysis contains significant scatter the values found by (D.6) and (D.9) can be quite different. A rough visualization of this can be obtained by picturing the smallest ellipse that can be drawn that envelopes all of the data points. A line connecting the largest and smallest abscissa values of the ellipse will approximate the regression of the y variable on the x variable, while the line connecting the maximum and minimum ordinate values will approximate the regression of the x variable on the y variable.

For the APC analyses the objective is to relate burst pressure and leak rate to bobbin voltage. This means that bobbin amplitude is depicted as the abscissa variable while burst pressure and leak rate are depicted as ordinate variables respectively. For the conventional regression analysis these are the corresponding choices for the regressor and regressed variables. However, if conditions dictate, an inverse regression may be performed, thus the depiction does not necessarily imply the direction of the regression analysis performed. The considerations discussed in the introduction indicate that the inverse regression is only useful if additional useful information can be gained from such an analysis.

The expansion of the model to include more terms, e.g., considering burst pressure to be related to the logarithm of the bobbin amplitude by a second order polynomial is still linear regression analysis. If the assumption of constant variance of the residuals is verified the application of least squares still results in the maximum likelihood estimators of the coefficients of the equation. If the prediction equation is non-linear in the coefficients, e.g., exponential, a transformation may be made to result in a linear equation, or non-linear regression techniques may be necessary. The use of a logarithmic transformation is common, and may result in a stabilization of the variance, i.e., a non-uniform variance before the transformation may become uniform as a result of the transformation.

Consideration of a non-linear regression model, e.g., logistic regression [13,14,15], is contained in the body of this report relative to determining the probability of leak as a function of bobbin amplitude.

D.3 Consideration of Variable Error

If the values of the regressed variable, say y , are subject to error but the regressor, x , is free from error, no bias will be introduced into the (regression predicted) mean value of y for a given x , although the variance will be greater due to the errors in the measurement of y . The calculated values of y are then unbiased estimates of the true values μ_y , assuming the error to also be normally distributed. The only effect of the errors in the measurement of y is to increase the variance of the residuals and render the estimate of y less reliable, i.e., the estimate will have larger inference bounds. If now x is also subject to measurement error the regression will be of observed values on observed values instead of true values on true values. If there is measurement error present in the predictor variable the slope obtained from the regression analysis will be biased [2,3,6,7,8,9,10,11], but the regression line will still pass through the centroid of the data. The standard regression analysis assumes that the regressor variable is known without error and that the regressed variable is a measured value subject to uncertainty. Thus, for example, the regression of burst strength, P on the logarithm of the bobbin amplitude, $\log(V)$, estimates the mean value P_k for which the observed value of bobbin amplitude is $\log(V_k)$. If the bobbin examination and evaluation technique were to be changed in the future to reduce the measurement errors the correlations based on current technology would have to be repeated.

If there is significant error present in the measurement of the variables the regression analysis may be performed using what is termed as the *error in variables* model. In this case it is assumed that the data measurements are of the form

(D.10)

where X and Y are the measurements corresponding to the true values of the variables x and y , and η and δ are their corresponding errors of measurement. For the predictor, say X , the total variance will be

(D.11)

It can be shown that when the measurement error is independent of the true value, the expected value of the calculated slope, a_1 , will be

(D.12)

where α_1 is the true value of the slope, or the value that would result if no measurement error was present, and

(D.13)

It is noted that a_1 would be found from equation (D.7) as before. A key point to note is that the calculated slope under predicts the true slope (without measurement error). If the measurement error is known, and is uniform, its effect on the analysis slope can be calculated directly and the appropriate slope to be used for prediction would be

(D.14)

When the error variance is known and can be expressed as a fraction of the variable variance the slope will be affected by a like amount.

When the error variance is not known, which is usually the case, an estimate of the true slope can be made using the partitioning technique developed by Wald ^[10] and subsequently improved upon by Bartlett ^[11]. The technique consists of partitioning the data into three groups based upon the ordered regressor variable. The line joining the centroids of the upper and lower groups is an unbiased and consistent estimator of the true slope. If the slope thus found is close to the slope determined without considering measurement errors then the measurement errors are considered to be not significant. The application of this technique must be done with caution since the order of the true values of the regressor variable(s) is not known, only the order of the measured variables. For the APC analyses the application of the Wald-Bartlett technique is restricted to estimating whether or not significant measurement error is present.

As an alternative, it may be assumed that the measurement errors are not significant, and a standard regression analysis performed. If the residuals are normally distributed about the regression line, inference bounds may be determined using the standard inference methods.

It is noted that if the magnitudes of the measurement errors associated with each of the variables, or their ratio, is not known, an "errors-in-variables" analysis does not lead to a criterion for the selection of the best regression direction. In general, the need for performing an "inverse" regression can be based on the determination of whether or not useful information beyond the conventional regression analysis will result.

D.4 Detection of Outliers

If the errors are normally distributed the application of LS to determine the coefficients of the regression equation minimizes the variance of these estimators. The coefficients are also the MLE's. A drawback of the LS technique is that it is not very robust. This means that the fitted line may not be the best estimator of the correct relationship because it can be significantly influenced by potentially outlying data. In addition, the resulting fit may be such that potential outliers become hidden if examined after the analysis is performed.

There are established methods for identifying influential data that may result in a distortion of the regression line. Such methods fall into the categories of regression diagnostics and robust regression. Robust regression methods are designed to be insensitive to potential outliers, and can be used to identify outliers based on the residual errors from the robust regression line. A rather simple example of improving the robustness of the fit would be simply minimize the sum of the absolute values of the residuals instead of the sum of the squares. This provides significant improvement if the outlier is in the y -direction for a y on x regression, but is not resistant to outliers in the x -direction.

One very robust technique is termed the "least median of squares," or LMS ^[12]. The best regression line (or polynomial) is the one for which the median of the squared residuals is a minimum. The drawbacks to this technique are that there is no closed form solution, and techniques for the determination of inference regions would be difficult to apply. However, the determination of a reasonable solution is quite easy using a computer. The algorithm proceeds by drawing sub-samples of a given size from the data set. For each sub-sample, regression line coefficients and the median of the squared residuals are calculated. The coefficients of the minimum median solution are designated as the LMS solution. A median based scale estimate (analogous to the standard deviation) is determined for the identification of outliers at a two-sided confidence level, or a one-sided confidence level.

The data for the APC were examined using the LMS robust regression program PROGRESS by Rousseeuw and Leroy. It is noted that the application of robust regression is not for the automatic deletion of improbable data points, only for the identification of potential outliers. The rejection of any data is then based on an evaluation of the circumstances surrounding the data collection to search for possible errors.

D.5 Selection of a Regression Coordinate System

For the analysis of continuous variable data four, alternatives were examined for each correlation. These choices are listed in Table D-1. For each case, the *correlation coefficient, r*, measuring the "goodness-of-fit" of the regression line was calculated.

Table D-1: Fitting Options Considered for LS Regression

Abscissa	Ordinate	Relation
Linear	Linear	
Logarithmic	Linear	
Linear	Logarithmic	
Logarithmic	Logarithmic	

The correlation coefficient is a measure of the variation of the data explained by the regression line, thus the largest value is indicative of the best fit. The expression for the square of the correlation coefficient, known as the *index of determination*, is

(D.15)

The index of determination is the proportion of the total variation about the mean of the predicted variable that is explained by the regression line. The scale combination yielding the largest index of determination, and, hence, correlation coefficient, was selected for the analysis. In the event that the predicted variable for the regression is the logarithmic transformation of a physical variable, the above calculation is performed on the untransformed variable. It is readily apparent, however, that for data with a range of several orders of magnitude, e.g., bobbin amplitudes ranging from _____, the use of a logarithmic scale is appropriate. It is also to be expected that the variation of observed voltages would be normally distributed about the log of the voltage. The same is true for the leak rate which ranged from _____ for specimens for which leaking was observed. It is to be noted that the use of a logarithmic transformation is commonly used for data with a large range as a variance stabilizing technique.

D.6 Selection of a Regression Direction

As noted in the introduction to this appendix, the bobbin amplitude does not cause the observed burst pressure and vice versa. The same is true for the relation between bobbin voltage and leak rate. Thus, the regression direction is not specified by the choice of variates.

The objective of performing the regression analysis is prediction. For all practical purposes the bobbin voltage will be used as a predictor of burst pressure and leak rate. However, the intended use does not automatically dictate the designation of the predictor and response variable roles for the regression analysis. The LS fit simply finds the line such that the variance of the responses is minimized relative to the regression line. As previously noted, once the LS fit has been performed either variable can be predicted from the other. In addition, inference regions or bands established for prediction in one direction may be similarly use in the reverse direction (although the terminology is changed to discrimination).

For a regression of y on x , the average of future values of y_0 for a given x_0 is bounded (confidence) with a level of confidence of $\geq(1-\alpha) \cdot 100\%$ by

(D.16)

where s^2 is the "standard error of regression," i.e.,

(D.17)

and $t_{1-\alpha/2, n-2}$ is found from the Student's t-distribution. Similarly, an individual future value of y_0 for a given x_0 is bounded (prediction) with a level of confidence of $\geq(1-\alpha)\cdot 100\%$ by

(D.18)

However, for a given y_0 the bounds on x_0 , referred to as discrimination bounds, are found by solving equation (D.18) for the values of x_0 that satisfy the equality, although care must be taken relative to the solution since real roots of equation (D.18) may not exist depending on the results of the data analysis.

If the scatter of the data is small, as for the burst pressure to bobbin amplitude correlation, the regressions of x on y and y on x will yield slopes that are similar. However, for APC analyses the data exhibit significant scatter for the leak rate to bobbin amplitude correlation and the two regression lines have significantly different slopes. In this case it is appropriate to select the regression line based on non-statistical considerations. Such considerations may be known end points of the regression line, e.g., burst pressure for non-degraded tubes, or comparison of the slope with theory based results. For either regression direction, inference regions can be determined.

As noted, equation (D.18) can be used to determine inference bounds regardless of the direction of the regression. In general the magnitudes of the inference bounds will not be identical. However, the confidence level statements are true for both bounds, i.e., one bound is not invalidated by the other. Thus, if a $\geq(1-\alpha)\cdot 100\%$ lower bound on the burst pressure from the regression of the burst pressure on the logarithm of the bobbin amplitude is higher than the corresponding lower bound from the inverse regression, it simply means that the confidence level of the inverse regression is $>(1-\alpha)\cdot 100\%$. Thus, if the residuals are verified to be normally distributed, the lower prediction bound may be taken as the higher of the prediction bounds established by performing the regression analysis in each direction.

D.7 Significance of the Regression

The significance of the regression is evaluated by calculating the improvement in the estimate of the predicted variable based on knowledge of the regressor variable. For the APC analyses this is the same as determining whether or not the estimate of the burst pressure or leak rate for a tube is improved by knowing the bobbin coil voltage amplitude. For a linear, 1st order regression this is the same as testing to determine if a zero slope is probable. If the confidence interval for the slope includes zero then the relationship between the predicted variable and the regressor could be accidental, i.e., due to random error. The actual determination may be made

by calculating the confidence interval on the slope, a_1 , to see if it includes zero, or by testing the null hypothesis that the true slope is zero. In practice this is stated as

(D.19)

If the null hypothesis, H_0 , is true, then ratio of the mean square due to regression (SSR) to the mean square due to error (SSE), i.e., the mean square of the residuals, follows an "F" distribution with the regression degrees of freedom (DOF) in the numerator and the residuals degrees of freedom in the denominator. For a linear analysis with k regressor variables and n data points, then

(D.20)

where $100 \cdot (1 - \alpha)\%$ is the associated confidence level. (Note that α is the area in the tail of the distribution.) If the true value of the slope is zero then both mean square (MS) Regression and MS Error are independent estimators of the true value of the error variance. Since they are both estimates they would not be expected to be exactly equal, however, it would be expected that they would be nearly equal so that their ratio would not be too far from unity. It is noted that the F ratio and the Index of Determination, r^2 , are both calculated from the sums of squares of the variables, so

(D.21)

and a critical value of r^2 for a selected critical α can be found as

(D.22)

If the value of r^2 found from the regression is greater than the critical value from (D.22) the null hypothesis, H_0 , i.e., that the slope is zero, would be rejected, and the alternate hypothesis, H_1 , that the true slope is not zero would be accepted. For example, consider

Then, from equation (D.22) we find a critical value of r^2 of and a critical value of r of . If the regression value of r^2 exceeds the regression is significant at a level greater than

For a 1st order regression, equation (D.20) can be rearranged as

(D.23)

i.e., a t distribution with $n-2$ DOF's. Given a value of r from the regression analysis, a value of t can be calculated and a significance level determined. For the same example as above, we consider $r^2 = \dots$ and $n = \dots$. From equation (D.23) we find $t = \dots$, and a significance level of $100 \cdot (1-\alpha) = \dots$, which agrees with the above determination. It is to be noted that for a small number of regressor variables and a large number of data points, the square of the correlation coefficient does not have to be very close to one to reject the null hypothesis and accept the alternate hypothesis that the slope is not equal to zero, thus implying that a correlation does exist.

D.8 Analysis of Regression Residuals

To use the results of the least squares analysis it is assumed that the expectation function is correct, that the response is given by the expectation function plus a disturbance, that the disturbance is independent of the response function, that each disturbance has a normal distribution about the response function value, that each disturbance has zero mean, that the disturbances (or weighted disturbances) have equal variances, and that the disturbances are independently distributed. The purpose of analyzing the residuals, i.e., the differences between the actual variable value and the predicted variable value, is to verify each of the assumptions inherent in performing the least squares analysis. There are a variety of plots that can be used for the analysis of the residuals, although not all may be judged necessary for each analysis. A plot of the residual values against the predicted values should be nondescript since the residuals should not be correlated with the predicted values. Such results indicate that the variance is approximately constant (as assumed), that there is no systematic departure from the regression curve, and that the number of terms in the regression equation is adequate. A frequency plot (histogram) of the residual values should appear to be similar to a normal distribution. A plot of the ordered residuals on normal probability paper should approximate a straight line. Any of these plots may be used to verify that the regression residuals are normally distributed, although the results are not obvious from the scatter plot. The normal probability plot offers the advantages that it can easily be used to determine if the mean is approximately zero, and a reasonable estimate of the standard deviation of the residuals may be read directly.

To prepare the cumulative normal probability plot, the residuals are sorted in ascending order and then plotted against an ordinate cumulative percent probability value given by

$$(D.24)$$

where n is the number of data points used in the regression and i is an index ranging from 1 to n . If a small number of outliers have been omitted from the regression analysis, but the depiction of their residuals is desired, n may be taken as the total number of data points and the residuals of the outliers included accordingly. This has the effect of compressing the spread of the outliers along the probability axis, but generally will not affect the conclusions relative to the linearity of the plot. The rationale for the cumulative probability values used is if the unit area under the normal curve is divided into n equal segments, it can be expected, if the distribution is normal, that one observation (residual) lies in each section. Thus, the i^{th} observation in order is plotted against the cumulative area to the middle of the i^{th} section. The factor of 100 is used to convert the scale to percent probabilities.

If the plotted residuals approximate a visually fitted straight line, it may be concluded that they are normally distributed about the regression curve. The residual value where the line crosses the 50% probability value is an estimation of the mean of the residuals, and can be used to verify that the mean is approximately zero. The residual distance from the 50% point to the 84% point is an approximation for the standard deviation of the residuals. If the residuals for the outliers have been included in the plot they will distort the results obtained for the mean and standard deviation, with the mean value being less affected.

For this type of plot, the outliers in the data, if any, will tend to appear on the far left in the lower half of the residual normal plot and on the far right in the upper half, i.e., large negative and positive residual values. The results from the normal probability plot may be used to determine the need for preparing any of the other plots, i.e., it may be apparent that no additional information would be available from a scatter plot.

D.9 References

1. Yamane, T., Statistics: An Introductory Analysis, 2nd Edition, Harper & Row, New York (1967).
2. Draper, N.R., and Smith, H., Applied Regression Analysis, Second Edition, Second Edition, John Wiley & Sons, New York (1981).
3. Hald, A., Statistical Theory with Engineering Applications John Wiley & Sons, New York (1952).
4. Weisberg, S., Applied Linear Regression, John Wiley & Sons, New York (1985).
5. Lipson, C., and Sheth, N. J., Statistical Design and Analysis of Engineering Experiments, McGraw-Hill, New York (1973).
6. Deming, W. E., Statistical Adjustment of Data, Dover Publications, New York (1964).
7. Mandel, J. The Statistical Analysis of Experimental Data, Dover Publications, New York (1984).
8. Davies, O. L. (Editor), Statistical Methods in Research and Production, Oliver and Boyd, London, England (1957).
9. Fuller, W.A., Measurement Error Models, John Wiley & Sons, New York (1987).
10. Wald, A. Fitting a Straight Line When Both Variables are Subject to Error, Annals of Mathematical Statistics, Vol. 11, pp. 284-300 (1940).
11. Bartlett, M.S., Fitting a Straight Line When Both Variables are Subject to Error, Annals of Mathematical Statistics, Vol. 5, pp. 207-212 (1949).

12. Rousseeuw, P.J., and Leroy, A.M., Robust Regression and Outlier Detection, John Wiley and Sons, New York (1987).
13. Hosmer, D.W., and Lemeshow, S., Applied Logistic Regression, John Wiley & Sons, New York (1989).
14. CSS. Statistica Users Manual, Statsoft (1991).
15. SAS/STAT User's Guide, Revision 6, Fourth Edition, Volume 2, Chapter 27, *The Logistic Procedure*, SAS Institute, Inc., Cary, North Carolina (1990?).